Ulm University Medical Center
Institute of Molecular Virology
Directors:
Prof. Dr. Frank Kirchhoff
Prof. Dr. Jan Münch

Development of advanced EPI-X4 derivatives for the treatment of non-Hodgkin lymphomas

Dissertation

to obtain the Doctoral Degree of Human Biology (Dr. biol. hum.)
at the Medical Faculty of Ulm University

Andrea Gilg

Born in Göppingen

2024

Dean of the Medical Faculty: Prof. Dr. Thomas Wirth

1st reviewer: Prof. Dr. Jan Münch

2 nd reviewer: Prof. Dr. Holger Barth

Day of Graduation: April 4th 2025

To my family.

Results gained in my thesis have previously been published in the following publications:

Gilg, A., Harms, M., Olari, L. R., Urbanowitz, A. K., Bonig, H. & Münch, J. Absence of the CXCR4 antagonist EPI-X4 from pharmaceutical human serum albumin preparations. *J. Transl. Med.* **19**, 1–5 (2021).

Harms, M., Fabech Hansson, R., **Gilg, A.**, Almeida-Hernández, Y., Löffler, J., Rodríguez-Alfonso, A., Habib, M. M. W., Albers, D., Ahmed, N. S., Abadi, A. H., Winter, G., Rasche, V., Beer, A. J., Weidinger, G., Preising, N., Ständker, L., Wiese, S., Sanchez-Garcia, E., Zelikin, A. N. & Münch, J. Development of N-Terminally Modified Variants of the CXCR4-Antagonistic Peptide EPI-X4 for Enhanced Plasma Stability. *J. Med. Chem.* **66**, 15189–15204 (2023).

TABLE OF CONTENTS

Abbreviations.....VII
1 Introduction 1
1.1 The CXCR4/CXCL12 axis 1
1.1.1 The CXCL12/CXCR4 axis in health 2
1.1.2 The CXCL12/CXCR4 axis in diseases 3
1.2 Lymphomas 5
1.2.1 Non-Hodgkin Lymphomas (NHL) 5
1.3 CXCR4 as therapeutic target in MCL and CLL 9
1.4 The endogenous CXCR4 antagonist EPI-X4 10
1.4.1 Generation and function of EPI-X4 10
1.5 Scope of the study 14
2 Materials and Methods 16
2.1 Materials 16
2.1.1 CXCR4 antagonists 16
2.1.2 Eukaryotic cells 17
2.1.3 Human blood plasma and serum 18
2.1.4 Proteins 18
2.1.5 Buffers and Media 20
2.1.6 Reagents and Kits 23
2.1.7 Consumables 24
2.1.8 Technical equipment 25
2.1.9 Software 26
2.2 Methods 27
2.2.1 Peptide synthesis 27
2.2.2 EPI-X4 27
2.2.3 Eukaryotic cells 28
2.2.4 Virology methods 30
2.2.5 Antibody competition assay 31
2.2.6 Cell signaling assays 31
2.2.7 Enzymatic stability 33
2.2.8 Animal experiments and animal replacement experiments 33
2.2.9 Statistical analyses 34
3 Results 36
3.1 EPI-X4 is absent in pharmaceutical HSA preparations. 36
3.2 Advanced EPI-X4 derivatives bind to CXCR4 and antagonizes CXCL12 mediated cell responses on human and murine lymphocytes. 38

3.2.1 EPI-X4 derivatives are active on human primary CD4+ T cells. 38
3.2.2 Advanced EPI-X4 derivatives act on murine CXCR4. 44
3.3 CXCR4 antagonizing effect of optimized EPI-X4 derivatives in Mantle cell lymphoma and chronic lymphocytic leukemia. 50
3.3.1 EPI-X4 derivatives antagonize CXCL12/CXCR4 signaling on MCL and CLL cell lines. 50
3.3.2 Efficacy of EPI-X4 derivatives on splenocytes derived from the Eμ-TCL-1 mouse model. 56
3.4 Further optimization strategies for EPI-X4 derivatives. 59
3.4.1 PEGylation of JM#173 and JM#29. 59
3.4.2 Diacid variants 64
3.5 Establishment of the HET-CAM model to determine peptide stability 72
4 Discussion 76
4.1 Pharmaceutical preparations of HSA do not contain EPI-X4. 76
4.2 EPI-X4 derivatives are antagonistically active on primary T cells. 76
4.3 EPI-X4 derivatives are less efficient on murine cells than on human cells. 79
4.4 Advanced EPI-X4 derivatives are promising drug candidates for advanced preclinical development for the treatment of Mantle cell lymphoma and chronic lymphocytic leukemia. 81
4.5 *In* vivo stability of EPI-X4 derivatives – Evaluating the impact of PEGylation and Albumin-binding. 83
4.6 Comparative analysis of newly generated diacid variants and monoacid versions: No clear advantages observed. 85
4.7 HET-CAM model is a reliable alternative to determine peptide stability *in vivo*. 87
4.8 Conclusion and future perspectives 88
5 Summary 90
6 References 92
7 Supplementary Information 126
8 Acknowledgements 130
9 Curriculum Vitae 131

ABBREVIATIONS

°C	Degrees Celsius
µ	micro
A20	BALB/c B cell lymphoma cell line
ACK	Ammonium-Chloride-Potassium
AIDS	acquired immunodeficiency syndrome
Akt	protein kinase B
Alb	albumin
ANOVA	analysis of variants
APC	antigen presenting cell
APC	Allophycocyanin
ARRRP	AIDS Research and Reference Reagent Program
ATCC	American Type Culture Collection
ATP	adenosine triphosphate
AUC	area under the curve
BA/F3	murine pro B cell line
Bcl-2	B cell lymphoma 2
B-CLL	CLL B cells
BCR	B cell receptor
BMSC	bone marrow stromal cells
BND D	5-Bromo-5-nitro-1,3-dioxane
BTK	Bruton's tyrosine kinase
BW5147	murine T lymphoblast cell line
Ca^{2+}	calcium ion
$CaCl_2$	calcium chloride
CAM	chorioallantoic membrane
cAMP	cyclic adenosine monophosphate
CCR	C-C motif chemokine receptor
CD	cluster of differentiation
Chol	cholesterol
CLL	chronic lymphocytic leukemia
CO_2	carbon dioxide
CSC	cancer stem cell
CXCL	C-X-C motif chemokine
CXCR	C-X-C motif chemokine receptor

d	dexter
Da	Dalton
DAG	diacylglycerol
dH_2O	distilled water
diMal	dimaleimide
DMEM	Dubelcco's Modified Eagle Medium
DPBS	Dubelcco's Phosphate Buffered Salin
DMSO	Dimethyl sulfoxide
DNA	deoxyribonucleic acid
dpi	day(s) post infection
DSMZ	Deutsche Sammlung von Mikroorganismen und Zellkulturen
ECL	extracellular loop
EDD	embryonic development day
EDTA	ethylenediaminetetraacetic acid
EDTA-Na_2 *2 H_2O	ethylenediaminetetraacetic acid disodium dihydrate
ELISA	enzyme-linked immunosorbent assay
EMT	epithelial to mesenchymal transmission
EPI-X4	endogenous peptide inhibitor of CXCR4
Erk	extracellular-signal regulated kinases
FACS	fluorescence-activated cell sorting
FCS	fetal calf serum
FDA	Food and Drug Administration
FDC	follicular dendritic cells
FSC-A	forward scatter parameter
g	gravity force
g	gram(s)
Gal	galactosidase
GDP	guanosine diphosphate
GLP-1	Glucagon-like peptide 1
Glu	glutamic acid (linker)
GPCR	G-protein coupled receptor
GRK	G-protein coupled receptor kinase
GTP	guanosine triphosphate
h	human
h	hour(s)

H_2SO_4	sulfuric acid
HBS	HEPES buffered saline
HCl	hydrochloric acid
HEK293T	human embryonic kidney 293 large T antigen cells
HeLa	Henrietta Lacks
HEPES	4-(2-hydroxyethyl)-1-piperazineethanesulfonic acid
HET-CAM	hen's egg test – chorionallantoic membrane
HG-3	human chronic B cell leukemia cell line
HIV	human immunodeficiency virus
HPLC	high performance liquid chromatography
HRP	horseradish peroxidase
HSA	human serum albumin
HSC	hematopoietic stem cell
IC_{50}	50 % inhibitory concentration
ICL	intracellular loop
IDL	intermediate differentiated lymphoma
Ig	immunoglobulin
IgHV	immunoglobulin heavy-chain variable region gene
IgV_H	immunoglobulin heavy chain variable
IL	interleukin
IP3	inositol 1,4,5-triphosphate
IPS-E	international prognostic score for early stage CLL
Jeko-1	human B cell lymphoma cell line
k	kilo
KCl	potassium chloride
KH_2PO_4	potassium dihydrogen phosphate
l	liter
LAM	lymphoma-associated macrophages
LAP	leucine aminopeptidase
LESTR	leucocyte-derived seven transmembrane receptor
log	logarithmic
LTR	long terminal repeat
m	monoclonal
m	milli
m	murine

m	meter
M	Molar (mol/l)
min	minute(s)
MAPK	mitogen-activated protein kinase
Maver-1	human lymphoblast cell line
MCL	mantle cell lymphoma
Mec-2	human B cell line
MeO	methoxy
MFI	mean fluorescence intensity
$MgCl_2$	magnesium chloride
MIPI	Mantle Cell Lymphoma International Prognostic Index
MSC	mesenchymal stromal cells
MWCL-1	human Waldenström's macroglobulinemia cell line
n	nano
n. d.	not determined
Na_2HPO_4 *$2H_2O$	di-sodium hydrogen phosphate dihydrate
NaCl	sodium chloride
NaEDTA	sodium ethylenediaminetetraacetic acid
$NaHCO_3$	sodium hydrogencarbonate
NaN_3	sodium azide
NaOH	sodium hydroxide
NEAA	non-essential amino acids
NH_2	amino group
NHL	non-Hodgkin lymphomas
NK	natural killer
NLC	nurse-like cell
OEG	oligo(ethylene glycol)
OVA	ovalbumin
p	phosphorylated
p24	capsid protein of HIV-1 (24 kDa)
p53	tumor suppressor protein (53 kDa)
Pal	palmitic acid
PBS	phosphate buffered saline
PCR	polymerase chain reaction
PE	phycoerythrin

PEG	poly(ethylene glycol)
PFA	paraformaldehyde
pH	*pondus Hydrogenii*
PI3K	phosphatidylinositol-3 kinase
PI3KCA	phosphatidylinositol-4,5-Bisphosphate 3-Kinase Catalytic Subunit Alpha
PIM	provirus integration site for Moloney murine leukemia virus 1
PKA	protein kinase A
PKB	protein kinase B
PKC	protein kinase C
PLC	phospholipase C
PTEN	Phosphatase and Tensin Homolog
REAL	Revised European-American Classification of Lymphoid Neoplasms
RLU	relative light units
rpm	rounds per minute
RPMI	Roswell Park Memorial Institute
RT	room temperature
s	second(s)
s.c.	subcutaneous
SAR	structure activity relationship
SCID	severe combined immune deficiency
SD	standard deviation
SDF-1	stromal-derived factor 1
SEER	Surveillance, Epidemiology, and End Result
SEM	standard error of mean
SLL	small lymphocytic lymphoma
SOX11	SRY-Box Transcription Factor 11
SRY	Sex-determining region Y protein
SSC-A	side scatter parameter
Ste	stearic acid
SupT1	human T lymphoblast cell line
SV	Simian virus
TAM	tumor associated macrophages
TCL-1	T cell leukemia/lymphoma 1A

tg	transgenic
TGR5	Takeda G protein-coupled receptor 5
TMB	3,3',5,5'-tetramethylbenzidine
TME	tumor microenvironment
TP53	tumor protein 53
T-PLL	T-prolymphocytic leukemi
TrtS	trityl
TZM-bl	HeLa-derived HIV-reporter cell line
UPEP	Ulm – Center for Peptide Pharmaceuticals
UV	ultraviolett
v/v	volume per volume
VCAM	vascular cell adhesion molecule
Vis	visible
VLA	very late antigen
w/v	weight per volume
WHIM	warts, hypogammaglobulinemia, infections, myelokathexis
WHO	World Health Organization
X4-tropic	CXCR4 tropic
ZAP-70	zeta chain of T cell receptor associated protein kinase 70

Table 1: Amino acid code.

Amino acid	1 letter code	3 letter code	Amino acid	1 letter code	3 letter code
Alanine	A	Ala	Leucine	L	Leu
Arginine	R	Arg	Lysine	K	Lys
Asparagine	N	Asn	Methionine	M	Met
Aspartic acid	D	Asp	Phenylalanine	F	Phe
Cysteine	C	Cys	Proline	P	Pro
Glutamic acid	E	Glu	Serine	S	Ser
Glutamine	Q	Gln	Threonine	T	Thr
Glycine	G	Gly	Tryptophan	W	Trp
Histidine	H	His	Tyrosine	Y	Tyr
Isoleucine	I	Ile	Valine	V	Val

1 Introduction

1.1 The CXCR4/CXCL12 axis

The C-X-C motif chemokine receptor 4 (CXCR4), formerly named leucocyte-derived seven-transmembrane receptor (LESTR) or Fusin, consists of 352 amino acids and belongs to the family of G-protein coupled receptors (GPCRs). Similar to other GPCRs, CXCR4 is composed of seven helices crossing the cellular membrane which are connected by three intracellular (ICL1-3) and three extracellular loops (ECL1-3)[1–3]. CXCR4 is widely expressed on cells of the human body, including cells of the hematopoietic system i.e. stem cells, but also epithelial and endothelial cells[4–8]. The best described ligand for CXCR4 is the cytokine C-X-C motif chemokine 12 (CXCL12), also known as stromal-cell derived factor 1 (SDF-1). CXCL12 belongs to the superfamily of CXC chemokines consisting of two cysteines separated by one amino acid[9]. Its genomic information is located on chromosome 10q11.1 and alternative splicing leads to two main isoforms of SDF-1, namely SDF-1α and SDF-1β. They differ structurally only in their C-terminal end which is proteolytically cleaved in case of SDF-1α but not SDF-1β[9,10]. The chemokine is evolutionary conserved between human and mice with up to 99 % of homology. It is present throughout the human body[9,11]. So far, 41 amino acids of CXCR4 have been identified to be crucial for the interaction with CXCL12 and are responsible for chemokine engagement, signal initiation and propagation, microswitch activation controlling G protein coupling and G-protein coupling itself[12].

Binding of CXCL12 to CXCR4 takes place in a two-step mechanism. First, CXCL12 interacts with the N-terminus of CXCR4 causing optimal orientation for the subsequent interaction with the receptor binding pocket via the CXCL12 N-terminal region[13–15]. Binding of CXCL12 to CXCR4 results in conformational changes of the receptor and phosphorylation of various amino acids located at the distal C terminal tail of the receptor by protein kinase C (PKC) and G-protein coupled receptor kinases (GRKs)[16–19]. This leads to the exchange of guanosine diphosphate (GDP) to guanosine triphosphate (GTP) and the dissociation of the G protein subunits α and βγ resulting in the activation of a complex signaling network (Figure 1)[3,8,16,20,21]. The βγ subunit influences the release of Ca^{2+} from their intracellular storage through the activation of the phospholipase C (PLC) leading to the generation of inositol 1,4,5-triphosphate (IP3) and diacylglycerol (DAG). PKC is then activated by DAG and in turn activates the mitogen-activated protein kinase (MAPK) along

with the intracellular Ca^{2+} released by IP3 leading to chemotaxis[16,20]. CXCR4 is mainly associated with the subunit $G\alpha_i$ subunit, but other Gα subtypes can also be coupled to CXCR4 leading to different intracellular responses upon stimulation[15,16,20,22,23]. Upon dissociation, $G\alpha_i$ inhibits adenyl cyclase and hence the generation of cyclic adenosine monophosphate (cAMP) and Protein kinase A (PKA) and also mediates the activation of phosphatidylinositol-3 kinase (PI3K)/Protein kinase B (Akt) pathway and Ras-MEK1/2-Erk1/2 pathway[16,20]. Through the activation of Akt, survival and cell cycle progression is mediated[20]. Activation of the Ras-MEK1/2-Erk1/2 pathway is associated with chemotaxis[20]. CXCR4/CXCL12 signaling is also mediated via G-protein independent pathways. Phosphorylated CXCR4 leads to the recruitment of β-arrestin resulting in receptor internalization via cathepsins[16,17,19,24,25]. Additionally, β-arrestin has been shown to play a role in chemotaxis, receptor-mediated Erk phosphorylation and Ca^{2+} mobilization[16,17,19,26,27].

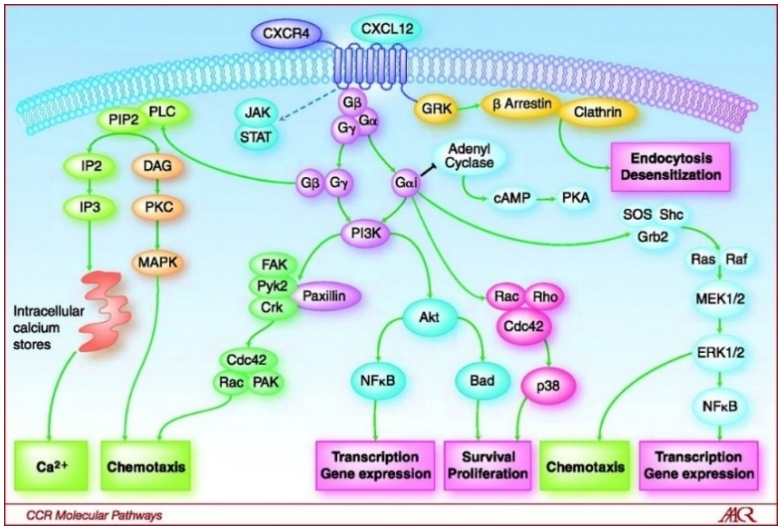


Figure 1. The C-X-C motif chemokine 12 (CXCL12) induces intracellular signaling pathways through the C-X-C motif chemokine receptor 4 (CXCR4). Upon binding of CXCL12 to CXCR4, the receptor undergoes conformational changes resulting in the dissociation of the coupled G-proteins α and βγ. This in turn initiates several intracellular signaling pathways through activation or inactivation of signaling proteins i.e. phosphatidylinositol-3 kinase (PI3K) and adenyl cyclase. This leads to Ca^{2+} flux, chemotaxis, survival, and cell proliferation. In addition, CXCL12/CXCR4 signaling leads to the recruitment of β-arrestin and to receptor endocytosis and desensitization. (From: Teicher and Fricker (2010)[8]. Reprinted with permission from American Association for Cancer Research)

1.1.1 The CXCL12/CXCR4 axis in health

CXCL12/CXCR4 signaling plays a pivotal role in embryonic development. Mice lacking either CXCR4 or CXCL12 experience embryonic lethality[28–30]. The CXCL12/CXCR4 axis is involved in functional organogenesis during development and contributes to B cell lymphopoiesis, bone-marrow myelopoiesis, fetal cerebellar development, cardiac ventricular septal formation, coronary artery development and effective organ vascularization.[28–36]. In adults, CXCR4 is highly involved in hematopoiesis. It has been

shown to play a crucial role in homing and retention of hematopoietic stem cells (HSCs) and progenitor cells to and within the bone marrow, where high concentrations of CXCL12 are found within the stem cell niches thereby controlling its trafficking, renewal and survival[37–41]. Furthermore, it is necessary for lymphoid and myeloid recolonization in the bone marrow as well as in the generation, development and proliferation of early hematopoietic progenitor cells[37,42]. CXCR4 is highly expressed on immune cells and crucial for the immune cell trafficking, their mobilization from the bone marrow, and the enrollment of immune responses. It is involved in homing of immune cells into lymph nodes in close proximity to sides of inflammation or infection[43–45]. Anti-inflammatory properties related to CXCR4 mediated signaling has been shown in case of atherosclerosis, where CXCR4 expression has been shown to limit the inflammation by improving the integrity of smooth muscle cells and the recruitment of progenitor cells. In line with this, CXCR4 deletions have been associated with increased leukocyte mobilization and hence enhanced atherosclerosis[46,47]. CXCR4 signaling also contributes to the adaptive immune through stabilization of the immunological synapsis formed by T cells and antigen presenting cells (APCs) leading to increased activation of T cells and cytokine production[48,49]. In addition, CXCR4 activation contributes to wound healing, angiogenesis and neovascularization[50–55].

1.1.2 The CXCL12/CXCR4 axis in diseases

Since it has been shown, that a functional CXCL12/CXCR4 axis is of high physiological relevance, it is not surprising that malfunctions of the CXCL12/CXCR4 axis lead to many pathophysiological conditions like diseases of the immune system and cancer.

Mutations within the gen locus coding for CXCR4 lead to truncations in the C-terminal tail to the receptor and are the causative agent of an immunodeficiency syndrome called WHIM (warts, hypogammaglobulinemia, infections, myelokathexis) syndrome. Truncated CXCR4 cannot be internalized leading to the loss of the negative feedback loop and hence to an overactivation of the receptor. This results in an accumulation of immune cells in the bone marrow (myelokathexis), reduced recruitment of immune cells to sites of infection and hence a decreased immune response[56–58]. In addition, upregulations of either CXCL12 and/or CXCR4 have been linked to the development of several autoimmune diseases i.e. psoriasis, rheumatoid arthritis and inflammatory bowel diseases[6,59–67].

Dysfunctional CXCL12/CXCR4 expression also plays a pivotal role in tumorigenesis of both solid tumors and hematological malignancies. CXCR4 is highly expressed on more than 20 different cancer types and overexpression is associated with disease progression and shorter survival of patients[68–73]. Tumorigenesis, also named carcinogenesis, is a multistep

process including at least three different stages: Initiation, promotion and progression[74]. It has been shown that, depending on the type of tumor, dysfunctional CXCR4 can contribute to each step of tumorigenesis. The causative agent of the initiation process is the presence of genetic mutations. In case of a B cell lymphoma subtype called Waldenström's macroglobulinemia, mutations within the coding region of CXCR4 have been identified in up to 40% of all patients. These mutations impair the desensitization and internalization of CXCR4 and thus prolong CXCR4 activation upon binding of CXCL12 associated with poorer outcome of the disease[75,76]. The step of cancer promotion, generally characterized by increased cell proliferation and decreased apoptosis of tumor cells and thus tumor growth, have been linked to (over-)activated CXCL12/CXCR4 signaling in various cancer subtypes[4,77–79]. Increased tumor growth through enhanced CXCL12 secretion is facilitated either directly from tumor cells in an autocrine manner or through the secretion of CXCL12 by cells present in the tumor microenvironment (TME)[79–81]. The formation of a TME contributes to the last step of the tumorigenesis, the progression of cancer. This stage is characterized by different mechanisms like the epithelial to mesenchymal transmission (EMT), tumor angiogenesis, metastasis as well as the immune escape of the tumors resulting in greater aggressiveness and higher malignant potential of the tumors. The EMT typically occurs during several physiological processes like embryonic development and tissue regeneration but also contribute to tumorigenesis. Thereby, epithelial cells undergo different biological changes resulting in a more mesenchymal phenotype and hence increased migratory capacity and invasiveness. CXCR4 contributes to EMT which facilitates the generation of cancer stem cell (CSCs), cancer metastasis and the progression of different types of tumors. Moreover, cancerous tissue which undergo EMT are associated with suppressed immune responses and increased resistance to chemotherapeutics[82–86]. $CXCR4^{high}$ expressing CSCs have been shown to have self-renewal properties contributing to tumor reinitiating processes after treatment and thus tumor survival and progression[87–90]. Expression levels of CXCR4 in cancer cells are associated with the formation of metastasis and hence higher aggressiveness of the tumor. Metastasis of $CXCR4^{high}$ tumors through the induction of CXCL12 lead to cell migration predominantly towards organs with high titers of CXCL12 like bone marrow or lungs where a secondary tumor arises[70,91–93]. Despite that, CXCR4/CXCL12 axis also contributes to TME, which is composed of different cells interacting in a direct or indirect manner with cancer cells. This results in cancer cell survival through gained pro-proliferative and anti-apoptotic signals from the TME, the escape from the immune system and chemotherapeutic resistance and hence tumor progression[94–96]. The

role of the CXCL12/CXCR4 axis within the TME will be described in more detail below for mantle cell lymphoma (MCL) and chronic lymphocytic leukemia (CLL), two subtypes of non-Hodgkin lymphomas (NHL).

1.2 Lymphomas

Hematological malignancies are a heterogeneous group of diseases accounting for approximately 6% of all cancers worldwide[97,98]

Lymphomas are hematological malignancies with more than 80 individual forms which were classified by the Revised European-American Classification of Lymphoid Neoplasms (REAL) in 1994 and adopted by the World Health Organization (WHO) into three different groups, namely Hodgkin lymphomas, B cell neoplasm, and T cell and NK cell neoplasms. The latter two subgroups are commonly known as non-Hodgkin lymphomas and lack the Reed-Sternberg cells which are abnormal mononuclear B lymphocytes characteristic for Hodgkin lymphomas[99–103].

1.2.1 Non-Hodgkin Lymphomas (NHL)

NHL are the most common hematopoietic malignancies with approximately 500,000 cases per year. The diseases are initiated in lymphocytes at different stages of development[104]. So far, more than 40 subtypes of NHL have been described with the majority (85-90%) being B cell neoplasms, followed by T cell neoplasms (~10%) and in rare cases NK-cell neoplasms[101–103,105–107]. Clinically, NHL are additionally classified into aggressive versus indolent forms.[105,108]. For some subtypes of NHL like mantle cell lymphoma or follicular lymphoma, driver gene mutations have been described. Moreover, additional factors are known to increase the risk to develop NHL, like gender and age, smoking and alcohol consumption, immunosuppression as well as several comorbidities[101,109–117]. Current therapy strategies for NHL includes surgery, radiation, chemotherapy and immunotherapy or combinations thereof[102].

1.2.1.1 Mantle cell lymphoma

Initially described in the 1970s and distinguished into centrocytic lymphoma, mantle zone lymphoma and intermediate differentiated lymphoma (IDL), these clinical pictures were later defined as one disease due to their morphological similarities. This disease was named mantle cell lymphoma (MCL) as it is postulated to arise in the inner mantle zone of lymphoid tissue[118–120]. It is a very rare subtype of non-Hodgkin lymphoma, accounting for approximately 5% of all NHL, with an incidence of around 1-2/100 000 per year. MCL

mainly develops in elderly persons with an median diagnosis age of approximately 65 years and affects men 3 times more than women[108,109,121,122]. Overexpression of cyclin D1 is the main hallmark of MCL, caused by a translocation of chromosomes 11 and 14 (t(11;14)) which has been firstly identified in 1979[108,123]. Survival prediction of MCL patients is nowadays based on the Mantle Cell Lymphoma International Prognostic Index (MIPI), which classifies MCL patients into 3 different risk groups: low, intermediate and high[124–126].These three groups differ in their mean survival, ranging from more than 5 years (low risk group) to 29 months (high risk group)[127]. Characteristic for MCL cells in comparison to untransformed B cells is a decrease of the cell surface molecule CD19 and an increase of CD20[128]. MCL is a very heterogeneous diseases including both indolent and highly aggressive variants where the latter one has been associated with deletions of TP53 (tumor protein 53), a protein acting as a tumor suppressor, reflecting a poorer overall survival[129–132]. In addition, tumor microenvironmental interactions contribute to tumor progression and survival (see Figure 2).

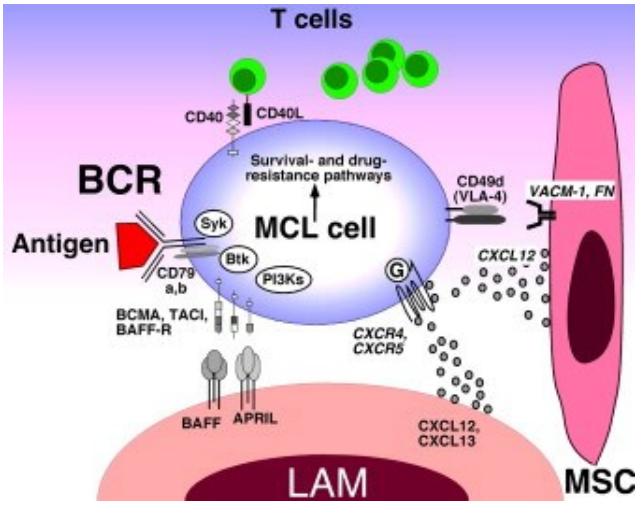


Figure 2. Mantle cell lymphoma (MCL) cells interact with their tumor microenvironment through cellular and molecular interactions. The tumor microenvironment (TME) of MCL cells contains T cells, mesenchymal stromal cells (MSC) and lymphoma-associated macrophages (LAM). They interact with MCL cells in various ways, e.g through direct interaction like CD40L/CD40 (Cluster of differentiation 40 ligand/ Cluster of differentiation 40) or VCAM-1/VLA-4 (vascular cell adhesion molecule-1/ very late antigen-4) or indirect interaction via the secretion of chemokines like CXCL12 which binds to its corresponding receptor CXCR4 expressed by MCL cells. (From: Burger and Ford (2011)[133]. Reprinted with permission from Seminars in Cancer Biology)

The B cell receptor (BCR) expressed by both healthy and malignant B cells plays a key role in cell function, growth, and differentiation. Although the exact role of BCR signaling in MCL is not yet fully understood, it is most likely an autoantigen stimulation of the BCR leading to constitutively active signaling and hence to survival of MCL cells[134,135]. CXCR4 overexpression contributes to disease progression and is associated with poorer outcome[136,137]. Expression levels of CXCR4 on MCL cells were shown to be upregulated by SOX11, a transcriptional regulator protein which is another prognostic marker for MCL aggressiveness and outcome prediction[138]. Elevated CXCR4 expression levels lead to increased cell migration and proliferation, enhanced transmigration and stronger adhesion to

stromal cells which are part of the TME. The latter one is associated with higher drug resistance through protection of MCL cells from drug-induced cytotoxic effects[138,139].
Current therapeutic options for MCL depend on the age of the patients, their health status as well as the line of treatment (first line treatment or after a relapse). They include classical chemotherapeutics like Chlorambucil or Bendamustin, and the use of Rituximab, a monoclonal antibody against CD20. Rituximab is applied either alone or in combination with chemotherapy or other targeting molecules like Ibrutinib or Venetoclax which block the Bruton's tyrosine kinase (BTK) or the B Cell lymphoma 2 (Bcl-2) protein, respectively. In some cases radiotherapy and stem cell transplantations are also considered[120,122].

1.2.1.2 B Cell Chronic Lymphocytic Leukemia

Chronic lymphocytic leukemia (CLL) is one of the most common B cell malignancy leading to an accumulation of neoplastic B cells in the peripheral blood, bone marrow and lymphoid tissue like lymph nodes and spleen[140,141]. A SEER (Surveillance, Epidemiology, and End Result) analysis showed, that CLL has an incidence of almost 6 per 100,000 people. It affects more men than women, independent of their ethnicity, and is mainly diagnosed at an higher age (68-84 years) and with extranodal involvement[141,142]. Although the name may suggest otherwise, the B cell chronic lymphocytic leukemia belongs to the NHL as it is mainly initiated in B cells accumulating in peripheral blood in contrast to the small lymphocytic lymphoma (SLL) which leads to the same disease, but here transformed cells are mainly found in the lymph nodes[143]. CLL B cells (B-CLL) are characterized by high protein expression levels of Bcl-2 and hypomethylation of its promotors as well as the upregulation of surface molecules cluster of differentiation (CD) CD5, CD23, and downregulation of CD19 and CD20[128,144,145].
Being one of more than 40 lymphoproliferative disorders, CLL needs to be clearly distinguishable from other lymphoproliferative disorders. This is assessed by e.g. blood tests and immunophenotyping[146]. However, several additional analyses are required to refine the diagnosis and outcome prediction, e.g. mutation status of the immunoglobulin heavy chain variable region (IgV_H) gene and expression levels of zeta chain of T cell receptor associated protein kinase 70 (ZAP-70), which facilitates BCR signaling. Differences among them lead to a high variation in the clinical course of the disease and survival rates of patients varying from only a few months up to more than 20 years[147–155]. CLL disease progression and tumor cell proliferation and survival rely on the TME which is composed of different cells: CD4+ T cells, natural killer cells (NK cells), nurse-like cells (NLC), bone marrow stromal cells (BMSC), follicular dendritic cells (FDC) and endothelial cells (Figure 3). Cells of the TME

enable the interaction with tumor cells in a direct or indirect way. These interactions lead to increased tumor cells proliferation and decreased apoptosis and facilitates their evasion from the immune system resulting in the progression and therapeutic resistance of CLL[156–164].

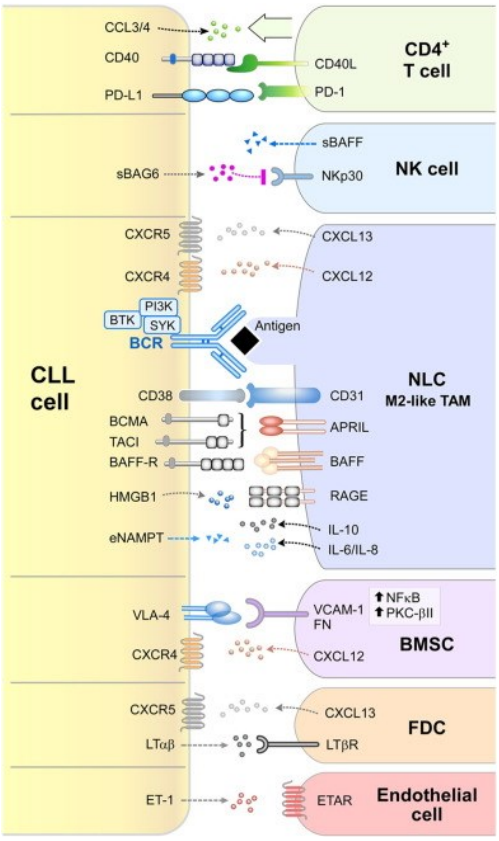


Figure 3. Interaction of chronic lymphocytic leukemia (CLL) cells with the tumor microenvironment. The tumor microenvironment of CLL cells contains T cells expressing the cluster of differentiation 4 (CD4+ T cells), natural killer (NK) cells, nurse-like cells (NLC), bone marrow stromal cells (BMSC), follicular dendritic cells (FDC) and endothelial cells. NLC are tumor associated macrophages (TAM) harboring characteristic features of macrophages subtype M2. Through direct and indirect interactions, CLL cells are capable to escape from the immune system and receive anti-apoptotic and pro-survival signals. Interaction with chemokines like CXCL12 or the C-X-C motif chemokine 13 (CXCL13) released by TME associated cells and direct cell-cell contact with surrounding cells in the TME through e.g. CD40 expressed on CLL cells and CD40L on the surface of CD4+ T cells contribute to tumor progression and chemotherapeutic resistance. (From: ten Hacken and Burger (2015)[165]. Reprinted with permission from BBA).

One of the microenvironmental interactions identified to contribute to disease progression is the CXCL12/CXCR4 axis. Elevated levels of CXCR4 have been determined on CLL cells in comparison to normal B cells[166–168]. CXCL12 is typically secreted by BMSC and NLC present in the TME. Increased expression levels of functional CXCR4 were shown to lead to CXCL12 mediated receptor endocytosis, Ca^{2+} mobilization, actin polymerization as well as cell migration[166,168–171]. Responsiveness of CXCR4 to CXCL12 has been associated with expression levels of ZAP-70, with a higher responsiveness for ZAP-70^{+} cells than for ZAP-70^{-} cells[172]. Expression levels of CXCR4 have been associated with overexpression of intracellular kinases in CLL, namely BTK and PIM (provirus integration site for Moloney murine leukemia virus 1), which is a serine/threonine kinase known to promote cell growth and survival. The inhibition of one of them leads to decreased CXCR4 expression[170,173–176]. Overexpression of CXCR4 has also been linked to the stimulation of the BCR, however CXCL12 mediated cell migration upon BCR stimulation is controversy discussed[177,178]. Additionally, inhibition of BTK has been shown to lead to redistribution of CLL cells from

the spleen and bone marrow to the circulation. This is most likely due to decreased CXCL12/CXCR4 interaction which has been shown to play a crucial role in adherence of CLL to stromal cell and its tropism to the bone marrow[166,175,179]. A protective role for CXCL12/CXCR4 axis has not only been shown in the bone marrow but also for a subset of cells, the so called nurse-like cells, in the blood through their secretion of CXCL12[180].

CLL is generally considered as an uncurable disease. Due to its heterogenicity, not all CLL patients receive treatment at the stage of diagnose, depending on their general health status, the progression of the disease and the international prognostic score for early stage CLL (IPS-E), which includes the mutation status of IgHv (immunoglobulin heavy-chain variable region gene), the amount of lymphocytes and the affected lymph nodes[181]. Classically, treatment options in CLL include chemotherapeutics like Chlorambucil, which was approved by the Food and Drug Administration (FDA) in 1957 and is commonly used in combination with the glucocorticoid prednisone, or nucleoside analogues like fludarabine[140,181–183]. An alternative to classical chemotherapy is the so called chemoimmunotherapy, which is the use of classical chemotherapeutics in combination with targeting monoclonal antibodies like Rituximab or Obinutuzumab[140,181,184]. Combinations of chemotherapeutic or monoclonal antibodies with inhibitors are also promising treatment options. Thereby, inhibitors like ibrutinib and venetoclax which specifically target signaling pathways associated with disease progression like BCR signaling and Bcl-2, respectively, are commonly used[140,181]. In addition, allogenic stem cell transplantation are also considered as possible treatment option[183].

1.3 CXCR4 as therapeutic target in MCL and CLL

Due to its contribution in numerous diseases, CXCR4 became a promising drug target within the last years. So far, several antagonists of CXCR4 have been developed, including small molecule compounds, peptides, and anti-CXCR4 antibodies. They have been shown to have anti-cancer and immunomodulatory properties leading to decreased tumor growth and metastasis and increased infiltration of cytotoxic T cells into the TME as well as reduced infection rates in WHIM patients[185–190]. Although some of them reached clinical trials up to phase III, there is still only one antagonist approved by the FDA so far, which is AMD3100[191,192]. Commercially available as plerixafor, the small bicyclam molecule AMD3100 was initially approved by the FDA in 2008 for the mobilization of HSCs prior autologous stem cell transplantation in patients suffering from multiple myeloma or non-Hodgkin Lymphoma[193]. However, besides its ability to induces the mobilization of HSCs,

AMD3100 was also shown to have anti-cancer properties by reducing tumor growth and metastasis in different types of cancers and is under clinical investigation for the treatment of e.g acute myeloid leukemia[186,187,194]. Potential therapeutic benefit in CLL and MCL patients by blocking CXCL12/CXCR4 interactions has been shown for AMD3100 and anti-CXCR4 antibodies *in vitro*. Treatment of CLL and MCL patients with either of them lead to decreased CXCL12 mediated signaling, cell death of CXCR4 expressing cancer cells, declined tumor burden and hence prolonged survival[139,168,195,196].

Thus, the recently discovered endogenous peptide inhibitor of CXCR4 (EPI-X4) and especially its advanced derivatives are promising drug candidates for the treatment of MCL and CLL.

1.4 The endogenous CXCR4 antagonist EPI-X4

1.4.1 Generation and function of EPI-X4

EPI-X4 was initially discovered during a hemofiltrate library screen as a peptide showing antiviral activity against human immunodeficiency virus 1 (HIV-1). Further characterization showed that EPI-X4 specifically blocks the entry of CXCR4-tropic HIV-1 into target cells. EPI-X4 is an evolutionarily conserved peptide with a molecular weight of 1830 Da and consists of 16 amino acids with the sequence LVRTYTKKVPQVXTPTL corresponding to the amino acids 408-423 of human serum albumin (HSA)[197].

HSA is the most abundant plasma protein in the human body[198–202]. It is produced by the liver under modest regulation by e.g. colloid osmotic pressure or certain hormones and inflammatory cytokines. With a plasma concentration ranging between 3.5-4.5 g/dl HSA represents more than 50% of total plasma protein content[198–201,203,204]. Albumin has a plasma half-life of around 19 days in humans and plays a key role in fluid distribution and generation of oncotic pressure within the human body[198–204]. Besides its function in inhibiting platelet function, it non-specifically binds certain compounds like enzymes and hormones thereby shuttling them to different sites of the human body[198,200–203]. Application of pharmaceutical human serum albumin is approved for the treatment of several diseases like nephrotic syndromes or liver injuries and diseases leading to loss of albumin[198,200–202,205]. Pharmaceutically it is generated from large pools of healthy plasma donors by e.g. cold alcohol fractionation or various column purification methods, followed by heat-sterilization and the addition of certain stabilizers necessary for the reduction of oxidative stress and the limitation of denaturation or aggregation[200,201,205,206].

EPI-X4 is generated from HSA under acidic conditions by aspartic proteases Cathepsin D and E. It can be produced by immature dendritic cells and neutrophils when supplemented with albumin, most likely by Cathepsin D and E which are part of the endo- and lysosomal protein degradation pathway and released by exocytosis during inflammation[197]. Besides its intracellular presence in endosomes and lysosomes, Cathepsin D is also present in extracellular spaces where it has been detected at sites of inflammation. Moreover, cathepsins are secreted by same types of cancer cells[207–210]. This makes it likely, that EPI-X4 can also be generated at those sites. Interestingly, with the exception of human breast milk, EPI-X4 was so far detected in body fluids under acidic conditions were Cathepsin D was found as well – either as precursor or in its mature form[197,211–217].

EPI-X4 is of great therapeutic potential as it directly interacts via its positively charged N-terminal region with the negatively charged minor binding pocket of CXCR4[218]. This interaction inhibits the binding of the CXCR4 antibody clone 12G5 to the extracellular loop 2 and the binding of its natural ligand CXCL12 thereby preventing CXCL12 mediated cellular effects like Ca^{2+} mobilization, receptor internalization, cell migration and invasion[197,210,212,218]. Besides its antagonistic properties, EPI-X4 has inverse agonistic effects on CXCR4 by reducing basal CXCR4 signaling[197]. EPI-X4 leads to cell mobilization of hematopoietic stem cells and neutrophils into the periphery after intraperitoneal injection into mice[197]. Moreover, its therapeutic benefit has been demonstrated in mouse models of airway hypereosinophilia. There, mice were treated intranasally with EPI-X4 prior to the allergen challenge using ovalbumin (OVA). EPI-X4 significantly inhibited the infiltration of immune cells into the lungs in the same range as AMD3100[219,197,212]. Although EPI-X4 has been proven to be safe and non-toxic, it is not the ideal drug candidate as it is only active in the µM range and rapidly degraded by Leucine-aminopeptidases (LAP) leading to an half-life of only approximately 20 min in human plasma[197,212,218,220].

1.4.1.1 Development of optimized EPI-X4 derivatives for therapy

A more active derivative of EPI-X4 is EPI-X4 WSC02 which was generated in a structure activity relationship (SAR) study which includes rational drug design and mutational analysis supported by molecular dynamics and docking stimulation[197]. For the sake of simplicity all EPI-X4 derivatives will be named hereafter without the prologue EPI-X4. WSC02 is a C-terminal truncated variant of EPI-X4 harboring four amino acids substitutions (L1I, Y4W, T5S, Q10C). It has stronger affinity to CXCR4 leading to enhanced antagonistic activities compared to EPI-X4. Like EPI-X4, WSC02 shows no cytotoxic effects in an

embryonic zebrafish model[75,219]. WSC02 was also active in Waldenström's macroglobulinemia *in vitro* and *in vivo*. Pretreatment of MWCL-1 cells, an established cell line of Waldenström's macroglobulinemia, for 30 min prior the injection into mice lead to impaired lymphoma progression. It significantly reduced cell engraftment leading prolonged median overall survival of the mice, while no effect was detected for EPI-X4[75].

A peptide developed in the second generation of optimized EPI-X4 derivatives is JM#21. Its amino acid sequence is based on WSC02 with three additional amino acids substitutions (V2L, K6R and V8L) (Table 2) leading to stronger interactions with the binding pocket of CXCR4 and thus increased antagonistic activity[212,218,219]. Indeed, JM#21 is up to 1420-fold more active than EPI-X4 in inhibiting cell migration and almost 35-fold more active than WSC02 in preventing HIV-1 infection[75,219]. Like EPI-X4 and WSC02, JM#21 has no cytotoxic effects in an embryonic zebrafish model[212,219] what makes it a promising candidate for the treatment of CXCR4 associated diseases. JM#21 has greater therapeutic effects than AMD3100. It has been shown that JM#21 prevents immune cell infiltration into lungs of mice suffering from airway hypereosinophilia. Moreover, JM#21 was shown to reduce the inflammatory score in atopic dermatitis mouse models. However, both, WSCO2 and JM#21 are rapidly degraded in human plasma by LAP leading to half-lives of only 10 min and 6 min, respectively[212,218–220]. Furthermore, JM#21 is rapidly eliminated *in vivo* which makes adequate systemic administration impossible[212].

1.4.1.2 Stability of optimized derivatives

EPI-X4 and its derivatives are exclusively degraded at the N-terminus and thereby lose their activity to interact with CXCR4. The N-terminus of CXCR4 is essential for effective binding of the peptides to CXCR4, and Alb(409-423), a variant lacking the first amino acid of EPI-X4, is considered to be inactive (see Table 2)[197,212,218].

Improved stability of JM#21 has been achieved by protecting the N-terminus from enzymatic degradation[212]. For this, the N-terminus of JM#21 was modified in different ways using unnatural or acetylated amino acid. JM#29 is a 12-mer variant of JM#21 which differs only in the first amino acid from its precursor. The replacement of 1-isoleucine by the unnatural amino acid d-leucin led to enhanced stability in plasma with a remaining activity of 98% and 63% after 2 h and 8 h, respectively, without losing CXCR4 specific antagonistic activity[212].

Binding studies of EPI-X4 with CXCR4 indicated that mainly the first seven amino acids are required for receptor interactions, thus further truncations were introduced to obtain derivatives with only 7 amino acids length[197,218]. To overcome the electrostatic repulsion between the binding pocket of CXCR4 and the C-terminal part of the peptide, the C-terminus

of these variants was modified by amidation[218,221]. This led to an non-toxic and even more stable peptide with almost no degradation after 8 h of incubation in human plasma, named JM#173[212,221]. *In vivo*, small peptides are prone to renal filtration[221–223], and peptides like JM#21 and JM#173 are rapidly eliminated from the blood stream[212,221]. In order to improve circulation half-lives of the peptides, EPI-X4 derivatives were designed, which are conjugated to albumin-linkers like fatty acids. Albumin has not only a relatively long-half life, it is also known to prevent proteins from renal elimination and accumulates in inflamed and cancerous tissue which in theory simplifies the transport of the derivatives to their desired destinations when administered systemically[222,224]. A prolonged half-life after coupling to fatty acids has already been shown for Liraglutide. It is a Glucagon-like peptide-1 (GLP-)1 analogue where the peptide is connected to steric acid via a glutamic acid linker. Through the binding to albumin, the half-life was extended up to 15 hours when administered subcutaneously (s.c.) in comparison to the peptide alone (1.5 h)[225,226]. To increase systemic half-lives, a SAR study was conducted, where EPI-X4 derivatives were coupled to fatty acids of different lengths. The most promising derivatives were JM#143, JM#194 and JM#198, which are coupled to either palmitic acid (C16) or stearic acid (C18) via a glutamic acid linker (Table 2)[212]. JM#143 strongly interacts with human serum albumin thereby being protected from enzymatic degradation by LAP without showing cytotoxic effects *in vitro* or *in vivo*[212]. Compared to JM#21, JM#143 had higher efficacy in an atopic dermatitis mouse model[212]. In addition, JM#143 remained active after circulating *in vivo* with 56% of its initial apparent activity after 2 h and 12% after 4 h, respectively, while JM#21 was fully eliminated after 10 min *in vivo*[212]. Stronger inhibitory effects and increased plasma stability have also been shown for JM#194, which is even more active than JM#143 (Table 2). Whereas between 4 and 8 hours after injection, the residual activity of JM#143 decreased, JM#194 was almost as active at 8 hours *in vivo* as after 4 hours[212]. Currently, the most promising EPI-X4 variant is JM#198, which strongly binds to CXCR4 and antagonizes CXCL12 mediated Erk phosphorylation *in vitro* in the nM range (Table 2). In addition, JM#198 has been shown to have excellent stability *in vitro* and *in vivo*. JM#198 remains completely active after a circulation time of 4 h in mice and is still 33% active after 8 h[212].

Table 2. Overview of the activities of the endogenous peptide inhibitor of C-X-C motif chemokine receptor 4 (EPI-X4) and advanced derivatives thereof used within this study.

Compound	Amino acid sequence	12G5	Human immunodeficiency Virus (HIV)	Phosphorylated Erk (pErk)	References
		50% inhibitory concentration (IC_{50}) [nM] ± SEM			
EPI-X4	LVRYTKKVPQVSTPTL	3167 ± 1416	15315 ± 8842	>100 000	[197,212,218–220]
JM#21	ILRWSRKLPCVS	264 ± 118	81 ± 41	1292 ± 646	[212,218,219,227]
JM#29	(d-L)LRWSRKMPCVS	310 ± 43	159 ± 13	3664 ± 877	[212]
JM#173	(d-I)LRWSRK-NH_2	263 ± 62	555 ± 29	6752 ± 2354	[212]
JM#143	ILRWSR(K-E-Pal)LPCVS	122 ± 32	137 ± 42	438 ± 82	[212]
JM#194	(d-L)MRWSR(K-E-Pal)-NH_2	5 ± 1	3 ± 1	50 ± 21	[212]
JM#198	ILRWSR(K-E-Ste)LPCVS	0.5 ± 0.1	64 ± 26	383 ± 147	[212]
AMD3100		499 ± 288	24 ± 14	2743 ± 1939	[212,219,220,227]
Alb(409-423)	VRYTKKVPQVSTPTL	>100 000			[197]

NH_2 = amidated C-terminus, Pal = palmitic acid, Ste = stearic acid

1.5 Scope of the study

EPI-X4 is a peptide corresponding to the amino acids 408-423 of human serum albumin with antiviral, anti-inflammatory and anti-cancer properties. Since pharmaceutical human serum albumin preparations, generated from healthy donors, are widely used for the therapy of different diseases like liver failure the **first aim** within this study was to clarify if EPI-X4 is present in those preparations thereby causing possible unwarranted effects upon application. Although EPI-X4 is only active in µM ranges, several derivatives of EPI-X4 have been generated so far with enhanced activity and plasma stability. However, their activity has neither been confirmed on human primary cells nor on murine cells. This is an important step in preclinical drug development as cell lines and human primary cells may differ in their morphology and cellular characteristics, leading to differences in CXCR4 expression and subsequent activation upon CXCL12 binding. In addition, differences within the amino acid sequence of CXCR4 between human and mice have been identified which might influence the activity of EPI-X4 and its advanced derivatives and hence the outcome in mouse models which are widely used in preclinical development. Therefore, the **second aim** was to examine whether the activity of EPI-X4 lead derivatives can be transferred to either of those cells. CXCR4 is highly overexpressed on several cancer types among them non-Hodgkin lymphomas. Hence, the **third aim** within this project was to investigate the efficacy of optimized EPI-X4 derivatives on two subtypes of non-Hodgkin lymphomas, namely mantle cell lymphoma and chronic lymphocytic leukemia. Although with the development of JM#198 an EPI-X4 derivative has been designed with improved activity and stability, it is still not suitable for clinical applications. Thus, the **fourth aim** of my thesis was to evaluate

the efficacy of EPI-X4 derivatives designed with further optimization strategies, namely PEGylation and coupling of dicarboxylic acids.

2 Materials and Methods

2.1 Materials

2.1.1 CXCR4 antagonists

2.1.1.1 Commercially available antagonists

The small molecule antagonist AMD3100 (Plerixaflor) was ordered at Sigma Aldrich and dissolved in dH_2O reaching a final concentration of 10 mM.

2.1.1.2 Peptides and peptide conjugates

Synthesized peptides were solved in phosphate buffered saline (PBS) or dimethyl sulfoxide (DMSO) in case of fatty-acid coupled variants reaching a stock concentration of 3 mM.

Table 3. EPI-X4 derivatives used and designed in the study.

Peptide	Amino acid sequence	Molecular weight [Da]
EPI-X4	LVRYTKKVPQVSTPTL	1832
JM#21	ILRWSRKLPCVS	1458
JM#29 M8L	(d-L)LRWSRKLPCVS	1476
JM#173	(d-I)LRWSRK-NH_2	957
JM#143	ILRWSR(K-Glu-Pal)LPCVS	1825
JM#194	(d-L)MRWSR(K-Glu-Pal)-NH_2	1343
JM#198	ILRWSR(K-Glu-Ste)LPCVS	1853
Alb(409-423)	VRYTKKVPQVSTPTL	1717
JM#226	ILRWSRK(-C16diacid)LPCVS	1726
JM#227	ILRWSRK(-Glu-C16diacid)LPCVS	1855
JM#228	ILRWSRK(-C18diacid)LPCVS	1754
JM#229	ILRWSRK(-Glu-C18diacid)LPCVS	1883
JM#230	ILRWSRK(-2xOEG-Glu-C18diacid)LPCVS	2173
JM#244	ILRWSRK(-C16diacid)-NH_2	1227
JM#245	ILRWSRK(-C18diacid)-NH_2	1255
JM#246	ILRWSRK(-Glu-C16diacid)-NH_2	1356
JM#247	ILRWSRK(-Glu-C18diacid)-NH_2	1384
JM#248	(d-L)LRWSRK(-C16diacid)-NH_2	1227
JM#249	(d-L)LRWSRK(-C18diacid)-NH_2	1356
JM#250	(d-L)LRWSRK(-Glu-C16diacid)-NH_2	1354
JM#251	(d-L)LRWSRK(-Glu-C18diacid)-NH_2	1384

NH_2 = amidated C-terminus, Pal = palmitic acid, Ste = stearic acid, Glu = glutamic acid linker, OEG = oligo(ethylene glycol)

Peptide conjugation of JM#29 and JM#173 was performed by the group of A. Zelekin and diluted in distilled water (dH_2O) at a stock concentration of 5mM.

2.1.2 Eukaryotic cells

2.1.2.1 Cell lines

HEK293T	Transformed adherent human embryonic kidney cell line, stably expressing simian virus 40 (SV40) large T-antigen[228]. Cells were obtained from the American Type Culture Collection (ATCC).
TZM-bl	HeLa-derived HIV-reporter cell line, stably expressing human surface receptors CD4 (cluster of differentiation 4), CCR5 (C-C motif chemokine receptor 5) and CXCR4, and *Escherichia coli*-derived β-galactosidase and *firefly luciferase* under transcriptional control of the HIV-1 long terminal repeat (LTR) promotor[229]. Cells were obtained from the National Institutes of Health AIDS Research and Reference Reagent Program (ARRRP).
SupT1	Human T lymphoblast cell line derived from an 8-year-old child with T cell lymphoblastic lymphoma. Cells were obtained from the American Type Culture Collection (ATCC).
Maver-1	Human lymphoblast cell line derived from an 82-year-old male with mantle cell lymphoma (DSMZ), kindly provided by Prof. Stilgenbauer, Ulm University Medical Center
Jeko-1	Human lymphoblast cell line isolated from a 78-year-old female with mantle cell lymphoma (DSMZ), kindly provided by Prof. Stilgenbauer, Ulm University Medical Center
HG-3	Human B cell line established from a 70-year-old man with chronic B cell leukemia (DSMZ), kindly provided by Prof. Stilgenbauer, Ulm University Medical Center
Mec-2	Human B cell line established from a 62-year-old man with chronic B cell leukemia (DSMZ), kindly provided by Prof. Stilgenbauer, Ulm University Medical Center
BW5147	Murine T lymphoblast cell line derived from the thymus of a mouse with lymphoma (ATCC TIB-47™), kindly provided from Hartmut Hengel, Freiburg
300-19	Murine pre-B lymphocytic cell line, kindly provided by Prof. Stilgenbauer, Ulm University Medical Center Ba/F3 IL-3 dependent murine pro B cell line from C3H mouse (DSMZ), kindly provided by Prof. Stilgenbauer, Ulm University Medical Center

A20	Murine B lymphoma cell line derived BALB/cAnN mouse (ATCC), kindly provided by Prof. Stilgenbauer, Ulm University Medical Center

2.1.2.2 Primary cells

CD4+ T cells	CD4+ T cells were isolated from human buffy coats derived from the German Red Cross Blood Donor Service Baden-Württemberg at Ulm University by negative selection as described in 2.2.3.2.1
Mouse splenocytes	Mouse splenocytes from the transgenic T cell leukemia/lymphoma 1A mouse model (Eμ-TCL1 mouse model) were isolated as described in section 2.2.3.2.2

2.1.3 Human blood plasma and serum

All experiments involving human blood were done with informed consent of all human subjects and reviewed and approved by the Institutional Review Board (Ethics Committee of Ulm University). All samples were anonymized before use.

For human plasma, blood from healthy donors was collected in EDTA containing blood collection tubes. Afterwards, tubes were centrifuged at 2,500 x g for 15 min and the plasma phase collected. Plasma from different donors was pooled and immediately aliquoted and stored at -80°C. For human serum, blood was collected in collection tubes containing clot activator and centrifuged for 10 min at 2,000 x g before serum phase was collected. Serum was pooled from different donors and stored as aliquots at -80°C.

2.1.4 Proteins

2.1.4.1 Chemokines

Human IL-2	Miltenyi Biotec
Recombinant human SDF-1α (CXCL12)	Peprotech
Recombinant murine SDF-1α (CXCL12)	Peprotech
Recombinant murine IL-3	Peprotech

2.1.4.2 Enzymes/Proteins

Viral proteins	
HIV-1 p24 protein	Abcam
Enzymes	
Cathepsin D from human liver	Sigma-Aldrich
Recombinant human Cathepsin E	rnd sytems

Trypsin/EDTA	PAN Biotech
Other proteins	
Bovine Serum Albumin	Sigma-Aldrich
Albumin, Human Serum, Non-denaturated	Calbiochem
Albumin Fraktion V, biotin-free	Roth
HSA(409-422) for Matrix	ImmunoGlobe Antikörpertechnik GmbH
HSA(407-424) for Matrix	ImmunoGlobe Antikörpertechnik GmbH

2.1.4.3 Antibodies and Dyes

Antibodies and Dyes for Flow Cytometry

Primary antibodies	
APC mouse anti-human CD184 clone 12G5	BD Bioscience
PE rat anti mouse CD184 antibody	BioLegend
PE rat anti-human CD184 clone 1D9	BD Pharmingen
Phospho-p44/42 MAPK (Erk1/2) (Thr202/Tyr204) (D13.14.4E) rabbit mAb	Cell Signaling
Phospho-p44/42 MAPK (Erk1) (Tyr204)/ (Erk2) (Tyr187) (D1H6G) mouse mAb	Cell Signaling
Phospho-Akt (Ser473) (193H12) Rabbit mAb	Cell Signaling
Isotype controls	
PE rat IgG2b, κ	BioLegend
APC mouse IgG2a, κ	BD Pharmingen
PE rat IgG2a, κ	BD Pharmingen
Rabbit (DA1E) mAb IgG	Cell Signaling
Mouse (E5Y6Q) mAb IgG2a	Cell Signaling
Normal rabbit IgG	Cell Signaling
Secondary antibodies	
Anti-rabbit IgG (H+L), $F(ab')_2$ fragment (Alexa Fluor 647 Conjugate)	Cell Signaling
Goat anti-Mouse IgG (H+L) Cross-Adsorbed Secondary Antibody, Alexa Fluor 488	Invitrogen
Dyes	
LIVE/DEAD™ Fixable Aqua Dead Cell Stain	Invitrogen

Antibodies for the EPI-X4 sandwich ELISA

The antibodies for detecting EPI-X4 were purified as described before[211].

Coating/Capture Antibody	
Rab IG-1185	ImmunoGlobe Antikörpertechnik GmbH
Detection Antibody	
Biotin GP2603#	ELISA Entwicklung
Streptavidin-Poly HRP20	Stereospecific Detection Technologies

Antibodies for the p24 ELISA

Coating antibody	
Monoclonal mouse anti-p24 Antibody (MAK183)	Exbio
Primary antibody	
Rabbit anti-p24 antibody	Eurogentec
Secondary antibody	
Goat anti-Rabbit IgG, Fc-HRP antibody	Dianova

2.1.4.4 Pharmaceutical human serum albumin (HSA) preparations

Albiomin	BIOTEST Pharma
Albunorm	Octapharma
Alburex	CSL Behring
Albutein	Grifols
Humanalbumin	Kedrion Biopharma
Human Albumin	CSL Behring
Human Albumin	TAKEDA
Plasbumin	Grifols

2.1.5 Buffers and Media

2.1.5.1 Buffers

Calcium Chloride Transfection

10x HBS	8.18% (w/v) NaCl, 5.94% (w/v) HEPES, 0.25% (w/v) Na_2HPO_4 x 2 H_2O

2x HBS	10x HBS diluted in H2O at a ratio of 1:5, adjusted to pH 7.12 and sterilized by filtration
2 M $CaCl_2$	Prepared in H_2O and sterilized by filtrations
P24 antigen ELISA	
Wash buffer	0.05% (v/v) Tween®20 in PBS
Blocking buffer	10% FCS (v/v) in PBS
Lysing buffer	1% (v/v) Triton X-100 in dH_2O
Dilution buffer	0.05% (v/v) Triton X-100, 0.05% Tween®20 in PBS
Antibody buffer	10% FCS (v/v), 0.05% (v/v) Tween®20 in PBS
Stop Solution	0.5 M H_2SO_4
EPI-X4 sandwich ELISA	
Buffer for coating antibody	100 mM $NaHCO_3$, 500 mM NaCl, 0.02% (w/v) NaN_3 in dH_2O and adjusted to pH 9.0. Used diluted with 50% (v/v) glycerol
Coating buffer	0.05 M $NaHCO_3$, 0.01% (w/v) NaN_3, 0.03% (w/v) BND D, in dH_2O and adjusted to pH 9.6
5x PBS	0.0405 M Na_2HPO_4*2 H_2O, 0.0075 KH_2PO_4, 0.68 M NaCl, 0.0135 M KCl in dH_2O, adjust to pH 7.1
50x washing buffer	2.5 % (v/v) Tween®20, 0.06% (w/v) BND D in 5x PBS, adjust to pH 7.1.
Assay buffer	0.02 M Na_2HPO_4*2 H_2O, 0.01 M EDTA-Na_2 * 2 H_2O, 0.2% (w/v) Albumin fraction V biotinfree, 0.12 M NaCl, 0.005% (v/v) chlorhexidine digluconate solution, 0.1% (w/v) gelatin hydrolysate, 0.05% (v/v) Tween®20, 0.002% (w/v) phenol red, 0.06% (w/v) BND D in dH2O, adjusted to pH 7.3
Matrix solution	10% (v/v) human serum, 1 mg/ml (w/v) Albumin Fraction V biotin free, 100 ng/ml (w/v) HSA(409-422), 100 ng/ml (w/v) HSA(407-424) in assay buffer
TMB substrate	TMB Super Sensitive One Component HRP Substrate
Stop Solution	0.5 M H_2SO_4
Flow cytometry	
FACS buffer	1% (v/v) FCS in PBS
Fixation buffer	2% (v/v) PFA in PBS

2.1.5.2 Cell culture media

SupT1 medium	RPMI (Roswell Park Memorial Institute) -1640 supplemented with 10% (v/v) heat-inactivated fetal calf serum, 2 mM L-glutamine, 100 units/ml penicillin, 100 µg/ml streptomycin and 10 mM HEPES (4-(2-hydroxyethyl)-1-piperazineethanesulfonic acid)).
Mec-2 medium	RPMI-1640 supplemented with 10% (v/v) heat-inactivated fetal calf serum, 2 mM L-glutamine, 100 units/ml penicillin and 100 µg/ml streptomycin
HG-3 medium	RPMI-1640 supplemented with 10% (v/v) heat-inactivated fetal calf serum, 2 mM L-glutamine, 100 units/ml penicillin and 100 µg/ml streptomycin
Maver-1 medium	RPMI-1640 supplemented with 20% (v/v) heat-inactivated fetal calf serum, 2 mM L-glutamine, 100 units/ml penicillin and 100 µg/ml streptomycin
Jeko-1 medium	RPMI-1640 supplemented with 20% (v/v) heat-inactivated fetal calf serum, 2 mM L-glutamine, 100 units/ml penicillin and 100 µg/ml streptomycin
300-19 medium	RPMI-1640 supplemented with 10% (v/v) heat-inactivated fetal calf serum, 2 mM L-glutamine, 100 units/ml penicillin, 100 µg/ml streptomycin, 1x non-essential amino acids and 50 µM β-mercaptoethanol
A20 medium	RPMI-1640 supplemented with 10% (v/v) heat-inactivated fetal calf serum, 100 units/ml penicillin, and 100 µg/ml streptomycin and 50 µM β-mercaptoethanol
Ba/F3 medium	RPMI-1640 supplemented with 10% (v/v) heat-inactivated fetal calf serum, 100 units/ml penicillin, and 100 µg/ml streptomycin and 10 ng/ml murine interleukin 3 (IL-3).
BW5147 medium	RPMI-1640 supplemented with 10% (v/v) heat-inactivated fetal calf serum, 1 mM sodium pyruvate, 100 units/ml penicillin, 100 µg/ml streptomycin and 50 µM β-mercaptoethanol
Migration medium	RPMI-1640 supplemented with 2 mM L-glutamine, 100 units/ml penicillin, and 100 µg/ml streptomycin and 0.1% (w/v) bovine serum albumin (BSA).

Starvation medium	RPMI-1640 supplemented with 1% (v/v) heat-inactivated fetal calf serum (FCS), 2 mM L-glutamine, 100 untis/ml penicillin, and 100 µg/ml streptomycin and 10 mM HEPES

2.1.6 Reagents and Kits

2-Mercaptoethanol 1000x	Gibco
5-Bromo-5-nitro-1,3-dioxane (BND D)	Stereospecific Detection Technologies
ACK Lysing Buffer (1x)	Lonza
BioFX® TMB Super Sensitive One Component HRP Microwell Substrate	Surmodics
Calcium Chloride ($CaCl_2$)	Sigma-Aldrich
CellTiter-Glo® Luminescence Cell Viability assay	Promega
Chlorhexidine digluconate solution	MP Biomedicals
CytoFlex Sheat Fluid	Beckman-Coulter
Dimethyl sulfoxide (DMSO)	Merck KGaA
di-Sodium hydrogen phosphate dihydrate ($Na_2HPO_4*2H_2O$)	Merck KGaA
Dubelcco's Modified Eagle Medium (DMEM)	Gibco
Dubelcco's Phosphate Buffered Saline (DPBS)	Gibco
Dynabeads^{TM} Human T-Activator CD3/CD28	Gibco
Ethylene**d**iamine **t**etraacetic **a**cid disodium dihydrate (EDTA-Na_2*2 H_2O)	Roth
Fetal Bovine Serum	Gibco
Formaldehyde 36% (39% w/v)	VWR chemicals
Gal-Screen™ β-Galactosidase Reporter Gene Assay System for Mammalian Cells	Thermo Fisher Scientific
Gelatin hydrolysate	MP Biomedicals
Glycerol	Sigma-Aldrich
HEPES ($C_8H_{18}N_2O_4S$)	Sigma-Aldrich
HEPES Buffer Solution (1M)	Gibco
Hydrochloric acid (HCl)	Merck KGaA
Isopropanol (70%)	Pharmacy of Ulm University Medical Center

L-Glutamine 200 mM	PAN Biotech
Magnesium Chloride ($MgCl_2$)	Sigma-Aldrich
MEM NEAA (100x)	Gibco
Methanol	Sigma-Aldrich
Mouse C57BL6 plasma NaEDTA	Innovative Research
Mycoplasma Test Kit PCR	Applichem
Pancoll human	PAN Biotech
Penicillin-Streptomycin	PAN Biotech
Phenol red	Merck KGaA
Potassium chloride (KCl)	Sigma-Aldrich
Potassium dihydrogen phosphate (KH_2PO_4)	Roth
RosetteSep Human CD4+ Enrichtment	Stemcell
Roswell Park Memorial Institute medium (RPMI Medium 1640)	Gibco
Sodium azide (NaN_3)	Sigma-Aldrich
Sodium Chloride (NaCl)	Merck KGaA
Sodium hydrogencarbonate ($NaHCO_3$)	Sigma-Aldrich
Sodium hydroxide solution (NaOH)	Merck KGaA
Sodium Pyruvate 100 mM (100x)	Gibco
Sulfuric acid (H_2SO_4)	Merck KGaA
Triton X-100	Sigma-Aldrich
Tween® 20	Sigma-Aldrich
Water HPLC Gradient grade	Fisher Chemicals

2.1.7 Consumables

Aluminium foil	Paclan
C-Fold Hand Towel	Tork
Combitips advanced	Eppendorf
Cryo Tubes	Sarstedt
Disposal bag	Sarstedt
ELISA plate, high binding	Sarstedt
Filtropur S 9.45	Sarstedt
Gloves	VWR

HTS-Transwell® 96 permable support with 5.0 µm pore, polycarbonate membrane	Corning
Kimtech Wipes	Kimberly Clark Professional
Luna™ Cell Counting Slides	Logos biosystems
MultiScreen™ MIC 5.0 µm Polycarbonate	Millipore
Reaction tubes (1.5 ml, 2 ml)	Eppendorf
Sealing Tape Sterile	Thermo Scientific
Serological pipettes (5 ml, 10 ml, 25 ml, 50 ml)	Sarstedt
S-Monovette® 7.5 ml K3E	Sarstedt
S-Monovette® 8.5 ml Z-Gel	Sarstedt
Tissue Culture Flasks (T25, T75, T175)	Sarstedt
Tissue Culture plates (6-well, 96-well)	Sarstedt
Trypan blue (0.4%)	Invitrogen
Tubes (15 ml, 50 ml)	Sarstedt

2.1.8 Technical equipment

Centrifuge 5810 R	Eppendorf
Centry™ 103 Minicentrifuge	Gilson
CytoFLEX flow cytometer	Beckman coulter
Explorer™ Semi-Micro Balance	Ohaus
Forma Steri-Cult CO_2 Incubator	Thermo Scientific
HERAfreeze™ Ultra-Low Freezer	Thermo Scientific
Herasafe™ KSP laminar flow hood	Thermo Scientific
Leica Mikroskop DMi1	Leica microsystems
Luna II™ Automated Cell Counter	Logos biosystems
Microplate Shaker	VWR
Mini Vortexter	Gilson
Multipette® M4	Eppendorf
Orion II Microplate Luminometer	Titertek Berthold
pH Meter SevenCompact	Mettler Toledo
Pipetman™ (P1000, P200, P20, P2)	Gilson™
Pipetus®	Hirschmann
Scout™ Portable Balance	Ohaus

ThermoMixer C	Eppendorf
Transferpette	Brand
VERSA max microplate reader	Molecular Devices
Vortex-Genie® 2	Scientific Industries

2.1.9 Software

BioRender	BioRender Multimedia and Design Software
CytExpert	Beckman coulter
FlowLogic	Inivai Technologies Pty. Ltd.
GraphPad Prism	GraphPad Software
Microsoft Office	Microsoft
Simplicity 4.02	Titertek Berthold
Softmax Pro™	Molecular Devices

2.2 Methods

2.2.1 Peptide synthesis

Peptides

EPI-X4 and its advanced derivatives were either synthesized by the Ulm Peptide Pharmaceutical (UPEP) core facility as described before[219] or ordered at KE biochem and quality controlled by the UPEP. Peptides were dissolved prior to use either in PBS or DMSO in case of fatty acid coupled variants.

Peptide-conjugates

Bioconjugation of JM#29 and JM#173 was performed by the group of Prof. Zelekin, Medical Polymer Chemistry Lab at Aarhus University, Denmark as described before[221]. Briefly, peptides were conjugated to polyethylene glycol (PEG) either via maleimide-cysteine coupling (monovalent and divalent telechelic variant) or through bis-sulfone cysteine coupling (Y-shaped dimer). For maleimide mono-conjugation, native peptides were mixed with monovalent maleimide reagent and incubated for 24-72 hours. Maleimide di-conjugation was performed by mixing diMal-PEG_{20kDa} with native peptide and mixture was incubated for 24 hours. Bis-sulfone conjugation was done by mixing native peptide with bis-alkylating reagent for 48-72 hours. All mixtures were purified by gel filtration and presence of peptide-conjugates analyzed using visible ultraviolet (UV-Vis) spectroscopy (280 nm) before peptide-conjugates were lyophilized. All peptide conjugates were dissolved in dH_2O prior to use.

2.2.2 EPI-X4

2.2.2.1 EPI-X4 specific enzyme-linked immunosorbent assay (ELISA)

Detection of EPI-X4 was performed by using a specific sandwich ELISA as described before[211] with minor modifications. Short, ELISA plates were coated with coating antibody at a concentration of 0.1 µg/ml in coating buffer. After one night at 4°C, plates were blocked for 1 hour at room temperature using washing buffer. Thereafter, plates were washed 5 times with washing buffer before freshly prepared matrix solution (50 µl/well) was applied. Next, analytes of concern, either pure or serially diluted 1:10 in assay buffer beforehand, were added (50 µl/well) as well as synthetic HSA(408-423) diluted in assay buffer reaching different concentration (as standard) using the same volume. Finally, 50 µl/well of biotin labeled antibody against the C-terminal domain was applied, too, and plates were incubated for 2 hours at room temperature under constant shaking (450 rpm). Afterwards, plates were washed 3 times with washing buffer before streptavidin labeled horseradish peroxidase

(HRP) was added to each well (100 µl/well of a 200 ng/ml solution prepared in assay buffer) and incubated for further 30 min using the same conditions. Next, plates were washed again 5 times using washing buffer before TMB substrate was applied (100 µl/well) and plates incubated for further 20 min at room temperature and 350 rpm. Reaction was stopped by adding H_2SO_4 as stop solution and optical densities were recorded within the next 10 min at 450/650 nm wavelength using an ELISA reader. Based on known concentrations of HSA(408-423) carried along as standard, standard curves were created on which the sample values were interpolated.

2.2.3 Eukaryotic cells

2.2.3.1 Handling cell lines

All cells were cultured at 37°C in a 5% carbon dioxide (CO_2) humidified incubator in T75 or T175 cell culture flasks. Cells were grown in their respective media as defined in section 2.1.2.1.

Cell lines were routinely tested by our technicians Daniela Krnavek and Nicola Schrott for mycoplasma contamination using a Mycoplasma Test Kit polymerase chain reaction (PCR).

2.2.3.2 Primary cells

2.2.3.2.1 Isolation of human primary CD4+ T cells

Human primary CD4+ T cells were isolated from lymphocyte concentrates (buffy coats) obtained from the German Red Cross Blood Donor Service Baden-Württemberg at Ulm University. For this, buffy coats were mixed with RosetteSep Human CD4+ T cell enrichment Cocktail (50 µl per 1 ml buffy coat) and incubated for 20 min at room temperature before diluted with PBS at a ratio of 1:1. Afterwards, blood/PBS mixture was carefully layed on top of prewarmed Ficoll using the same volume ratio before centrifugated at 1200 x g for 20 min (acceleration 5, no brake). Thereafter, CD4+ T cells present in the interphase between plasma an Ficoll were collected and washed once with PBS reaching a final volume of 50 ml. Supernatant was removed after centrifugation at 1300 rpm for 5 min (acceleration 9, brake 9) and remaining erythrocytes were destroyed by resuspension the cell pellet in 5 ml Ammonium-Chloride-Potassium (ACK) Lysing buffer. After 5 min incubation at room temperature, cells were washed once again with PBS as described above, before remaining cells were cultured in SupT1 growth media supplemented with 10 ng/ml IL-2 and 12.5 µl CD3/CD28 beads per 1 * 10^6 cells reaching a final concentration of 1.5 * 10^6 cells/ml for three days.

2.2.3.2.2 Isolation of splenocytes from Eμ TCL-1 mouse model.

Spleens of Eμ-TCL1 mice were dissected by members of the group of Prof. Stilgenbauer, Ulm University Medical Center, as described in section 2.2.8.2. For the extraction of mononuclear cells out of murine spleen, spleens are cutted and filled up with PBS reaching a final volume of 30 ml. Afterwards, 5 ml cell suspension are carefully layed over 5 ml BioColl in a 15 ml falcon and centrifuged at 2800 rpm with acceleration 5 and brake 1 for 20 min at 4°C. Afterwards, interphase is collected into a new 50 ml falcon and filled up with PBS to 50 ml final volume in a ratio of 1:1 and centrifuged or 5 min at 4°C with 1200 rpm, acceleration 9 and brake 9. Supernatant is carefully removed, and cell pellet resuspended in PBS and filled up with it to 30 ml. Afterwards, cells are diluted with PBS in a ratio of 1:6 (100 µl cell suspension + 500 µl PBS) and cells are count using Vi-CELL XR. Next, cells are centrifugated again for 5 min at 4°C (1200 rpm, acceleration 9, brake 9) and resuspend in freezing medium (90% FCS + 10% DMSO) reaching a final concentration of approximately $50*10^6$ per ml and kept at liquid nitrogen until further use.

2.2.3.3 Viability assays

To determine cell toxicity of newly developed EPI-X4 derivatives, 50,000 SupT1 cells were treated with different concentrations of them for 24 hours at 37°C, 5% CO_2. Afterwards, cells were washed once with PBS before 50 µl of LIVE/DEAD™ Fixable Aqua Dead Cell Stain (1:1,000 diluted in PBS) were applied for 10 min at room temperature protected from light. Cells were washed 3 times with FACS buffer (1% FCS in PBS) before fixed using 2% PFA (paraformaldehyde) in PBS. Fixation process was carried out for 10 min at 4°C protected from light. Fixation solution was removed, and cells resuspend in FACS buffer before analyzed using flow cytometry. Discrimination of living cells and dead cells was carried out using side scatter area (SSC-A) and respective fluorescence of the used stain.

2.2.3.4 Calcium phosphate transfection of 293T cells

The day before transfection, 700,000 HEK293T cells were seeded in 6 well plates. The next day, medium was replaced with 2 ml of growth medium. Meanwhile, 5 µg of desoxyribonucleic acid (DNA) was mixed with 2 M $CaCl_2$ (13 µl) and filled up with dH_2O reaching a final volume of 100 µl. Next, 100 µl 2x HBS was added dropwise. Afterwards, mixture was vortexed carefully before added dropwise to the cells. After an incubation time of 8-16 hours, medium was replaced.

2.2.4 Virology methods

2.2.4.1 Generation of virus stocks

HIV-1 virus stocks were kindly generated by Daniela Krnavek, Institute of Molecular Virology, Ulm University Medical Center. Generally, infectious virus stocks are produced in HEK293T cells by transfecting them with proviral DNA using the calcium phosphate transfection method as described above. Two days after, virus stocks were harvested by collecting the supernatant which was centrifuged for 3 min at 1,300 rpm to remove cell debris. Afterwards, aliquots of virus containing supernatant were prepared and stored at -80°C until further use.

2.2.4.2 HIV-1 p24 antigen ELISA

Quantification of virus stocks was done by Daniela Krnavek, Institute of Molecular Virology, Ulm University Medical Center. This is done by performing an antigen ELISA to detect HIV-1 p24 capsid antigen. Therefore, monoclonal anti-p24 antibody MAK183 was diluted in PBS and used as coating antibody on 96-well flat-bottom absorption microplates (50 ng/well). After an overnight incubation at room temperature in a humidified chamber, plates were washed and blocked for 2 hours at 37°C using 150 µl blocking solution. Meanwhile, HIV-1 samples were lysed with 1% (v/v) Triton X-100 and serially diluted before added to the washed plates. HIV-1 p24 antigen protein was serially diluted (2-fold) starting at a concentration of 12.5 ng/ml and used as standard. Samples and standard were incubated overnight. The day after, plates were washed and rabbit anti-p24 antibody was diluted in antibody buffer (1:1,000 dilution) and added to the washed plates (100 µl/well). After an incubation at 37°C for 1 hours, plates were washed again before TMB substrate was applied to each well (100 µl/well). The reaction was stopped after an incubation for 20 min at room temperature at 450 rpm by the addition of 100 µl 0.5 M H_2SO_4. Absorbance was measured at 450 nm and baseline corrected at 650 nm using Versa max microplate reader. Virus stocks were quantified by interpolating the measured absorption from the standard curve.

2.2.4.3 HIV-1 infectivity assay using TZM-bl cells.

To determine the anti-HIV-1 activity of advanced EPI-X4 derivatives, HIV-1 infectivity assays were performed using TZM-bl reporter cells. For this, 10 000 cells/well in 100 µl growth medium were seeded into 96-well flat-bottom plates and incubated overnight at 37°C, 5% CO_2. The next day, media was exchanged to infection media (70 µl/well) and cells were incubated with 10 µl of serially diluted peptides and controls for 10 min at 37°C, 5% CO_2 before inoculated with virus diluted 1:50 in infection media (20 µl/well). Three days

post infection (dpi) infection was determined by β-galactosidase assay. Therefore, media was removed and 40 µl/well Gal-Screen substrate/buffer A (diluted 1:8 in PBS) was added and incubated for 30 min at room temperature whereby cells were lysed, and the substrate is converted by the released β-galactosidase of infected cells leading to the release of luminescence. Afterwards, 35 µl of each well was transferred to white 96-well plates luminescence is measured as relative light units per second (RLU/s) using the Orion II Microplate Luminometer. Values were background subtracted (uninfected cells) and normalized to infected cells treated with PBS only which was set as 100% infection.

2.2.5 Antibody competition assay

Determination of binding efficacy of CXCR4 ligands is based on a competition with fluorescently labelled anti-CXCR4 antibody (clone 12G5) as described before. The used antibody clone interacts with the extracellular loop ECL2 of CXCR4 nearby the orthosteric binding pocket. This interaction is blocked by compounds binding to this region and dependent on the CXCR4 ligand regarding their concentrations and affinity towards CXCR4. Therefore, cells of interest were resuspended in FACS buffer (PBS+1% FCS) at a concentration of $0.5*10^6$ cells/ml and 100 µl per well were seeded into a 96-well V-bottom microtiter plates. After removing buffer, cells were precooled at 4°C for 20 min. Meanwhile, ligands of interest were serially prediluted in pre-cooled PBS and CXCR4 antibody 12G5 coupled to the fluurophore APC (Allophycocyanin) was prediluted in FACS buffer reaching a final concentration of 0.49 nM. Binding competition was initiated by the addition of 15 µl diluted compound and immediately afterwards 15 µl antibody to the cells. In case of plasma samples involved, mixture was carefully mixed after cell addition. After an incubation of 2h at 4°C protected from light, unbound antibody was removed by 2 washing steps using FACS buffer before cells were resuspended in 100 µl 2% PFA for fixation. Mean fluorescence intensity of cell-bound antibody was analyzed using FACS CytoFLEX. For further calculations, MFI values of isotype controls were subtracted and normalized to the control wells containing only PBS and 12G5 antibody. 50% inhibitory concentration (IC_{50}) values were calculated using the non-linear regression model in GraphPad Prism.

2.2.6 Cell signaling assays.

2.2.6.1 Akt and Erk phosphorylation

To investigate the known downstream effect of CXCL12/CXCR4 interaction, namely the phosphorylation of intracellular Akt and Erk, cells of interest were stimulated in the presence of absence of CXCR4 ligands with CXCL12 before stained with antibodies for

phosphorylated Akt (pAkt) and phosphorylated Erk (pErk) and analyzed via flow cytometry. Therefor, 100 000 cells of interest in 100 µl starvation medium were seeded per well into a 96-well V-bottom microtiter plate and incubated for 2 h at 37°C, 5% CO_2. For determination of CXCL12 induced effects, cells were stimulated with 5 µl CXCL12 (100 ng/ml final concentration) for different time frames (30 min, 15 min, 5 min, 2 min and 0 min). Inhibitory effects of CXCR4 compounds were ascertained by pretreatment of the cells with compounds of interest in different concentrations before stimulated with CXCL12 (100 ng/ml final concentration). Reactions were stopped with 20% PFA and incubated at 4°C for at least 15 min. Afterwards, cells were permeabilized with ice cold methanol (100 µl/well) for 10 min at 4°C. Methanol was removed, cells were washed once with FACS buffer before 30 µl/well primary antibody were added for 1 hour at 4°C to detect pAkt and pErk. After washing the cells twice with FACS buffer to get rid of unbound primary antibodies respective secondary antibodies were added (30 µl/well) and incubated for 30 min at 4°C protected from light. Cells were washed again twice with FACS buffer and fixed in 2%PFA before analyzed by flow cytometry. Changes of pAkt and pErk levels were determined by subtraction mean fluorescence intensity (MFI) values of the respective isotype controls before normalized to the unstimulated PBS control.

2.2.6.2 Cell migration

Induction of cell migration by CXCL12 was analyzed by the boyden chamber assay using 96-well transwell migration plates with 5 µm polycarbonate membrane. For this, 75 000 cells of interest were seeded in migration medium into the upper chamber of the transwell system with or without CXCR4 inhibiting compounds reaching a final volume of 50 µl. Cells were allowed to settle down for around 15 min. Meanwhile, 96-well V-bottom microtiter plates which were used as lower chamber were filled with 200 µl migration medium with or without 100 ng/ml CXCL12 and different concentrations of CXCR4 inhibiting compounds of interest. In case of migration plates from Sigma Aldrich, lower chamber of the transwell system was used whereby a final volume of 170 µl of Media supplemented with or without 100 ng/ml CXCL12 and compounds of interest as described above. Afterwards, upper and lower chamber were carefully combined and incubated for 4 h at 37°C, 5% CO_2. Relative cell migration was analyzed using Cell-Titer Glo assay. For this, upper chamber was removed, and lower chamber was centrifuged at 1300 rpm for 3 min before media was displaced with 100 µl/well CellTiter-Glo reagent (1:2 diluted in PBS) and incubated for 10 min at RT protected from light. Relative Light Units per second (RLU/s) of each well was determined using an Orion II Microplate Luminometer. Relative migration was then

determined after subtraction of unspecific migration (cells migrated in the absence of CXCL12) and normalization, first to the input control (seeded cells directly added to the lower chamber) and second to the CXCL12 only control.

2.2.7 Enzymatic stability

2.2.7.1 Microtiter based stability determination.

Plasma stability of compounds was determined by spiking the compounds into plasma obtained from humans, mice and hen's egg test – chorionallantoic membrane (HET-CAM) models, respectively, reaching a final concentration of 20 µM if not otherwise mentioned. First samples, corresponding to t = 0 minutes were taken immediately and frozen at -80°C. Remaining mixture were incubated at 37°C, 350 rpm. At timepoints of interest, further samples were taken and stored at -80°C as well. Remaining functional activity of samples were determined using antibody competition assay was performed as described in section 2.2.5. Note, highest plasma concentration of cells was 50% due to the 1:2 dilution with 12G5-APC antibody.

2.2.8 Animal experiments and animal replacement experiments

2.2.8.1 Pharmacodynamic studies

Mice for pharmacodynamic studies

Mouse experiments were performed by Gordon Winter and Jessica Löffler, Department of Nuclear Medicine, Ulm University Medical Center in compliance with the Directive 2010/63/EU. All experiments were approved by the regulatory authority of the state of Baden-Württemberg (Registration No. 1375) and in accordance with German animal protection laws. Peptides of interest were solved in DMSO or PBS as described in section 2.1.1.2 and diluted in 0.9% NaCl (sodium chloride) reaching a final concentration of 700 µg/ml or 7 mg/ml. 100 µl were injected into the tail vein of C57BL6 mice (700 µg/ml stock solution) or SCID mice (7 mg/ml stock solution). After 4 hours, mice were sacrificed by cervical dislocation and blood obtained by heart punctation. Collected blood was diluted with 0.16 M NaEDTA (sodium ethylenediaminetetraacetic acid) in a ratio of 19:1 and centrifuged at 2000 x g for 20 min at 4°C and obtained plasma was stored at -80°C until further analysis.

Chicken embryos for pharmacodynamic studies

Chicken egg handling and peptide injections were done by Gordon Winter and Jessica Löffler, Department of Nuclear Medicine, Ulm University Medical Center. Chicken eggs were obtained from Lohmann Süd at embryonic development day (EDD) 0 and incubated at

37.8°C, 63% humidity under constant agitation (3 min every 2 hours). The eggshell was carefully opened at EDD 2 and eggs further incubated at 37.8°C and 63% humidity either until EDD 14 for blood donation or until EDD 15/16 for peptide injection. Peptides of interest were dissolved either in NaCl (JM#21) or DMSO (JM#198) and further diluted in 0.9% NaCl reaching a final stock concentration of 700 µg/ml. 100 µl of stock solution was then injected into a prominent vessel of the chorioallantoic membrane (CAM) and incubated for indicated time points. Blood was obtained from a prominent vessel of the CAM and diluted with 0.16 M NaEDTA in a ratio of 19:1. After centrifugation at 2000 x g for 20 min at 4°C plasma was obtained and stored at -80°C for further analysis. Chicken eggs were sacrificed afterwards by cervical dislocation.

2.2.8.2 Experiments involving Eµ-TCL1 mouse model.

Animal experiments involving the Eµ-TCL1 mouse model were performed by members of the group of Prof. Stilgenbauer, Ulm University Medical Center in accordance with the approval from the institutional animal welfare committee and regulations of the Government of Baden-Württemberg/Regional Council of Tübingen (Registration No. 1124 and 1128). Therefore, splenocytes derived from leukemic Eµ-TCL1 mice were propagated in immunocompetent female C57BL6/J (Charles River) recipient mice. This was done by injecting 20 million mononuclear cells into the tail vein of recipient mice. The animals were euthanized at a human endpoint based on disease severity, changes in mobility, and signs of suffering in accordance with the institutional animal welfare committee.

Dissection of Eµ-TCL1 mice

Dissection of Eµ-TCL1 mice were performed by members of the group of Prof. Stilgenbauer, Ulm University Medical Center. Mice were placed into the euthanasia chamber which will be filled afterwards with CO_2. After 3 min of CO_2 inhalation, mice were taken out of the chamber and checked for interdigital reflex. Euthanized mice were sprayed with 70% ethanol and fixed on the dissection board before cervical dislocation is performed and mice are dissected to remove the spleen. The spleens are further processed aseptically as described in section 2.2.3.2.2

2.2.9 Statistical analyses

Statistical analysis was performed in GraphPad Prism (version 8.3.0). IC_{50} values were determined by non-linear regression. For half-life calculations, the area under the curves (AUC) for each time point were calculated and activities were then determined ((AUC (t = 0) / AUC (t)) x 100) for each time point and half-lives determined using the One-Phase-

Decay model. Differences between groups were tested for statistical significance as indicated in the respective figure legends.

3 Results

3.1 EPI-X4 is absent in pharmaceutical HSA preparations.

Human serum albumin (HSA) is the most abundant protein in the human plasma and is involved in many physiological processes like the inhibition of platelet aggregation as well as the transport of several cytokines, hormones and waste products[198–203]. Pharmaceutical preparations of human serum albumin have long been approved for the treatment of several diseases including liver injuries which are associated with the loss of body-own serum albumin[198,200–202,205]. Since it has been shown, that EPI-X4 can enzymatically be generated from human albumin under acidic conditions[197], I first focused on the question if EPI-X4 is present in pharmaceutical HSA preparations. Pharmaceutical HSA preparations are generated from pooled human plasma by different purification methods under different conditions ranging from a pH of 4.5 (acidic) to a pH of 7.2 (neutral) and the use of different stabilizers which might result in EPI-X4 generation during preparation or storage[198,200,206]. For this, eight different commercially available HSA preparations (listed in Table 4) were analyzed for the presence of EPI-X4 by using a specific sandwich-ELISA. All of them were serially diluted and applied to plates coated with an EPI-X4 antibody binding to the N-terminus of the peptide before incubation with an antibody specific for the EPI-X4 C-terminus and detected with an HRP-conjugated secondary antibody as described before[211]. Concentrations of EPI-X4 were determined by interpolation of the obtained values against a standard curve of synthetic EPI-X4. However, EPI-X4 was not detected in any of the tested pharmaceutical HSA preparations at neutral pH (Figure 4, pH 7).

Since it has been shown that EPI-X4 can generated by acidification of human plasma[197], I next tested whether the acidification of pharmaceutical HSA leads to the release of EPI-X4. For this, four of the previously tested pharmaceutical HSA preparations were acidified to pH 4 and incubated at 37°C for 4 h before applied to the EPI-X4-specific sandwich ELISA. EPI-X4 was not detected in any of the acidified preparations (Figure 4, pH 4 left). Only the addition of Cathepsin D and E to acidified pharmaceutical HSA preparations (Figure 4, pH 4 right) led to the generation of detectable concentrations of EPI-X4 (51-54 µg/ml) with no significant differences between the tested preparations (Figure 4, Table 4). Considering the molecular weights of albumin (66.5kDa) and EPI-X4 (1.83 kDa) and the concentration of albumin used within this study (4 mg/ml), a complete digestion would lead to theoretical EPI-X4 concentrations of approximately 110 µg/ml. Thus, in all HSA preparations the

addition of Cathepsin D and E lead to the degradation of approximately half the albumin regardless of the presence of different stabilizers.

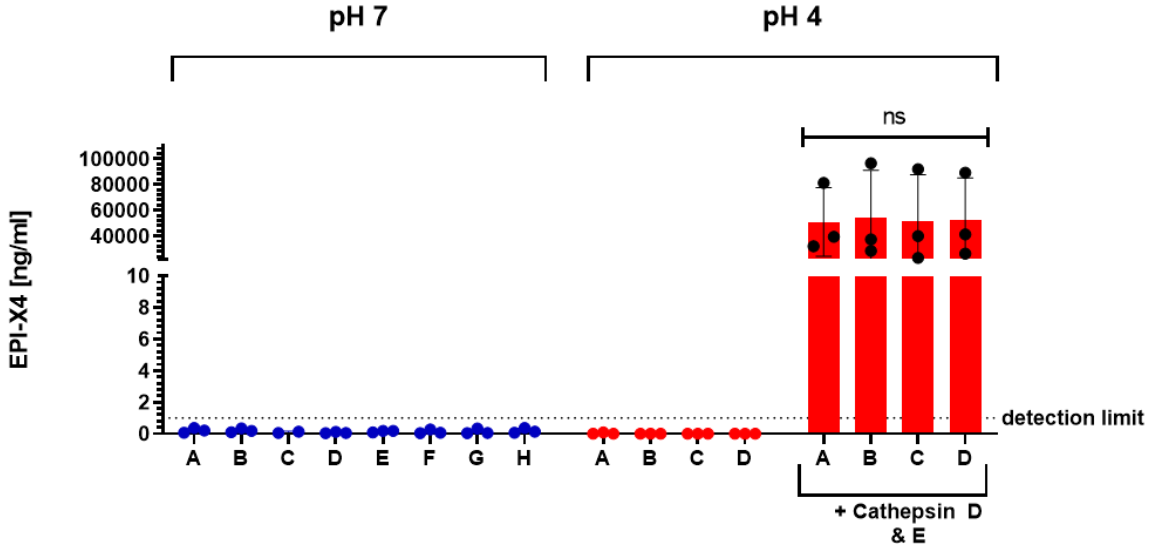


Figure 4. The endogenous peptide inhibitor of the CXCR4 (EPI-X4) can be generated in pharmaceutical human serum albumin (HSA) preparations in the presence of Cathepsin D and E under specific conditions. Naïve pharmaceutical HSA preparations (pH 7) were analyzed for the presence of EPI-X4 using a specific sandwich enzyme-linked immunosorbent assay (ELISA)[211]. Pharmaceutical HSA preparations were acidified to pH 4 reaching a final concentration of 4 mg/ml with (right) or without (left) the addition of Cathepsin D & E and incubated for 4 h at 37°C before applied to the ELISA. Optical densities (ODs) were detected and EPI-X4 concentrations interpolated from a standard curve of synthetic EPI-X4. Shown data represent means from n=3 individual experiments ± SD. Dotted line indicates the detection limit of 1 ng/ml. Statistical analysis was done using a 2way ANOVA with Turkey's multiple comparisons test; ns=not significant). Modified from Gilg *et al* (2021)[230] (CC BY 4.0, https://creativecommons.org/licenses/by/4.0).

Table 4. Pharmaceutical human serum albumin (HSA) preparations used in this study.

Code	Product	HSA concentration	Supplier	EPI-X4 concentration [µg/ml][a]		
				pH 7	pH 4	pH 4+ Cathepsin D+E
A	Albutein	200 g/l	Grifols	<detection limit.	<detection limit.	51 ± 15
B	Plasbumin	200 g/l	Grifols	<detection limit.	<detection limit.	54 ± 21
C	Human Albumin	200 g/l	CSL Behring	<detection limit.	<detection limit.	52 ± 21
D	Albiomin	200 g/l	BIOTEST Pharma	<detection limit.	<detection limit.	52 ± 19
E	Albunorm	200 g/l	Octapharma	<detection limit.	n.d.	n.d.
F	Humanalbumin	200 g/l	Kedrion Biopharma	<detection limit.	n.d.	n.d.
G	Alburex	50 g/l	CSL Behring	<detection limit.	n.d.	n.d.
H	Human Albumin	50 g/l	TAKEDA	<detection limit.	n.d.	n.d.

[a]Concentrations of EPI-X4 determined via enzyme-linked immunosorbent assay (ELISA) using HSA concentrations corresponding to either the supplier's specifications (pH 7) or 4 mg/ml (pH 4), n.d.= not determined

3.2 Advanced EPI-X4 derivatives bind to CXCR4 and antagonizes CXCL12 mediated cell responses on human and murine lymphocytes.

Optimized EPI-X4 derivatives have been shown to antagonize CXCL12 mediated cellular responses upon binding to CXCR4. However, so far, their antagonistic efficacy has mainly been analyzed on the human leukemia cell line SupT1, which expresses high levels of CXCR4 and is therefore sensitive to CXCL12 induced activation[212,218–220,227]. Immortalized cancer cell lines often harbor many different specific mutations, that can alter their response to stimuli or therapeutics. To gain a more insight into the effects of EPI-X4 derivatives in a more physiological relevant context, I tested the efficacy of EPI-X4 lead derivatives in isolated primary human CD4+ T cells, which can be main drivers in (auto)inflammatory diseases and contribute to the tumor microenvironment[231–234]. Furthermore, to predict the transferability from mouse to human, I investigated the effect of the EPI-X4 derivatives in murine cells as mouse models are often used in preclinical studies to test drug efficacies. For this, I used a panel of EPI-X4 derivatives: (1) JM#21, a highly active but unstable derivative of EPI-X4[75,212,218,219], (2) JM#29 M8L and JM#173, more stable variants of JM#21 through the protection of the N-terminus by an unnatural amino acid (d-L) and the additional amidation of the C-terminus in case of JM#173[212,221] and (3) the fatty acid coupled derivatives JM#143, JM#194 and JM#198, highly active and stable variants of JM#21[212]. In addition, EPI-X4 itself, its inactive variant Alb(409-423) and AMD3100, the only FDA-approved CXCR4 antagonist, have been used as controls. All sequences are presented in section 1.4.1.2, Table 2.

3.2.1 EPI-X4 derivatives are active on human primary CD4+ T cells.

In order to evaluate the affinity and antagonistic activity of EPI-X4 derivatives in a more physiological context, the efficacy of EPI-X4 derivatives were validated on human primary CD4+ T cells which were isolated from human leucocyte concentrations obtained from the *DRK Blutspendezentrale* using a Ficoll gradient and negative selection. First, the expression levels of CXCR4 on the isolated cells from ten representative donors were analyzed using flow cytometry. For this, cells were stained with two fluorescently labelled anti-CXCR4 antibodies, clone 12G5 or 1D9, targeting the extracellular loop 2 (ECL2) and the N-terminus of CXCR4, respectively, or the corresponding isotype controls. CXCR4 expression was detected on CD4+ T cells with both antibodies (Figure 5b and c).

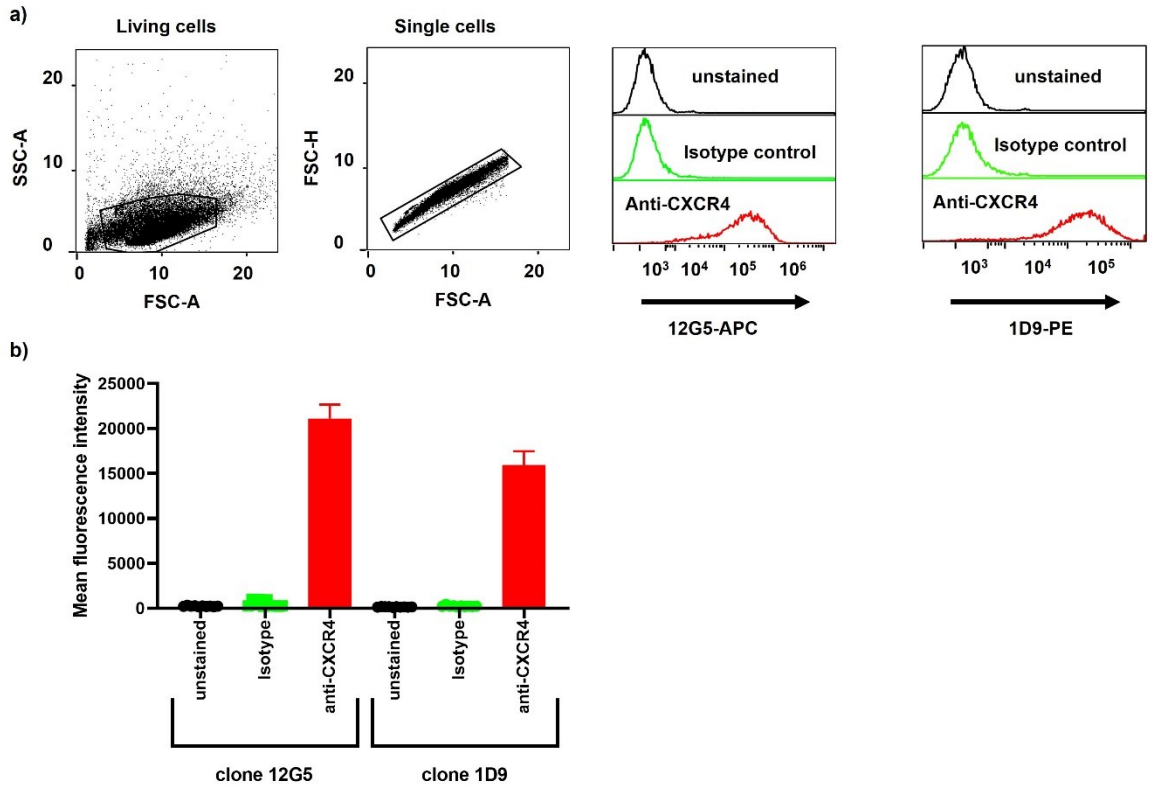


Figure 5. CXCR4 expression on human primary CD4+ T cells. 100,000 CD4+ T cells, isolated from human leucocyte concentrations, were seeded in fluorescence activated cell sorting (FACS) buffer consisting of phosphate buffered saline (PBS) supplemented with 1% fetal calf serum (FCS) and stained with two anti-CXCR4 antibodies, namely clones 12G5 and 1D9, coupled to the fluorophores APC (Allophycocyanin) and PE (phycoerythrin), respectively. After an incubation of 1 hour at 4°C, cells were washed twice with FACS buffer and fixed with 2% paraformaldehyde (PFA) and analyzed via flow cytometry. (a) Shown is the gating strategy using the area(-A) and the high (-H) of the forward and side scatter (FSC and SSC, respectively) and the stacked histograms of cells left unstained (black) or stained with the isotype control (green) or anti-CXCR4 antibody (red) of one representative donor. (b) Mean fluorescence intensity (MFI) from n=10 individual donors for anti-CXCR4 clone 12G5 and 1D9, measured in triplicates, ± SEM.

I next evaluated the binding efficacy of the current EPI-X4 lead derivatives using a previously described antibody competition assay[220] and compared the observed IC_{50} values with previously published data[197,212,218–221,227]. Compounds of interest were serially diluted in PBS and applied to the isolated CD4+ T cells along with a constant concentration of fluorescently labelled CXCR4 antibody (clone 12G5). This antibody binds to the second extracellular loop (ECL2) of CXCR4 and competes with receptor ligands for binding depending on the concentrations and binding affinity to the receptor[220]. After 2 hours of incubation at 4°C bound antibody was analyzed by flow cytometry and the half maximal inhibitory concentration (IC_{50}) for each compound calculated in GraphPad Prism using a non-linear regression model. As expected, all tested compounds with the exception of the inactive variant Alb(409-423) dose dependently inhibited antibody binding to CXCR4 (Figure 6a, Table 5). EPI-X4 replaced the antibody with an IC_{50} of ~2.8 µM, while its advanced derivatives were more active with activities between 22 nM (JM#143) and 499 nM (JM#29 M8L). Most tested EPI-X4 derivatives were more active than AMD3100 (IC_{50} =

537 nM). While most of the derivatives were as active on CD4+ T cells as on SupT1 cells (Figure 6b), JM#194 and JM#198 were around 7-fold and 55-fold, respectively, less active on CD4+ T cells than on SupT1 cells (IC_{50}= 36 nM vs. 5 nM and 28 nM vs. 0.5 nM, respectively). Only JM#143 was 5-fold more potent on CD4+ T cells than on SupT1 cells (IC_{50} 22 nM vs. 122 nM)[197,212,218–221,227]. Overall, binding efficacy of the tested EPI-X4 derivatives were comparable between SupT1 cells and CD4+ T cells with a correlation coefficient of r=0.9947 indicating that binding efficacies can be easily transferred from SupT1 cells to the more physiological relevant CD4+ T cells. However, reduced binding activity of JM#198 and JM#194 on CD4+ T cells might be due to batch related differences and thus differences during peptide synthesis. Nevertheless, both EPI-X4 derivatives are still highly active in binding to CXCR4.

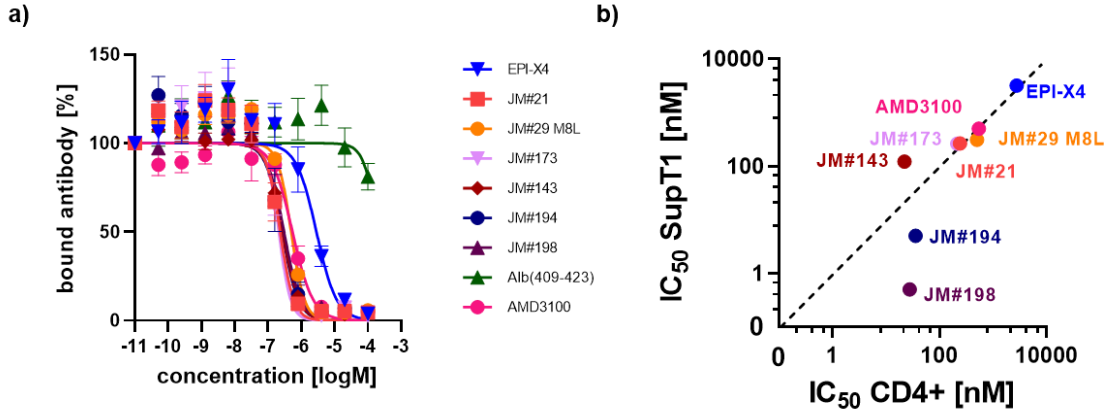


Figure 6. Advanced EPI-X4 derivatives bind to CXCR4 on CD4+ T cells. Advanced EPI-X4 derivatives and controls were serially diluted in cold PBS and applied to human primary CD4+ T cells together with a constant concentration of the fluorescently labelled anti-CXCR4 antibody clone 12G5. After 2 hours at 4°C, unbound antibodies were removed, and cells fixed with 2% PFA before fluorescence intensities were detected using flow cytometry. (a) Shown are normalized dose-response curves of all compounds tested. Data are derived from n=3 donors ± SEM. (b) 50% inhibitory concentration (IC_{50}) values of EPI-X4, its advanced derivatives and AMD3100 obtained by antibody competition assay for CD4+ T cells were plotted against published data for the human T lymphoblast cell line SupT1[197,212,218–221,227]. The dotted line indicates a perfect correlation with a Pearson correlation coefficient of r=1.0.

Stimulation of CXCR4 by CXCL12 leads to the phosphorylation of different intracellular signaling molecules, e.g. Protein kinase B (PKB), also known as Akt, and Erk (extracellular-signal regulated kinase). To test, if isolated CD4+ T cells are responsive to CXCL12, cells were stimulated with 100 ng/ml CXCL12 for different times, stained for intracellular phosphorylated Akt (pAkt) and phosphorylated Erk (pErk) and analyzed in flow cytometry. Both, pAkt and pErk peaked two minutes after stimulation with CXCL12 (Figure 7a and b). Maximum induction of pAkt was around 15-fold, whereas pErk induction was on average 7-fold, compared to unstimulated cells.

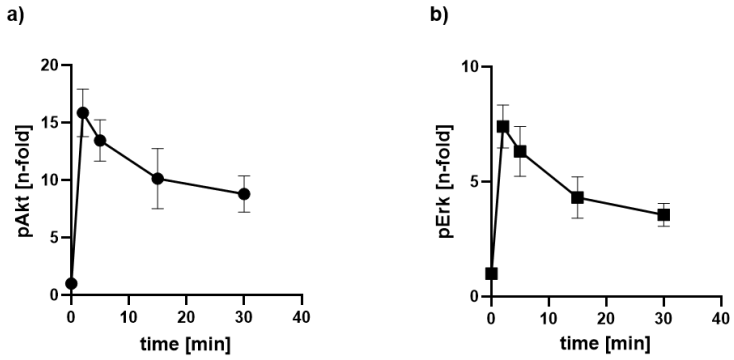


Figure 7. CXCL12 induces Akt and Erk phosphorylation in human primary CD4+ T cells. 100,000 human primary CD4+ T cells were stimulated with 100 ng/ml CXCL12 and stimulation was stopped by the addition of 10% PFA after indicated times. Cells were stained for phosphorylated Akt (pAkt) (a) and phosphorylated Erk (pErk) (b) after membrane permeabilization. Fluorescence intensities were analyzed using flow cytometry. Obtained values were normalized to the unstimulated cells (t=0 min) and plotted as n-fold induction over time. Shown data are derived from n=3 donors, measured at least in triplicates ± SEM.

Next, I tested for the inhibition of Akt and Erk phosphorylation by optimized EPI-X4 derivatives. For this, cells were preincubated with serially diluted compounds or buffer for 10 min and afterwards stimulated with 100 ng/ml CXCL12 for 2 min. Dose-response curves were generated by subtracting the background signals derived from unstimulated and untreated cells and normalized to cells which were stimulated with CXCL12 in the absence of compounds (see Figure 8a and b)

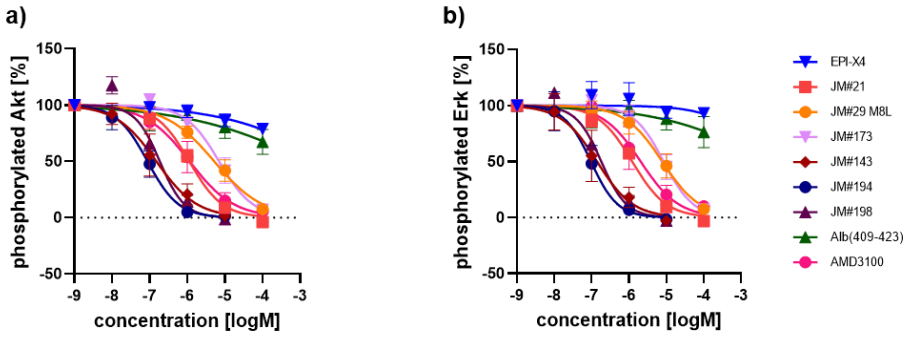


Figure 8. Advanced derivatives of EPI-X4 inhibit CXCL12 induced Akt and Erk phosphorylation in human primary CD4+ T cells in a dose-depended manner. 100,000 CD4+ T cells were pre-treated with serially diluted compounds for 10 min. Afterwards, cells were stimulated with 100 ng/ml CXCL12 for 2 min and then stained for intracellular pAkt and pErk. Mean fluorescence intensities (MFI) were determined using flow cytometry. Signals, induced by unstimulated cells were subtracted and normalized to cells stimulated with CXCL12 in the absence of compounds. Shown are dose-response curves for the inhibition of pAkt (a) and pErk (b). Data are derived from n=3 donors, measured at least in triplicates ± SEM.

IC_{50} values were determined by non-linear regression curve-fit using GraphPad Prism (Table 5). As expected from previously published data, neither EPI-X4 nor its inactive variant Alb(409-423) reached 50% inhibition at the highest concentration tested (100 µM). Indeed, previously published data on SupT1 cells as well as on Waldenstroem's macroglobulinemia cells showed IC_{50} values of EPI-X4 for pErk inhibition of >100 µM[75,212,219]. All other derivatives as well as AMD3100 showed a dose-dependent inhibition of pAkt and pErk. While JM#29 M8L and JM#173 were less potent in inhibiting pAkt (IC_{50}s=7 µM and 9 µM,

respectively) and pErk (IC_{50}s = 9 µM and 10 µM, respectively) than AMD3100 (IC_{50} = 2 µM and 3 µM, respectively) all other advanced derivatives were more active. The strongest inhibition was observed for the fatty acid coupled variants JM#143, JM#194 and JM#198 with IC_{50} values in the nM range. JM#194 was the most potent variant in antagonizing CXCL12 mediated phosphorylation of Akt and Erk in CD4+ T cells (IC_{50}= 99 nM and 112 nM, respectively). Most of the tested derivatives display comparable activities in CD4+ T cells compared to published activities in SupT1 cells [212,219,227] with a Pearson correlation coefficient of r=0.9235 (Figure 9).

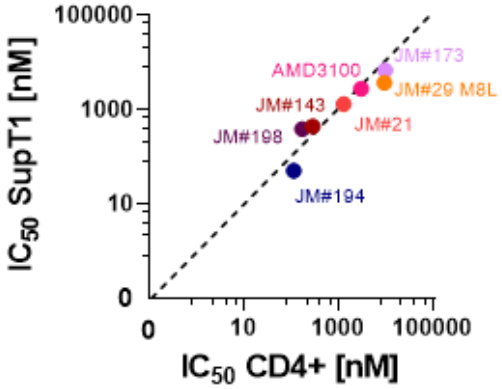


Figure 9. Comparison of IC_{50} values obtained for Erk inhibition between SupT1 cells and human primary CD4+ T cells. IC_{50} values of optimized EPI-X4 derivatives as well as AMD3100 in inhibiting CXCL12 mediated Erk phosphorylation determined on human primary CD4+ T cells were plotted against the published IC_{50} values obtained on SupT1 cells[212,219,227]. The dotted line indicates a perfect correlation with a Pearson correlation coefficient of 1.0.

CXCL12 is a chemokine inducing chemotaxis along a gradient upon binding to CXCR4. In order to analyze cell migration towards CXCL12, a transwell migration assay system was used. Briefly, 75,000 CD4+ T cells were seeded in migration media into the upper compartment of the system and allowed to settle down for approximately 15 min. In the meantime, the lower compartment was filled up with migration media containing 100 ng/ml CXCL12 or dH2O as negative control. The reaction was started by combining both systems and cells were allowed to migrate through the membrane for 4 hours. Afterwards, migrated cells present in the lower compartment were analyzed by quantifying ATP (adenosine triphosphate) levels using CellTiter-Glo® and normalized to the number of cells seeded (input control). As shown in Figure 10, CXCL12 induced migration of 57% of the of human primary CD4+ T cells compared to spontaneous migration measured in the absence of CXCL12 (10%).

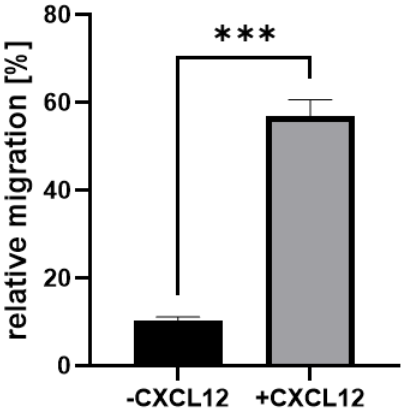


Figure 10. CXCL12 induces cell migration of human primary CD4+ T cells. Migration towards a CXCL12 gradient was analyzed using a transwell migration system with a pore size of 5 µm. For this, 75,000 human CD4+ T cells were seeded into the upper compartment of the system and allowed to settle down for around 15 min. Meanwhile, the lower compartment was filled up with migration media containing 100 ng/ml CXCL12 or dH_2O (distilled water) as negative control. The upper compartment was carefully placed onto the lower chamber and cells were allowed to migrate for 4 hours at 37°C. Afterwards, relative migration was analyzed using CellTiter-Glo® viability assay. Shown data are derived from n=3 donors, measured at least in triplicates ± SEM. Significance was calculated using an unpaired t-test, ***=p ≤0.001.

All advanced EPI-X4 derivatives inhibited CXCL12 induced cell migration of human primary CD4+ T cells in a dose-dependent manner (Figure 11). With the exception of JM#29 M8L, derivatives were either as active as AMD3100 (IC_{50}=1735 nM) or even more active in case of the fatty acid variants. Also here, JM#194 the most active derivative with an IC_{50} value of 32 nM which is 54-fold more potent than AMD3100. However, AMD3100 was described to be more potent on SupT1 cells than on the herein used CD4+ T cells (IC_{50} = 60 nM compared to 1735 nM)[219], thus, demonstrating the importance of testing therapeutics in different cellular systems. Overall, the herein showed data demonstrate that EPI-X4 derivatives are highly active on primary CD4+ T cells indicating their therapeutic potential in (auto)inflammatory diseases as well as in targeting CD4+ T cells within the tumor microenvironment.

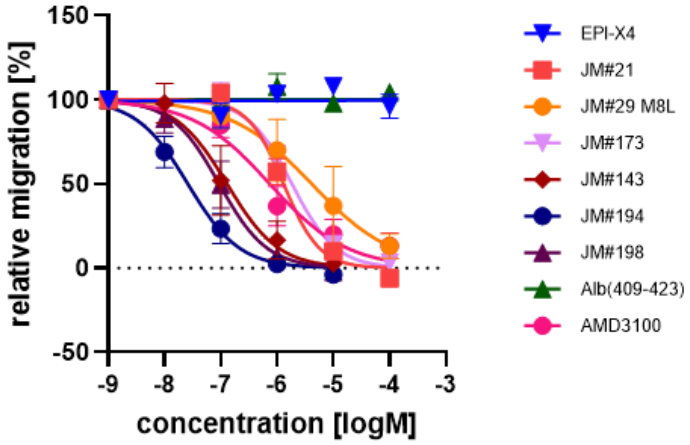


Figure 11. CXCL12 mediated cell migration of human primary CD4+ T cells is inhibited by advanced EPI-X4 derivatives in a dose-dependent manner. Human primary CD4+ T cells treated with potential CXCR4 antagonists were seeded into the upper chamber in a transwell chamber system (5 µm pore size) and allowed to settle down for around 15 min. Meanwhile, the lower compartment was filled up with migration media containing 100 ng/ml CXCL12 or no CXCL12 in the presence or absence of the compounds of interest. The migration time was started by combining the upper and lower chamber and stopped after 4 hours. Afterwards, a CellTiter-Glo® assay was performed and relative migration determined by subtracting unspecific migrate cells in the absence of CXCL12 followed by normalization to the number of cells seeded. Shown data are derived from n=3 donors ± SEM.

Table 5. Overview of efficacy of EPI-X4 and its advanced derivatives on human primary CD4+ T cells.

Compound	12G5[a]	pErk[b]	Phosphorylated Akt (pAkt)[b]	Migration[c]
	IC_{50} ± SEM [nM]			
EPI-X4	2736 ± 679	>100 000	>100 000	>100 000
JM#21	241 ± 51	1281 ± 311	1161 ± 283	1459 ± 262
JM#29 M8L	499 ± 47	9406 ± 4250	6697 ± 2570	14863 ± 13367
JM#173	213 ± 27	9744 ± 4853	8765 ± 3990	1857 ± 438
JM#143	22 ± 2	285 ± 219	233 ± 100	649 ± 480
JM#194	36 ± 23	112 ± 53	99 ± 30	32 ± 12
JM#198	28 ± 10	170 ± 29	182 ± 17	352 ± 176
Alb(409-423)	>100 000	>100 000	>100 000	>100 000
AMD3100	537 ± 149	3002 ± 1740	1704 ± 766	1735 ± 1355

[a]Competition with the CXCR4 antibody (clone 12G5), [b]Inhibition of CXCL12-dependent Erk or Akt phosphorylation, [c]Inhibition of cell migration towards a CXCL12 gradient. Data represent means of n=3 individual experiments ± SEM

3.2.2 Advanced EPI-X4 derivatives act on murine CXCR4.

The initial assessment of potential drug efficacy is commonly conducted using pre-clinical mouse models *in vivo*. EPI-X4 and some of its optimized derivatives have demonstrated therapeutic potential when applied topically in different mouse models[75,197,212,219]. However, it has never been shown that optimized peptides directly interact with murine CXCR4. I herein evaluated the effect of EPI-X4 and its advanced derivatives as well as AMD3100 on the CXCL12/CXCR4 axis using murine cell lines. The cell lines I used were the murine T lymphoblastic cell line derived BW5147 and three different murine B cells lines (300-19, Ba/F3, and A20).

I first determined the relative expression levels of CXCR4 using the murine specific anti-CXCR4 antibody L276F2-PE and analyzed the binding of it via flow cytometry. As shown in Figure 12, all tested cell lines express CXCR4 with the highest expression levels detected on A20 cells and BW5147.

Unfortunately, assessing binding kinetics to murine CXCR4 could not be determined by the previously established competition assay since the human specific anti-CXCR4 antibody clone 12G5 does not bind to murine CXCR4 (see Supplement Figure 1a). This is most likely due to the differences between murine and human CXCR4 in the amino acids at position 176 (N→D), 179 (Q→E) and 180 (and G→A) as highlighted in Supplement Figure 1b). These amino acids have been shown to be crucial for binding of the anti-CXCR4 antibody clone 12G5 and especially the latter two have been associated with a complete loss of antibody binding[235]. Therefore, the determination of binding efficacy of EPI-X4 and its advanced derivatives to murine CXCR4 using the antibody competition assay as it was done for human primary CD4+ T cells was not possible. Hence, I only determined the antagonistic efficacy

of all compounds on all murine cell lines. First, cells were stimulated with 100 ng/ml CXCL12 and phosphorylation levels of Akt and Erk were determined as described above to prove the responsiveness to CXCL12.

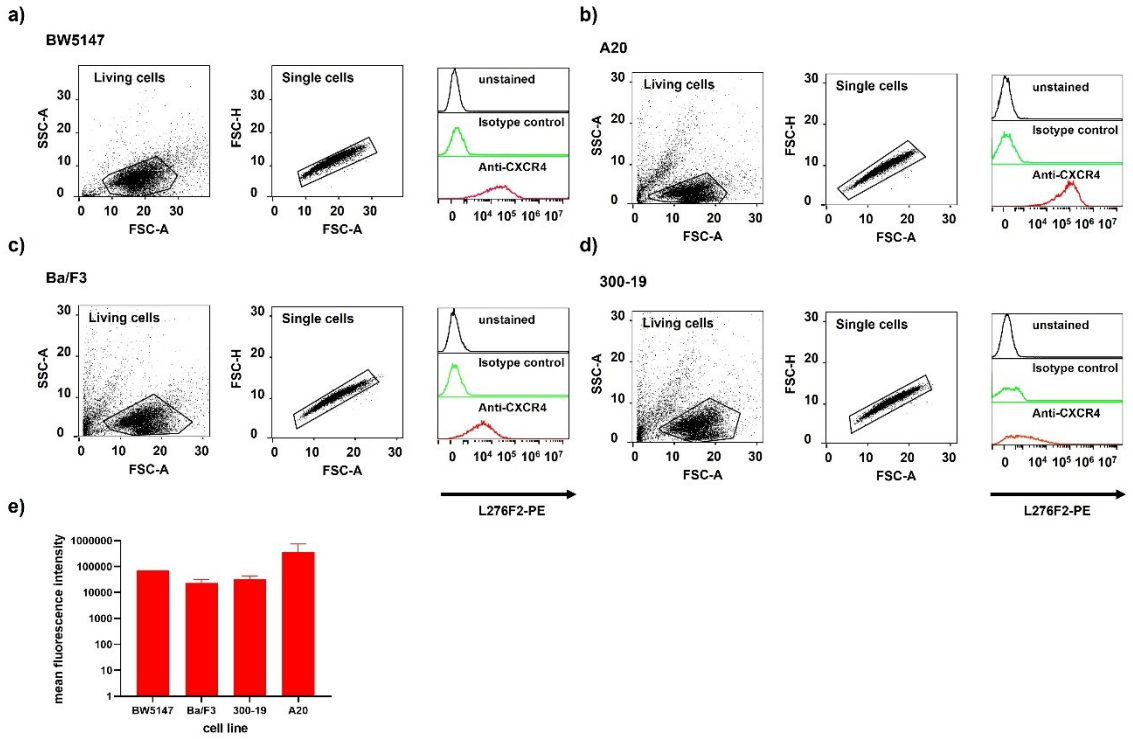


Figure 12. CXCR4 expression on murine cell lines. 100,000 cells of interest were stained with murine anti-CXCR4 antibody L276F2-PE for 1 hour at 4°C. Afterwards, unbound antibodies were removed, and cells fixed with 2% PFA before mean fluorescence intensities (MFI) were determined by flow cytometry. (a-d) Representative dot plots for the gating strategy using SSC-A, FSC-A and FSC-H for each cell line and a stacked histogram overlay of unstained cells (black), cells stained with the respective isotype control (green) and cells stained with anti-CXCR4 antibody (red). (e) MFI values of each cell line derived from n=1-3 independent experiments, performed in triplicates ± SEM.

Interestingly, 300-19 cells were less responsive to CXCL12 stimulation than all other cell lines tested as the addition of the chemokine did not alter phosphorylation status of Akt and Erk above 2-fold as displayed in Figure 13a and b. In contrast, Ba/F3 had the highest response after CXCL12 stimulation with an increase of almost 8-fold for pErk and around 15-fold for pAkt compared to t=0. For A20, a 3-fold increase of both, Akt and Erk was observed. In contrast, phosphorylation of Erk (around 5-fold) but not Akt was detected for BW5147 cells. Expression levels of CXCR4 do not correlate with CXCL12 induced phosphorylation as the cell line with the highest CXCR4 expression (A20) is not the one showing the highest response to CXCL12 (Ba/F3). To test for antagonistic effects of optimized EPI-X4 derivatives, the cell lines with the best CXCL12 responsiveness (Ba/F3, A20 or BW5147) were pretreated with different concentrations of the compounds for 10 min before simulated with 100 ng/ml murine CXCL12. Afterwards, cells were analyzed for intracellular pAkt and pErk levels using flow cytometry and dose-response curves generated

as shown in Figure 14a and b. IC_{50} values were calculated using the non-linear regression model in GraphPad Prism as described before and listed in Table 6.

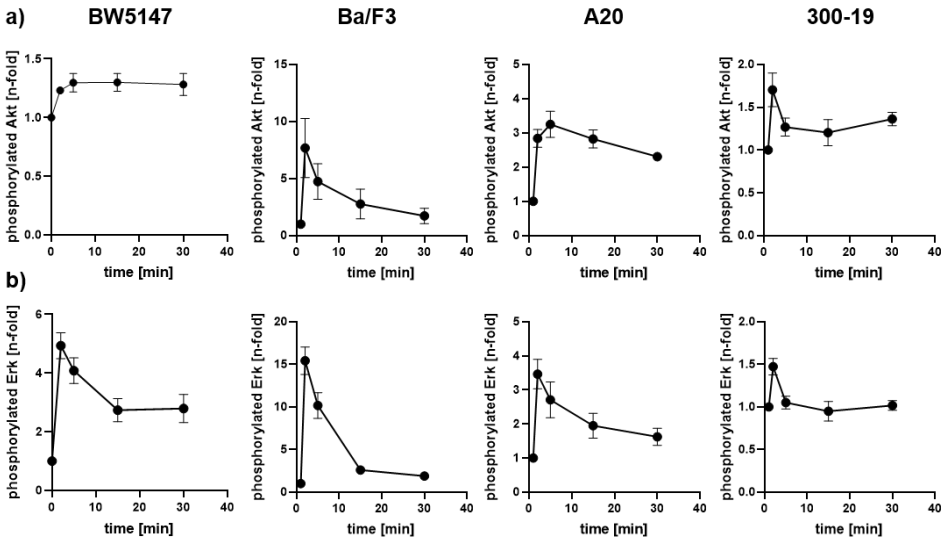


Figure 13. Phosphorylation of Akt and Erk after CXCL12 stimulation. Cell lines of interest were simulated with 100 ng/ml CXCL12 for defined timepoints. The reaction was stopped by the addition of 10% PFA and cells subsequently stained for their intracellular pAkt and pErk levels and analyzed using flow cytometry. Fluorescence values were normalized to the unstimulated control (t=0) and plotted as n-fold induction over time for phosphorylated Akt (a) and phosphorylated Erk (b), respectively. Data are derived from n=3 individual experiments measured at least in triplicates ± SEM.

While EPI-X4 and its inactive variant Alb(409-423) showed no or minor alterations in Akt and Erk phosphorylation levels in all cell lines tested, most of the advanced derivatives were antagonistically active with different activities between the murine cell lines used. JM#21 was more active in inhibiting Erk phosphorylation in Ba/F3 and BW5147 cells with IC_{50} values of approximately 8 µM, than in A20 cells with an IC_{50} value of around 33 µM and was therefore less active than in human cells (~1 µM) (see also section 3.2.1). Similarly, different antagonistic activities between cell lines were observed for JM#194, which was highly active in Ba/F3 cells but did not reach 50% inhibition of CXCL12 induced Erk phosphorylation in BW5147 cells at the highest concentration used (10 µM). Similar inhibitory variations were detected for JM#29 M8L, for which the IC_{50} values ranged from approximately 3 µM for pErk inhibition in BW5147 cells to >100 µM in A20 cells. A lower activity in A20 cells (IC_{50}=~8 µM) compared to Ba/F3 cells (IC_{50}=~1 µM) and BW5147 cells (IC_{50}=~3 µM) was also observed for AMD3100. The fatty acid coupled variants JM#143 and JM#198 showed the strongest inhibition in CXCL12 induced Akt and Erk phosphorylation in all cell lines tested with IC_{50} values mostly in the nM range with the exception of BW5147 where an IC_{50} value of around 1 µM for pErk inhibition was determined for JM#198.

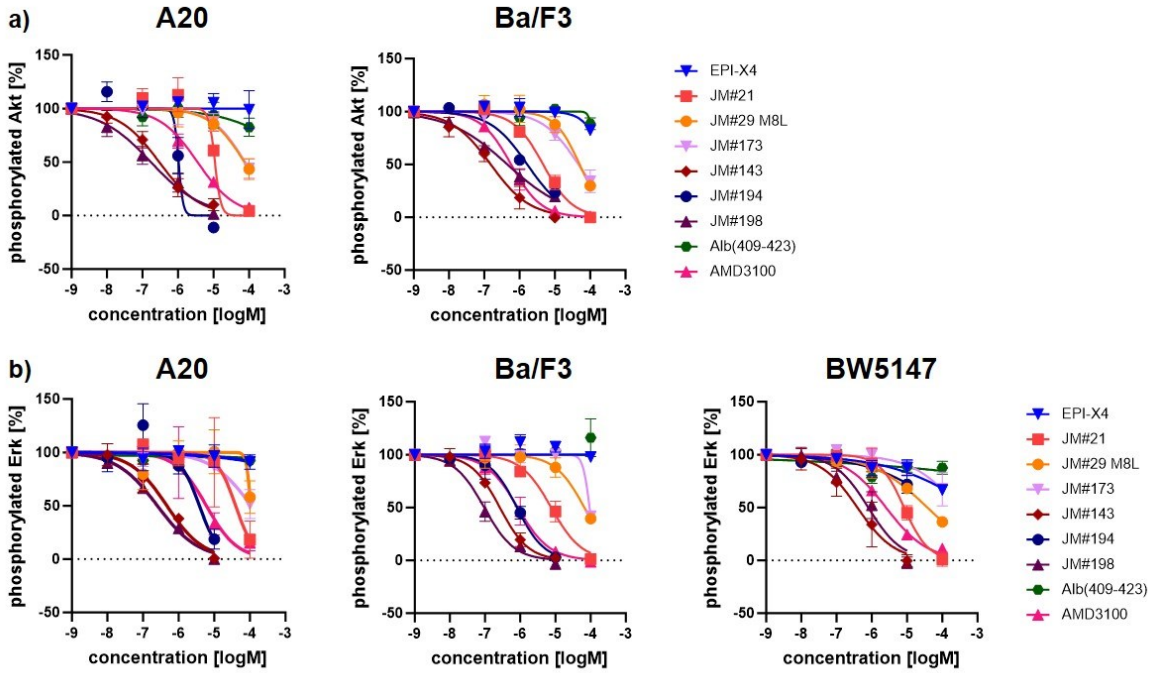


Figure 14. CXCL12-induced Akt and Erk phosphorylation is dose-dependently inhibited by advanced EPI-X4 derivatives. Cells were pretreated with compounds for 10 min before stimulation with 100 ng/ml CXCL12 for 2 min and subsequently stained for intracellular pAkt and pErk levels. Analysis was performed using flow cytometry and fluorescence intensities (subtracted from unstimulated cells) were normalized to cells stimulated with CXCL12 in the absence of compounds. Shown are dose-response curves for the inhibition of Akt phosphorylation (a) and Erk phosphorylation (b) derived from n=3 individual experiments measured at least in triplicates ± SEM.

Table 6. Overview of antagonistic efficacies in murine cell lines upon CXCL12 induced Akt and Erk phosphorylation.

Compound	pErk IC_{50} ± SEM [µM]			pAkt IC_{50} ± SEM [µM]	
	A20	Ba/F3	BW5147	A20	Ba/F3
EPI-X4	>100	>100	>100	>100	>100
JM#21	33.7 ± 22.3	8.32 ± 1.95	8.31 ± 2.47	8.34 ± 3.24	5.01 ± 1.60
JM#29 M8L	>100	66.17 ± 21.01	3.72 ± 0.79	75.71 ± 24.74	55.01 ± 17.23
JM#173	>100	90.62 ± 4.47	>100	70.59 ± 21.72	65.89 ± 36.17
JM#143	0.50 ± 0.22	0.27 ± 0.06	0.69 ± 0.55	0.40 ± 0.19	0.22 ± 0.13
JM#194	4.83 ± 1.28	0.78 ± 0.10	>10	1.06 ± 0.13	1.66 ± 0.29
JM#198	0.25 ± 0.02	0.12 ± 0.02	1.03 ± 0.4	0.26 ± 0.14	0.51 ± 0.21
Alb(409-423)	>100	>100	>100	>100	>100
AMD3100	7.71 ± 5.15	1.01 ± 0.39	2.72 ± 0.46	14.30 ± 10.66	0.66 ± 0.24

Overall, tested compounds were more potent in inhibiting Erk phosphorylation in Ba/F3 cells than A20 cells (Supplement Figure 2, Figure 15a). Almost similar potencies were detected between Ba/F3 cells and BW5147 (Supplement Figure 2b) with the exception of JM#29 M8L which was less potent in inhibiting Erk phosphorylation in Ba/F3 cells than in BW5147 cells and JM#21 which showed similar potency between both cell lines. Nearly comparable potencies were detected for A20 and BW5147 cells with only minor differences in case of AMD3100 and JM#143 and moderately difference observed for JM#21 which was around 4 times more potent on A20 cells than BW5147 cells (Supplement Figure 2c). In addition, mostly all compounds were more potent in human primary CD4+ T cells than in murine cells

(Supplement Figure 2, Figure 15d-f) with the exception of AMD3100 and JM#29 M8L showing stronger potency on Ba/F3 cells (3 times) and BW5147 cells (6 times), respectively. Although EPI-X4 has been shown before to antagonize CXCL12 mediated migration of Ba/F3 cells at a concentration of 100 µM[197], no antagonistic activity was observed for the inhibition of CXCL12 induced Akt and Erk phosphorylation. This is most likely due to different concentrations of CXCL12 used here (100 ng/ml) which is around 8-fold lower than used by Zirafi *et al.* (100 nM)[197]. In addition, in comparison to hCXCR4, these data indicate differences in binding to mCXCR4 and hence antagonistic activities.

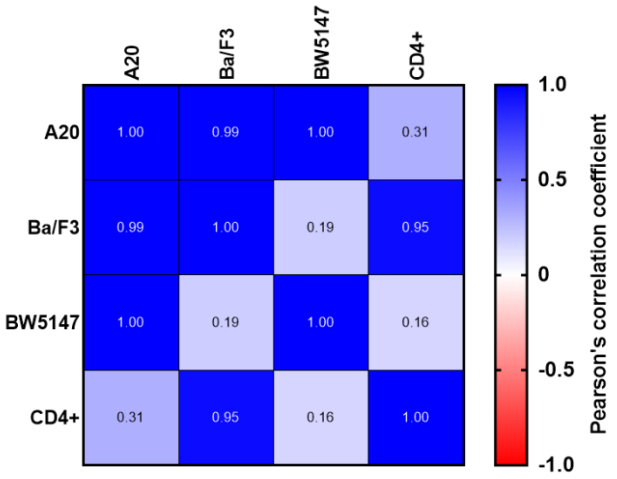


Figure 15. Comparison of the IC_{50} values for inhibition of Erk phosphorylation in murine cells and human primary CD4+ T cells. Correlation matrix of IC_{50} values determined for inhibition of Erk phosphorylation for the murine cell lines Ba/F3, A20 and BW5147 and the human primary CD4+ T cells. Values represent the Pearson correlation coefficients determined for pErk inhibition in all cell lines tested.

In general, strong correlation was detected between IC_{50} values determined in murine cell lines A20 and Ba/F3 (r=0.99), and A20 and BW5147 (r=1.00), respectively, for the inhibition of CXCL12 induced Erk phosphorylation (Figure 15). In contrast, values obtained in A20 cells and BW5147 cells only weakly correlate with efficacies determined in CD4+ T cells (r=0.31 and r=0.16, respectively) whereas a strong correlation was detected between values obtained in Ba/F3 cells and CD4+ T cells (r=0.95). Thus, the efficacies of advanced EPI-X4 derivatives differ between the murine cell lines and were in general weaker than in human cells. Differences in binding and antagonistic activities between human CXCR4 (hCXCR4) and murine CXCR4 (mCXCR4) has not only been shown before for AMD3100 but also for other CXCR4-specific peptides like FC-131[236–239].

Although CXCL12 induced intracellular phosphorylation of Akt and/or Erk was detected for A20, Ba/F3 and BW5147 cells, only the latter one showed a significant cell migration towards a 100 ng/ml CXCL12 gradient. As depicted in Figure 16, BW5147 cells reached a CXCL12-specific migration of approximately 14%. Neither the murine B cell lines A20 nor Ba/F3 showed CXCL12-specific migration over 2%. Therefore, changes in CXCL12-mediated cell migration in the presence of CXCR4 targeting compounds were assessed only for BW5147 cells.

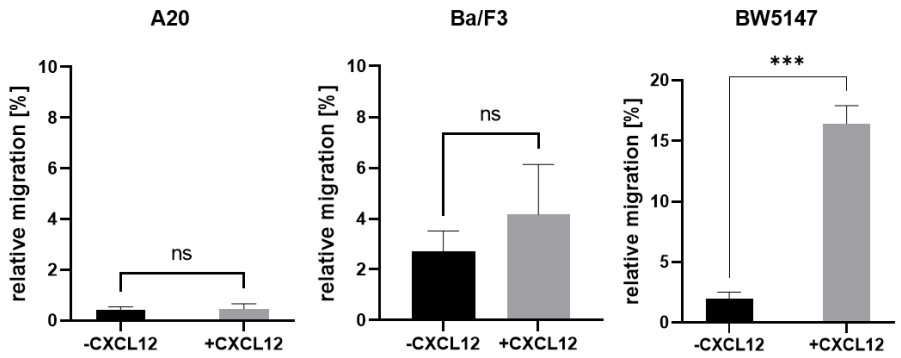


Figure 16. CXCL12 induces cell migration of murine cell lines. CXCL12 induced cell migration of murine B cell lines A20 and Ba/F3 and murine T cell line BW5147 was assessed using a transwell migration assay system. Therefore, 75,000 cells were seeded into the upper chamber of the system and allowed to settle down for around 15 min. In the meantime, the lower chamber was filled with assay buffer containing 100 ng/ml CXCL12 or dH_2O. Both chambers were combined, and cells allowed to migrate towards the lower chamber for 4 hours at 37°C. Afterwards, relative migration was determined by CellTiter-Glo® viability assay in the lower chamber. Shown data are derived from n=3 individual experiments, performed in triplicates ±SEM. Significant differences were calculated using an unpaired t-test, ns=not significant, ***=p<0.001.

For this, migration towards a CXCL12 gradient (100 ng/ml) was evaluated in the presence of the most potent peptides (JM#143 and JM#198) as well as JM#21. In addition, the inhibitory activity of AMD3100 was evaluated. As shown in Figure 17, all tested compounds inhibited CXCL12 induced migration in a dose-dependent manner. At a concentration of 10 µM, almost full inhibition (>95%) was observed for all compounds tested except for JM#143, which showed about 87% inhibition.

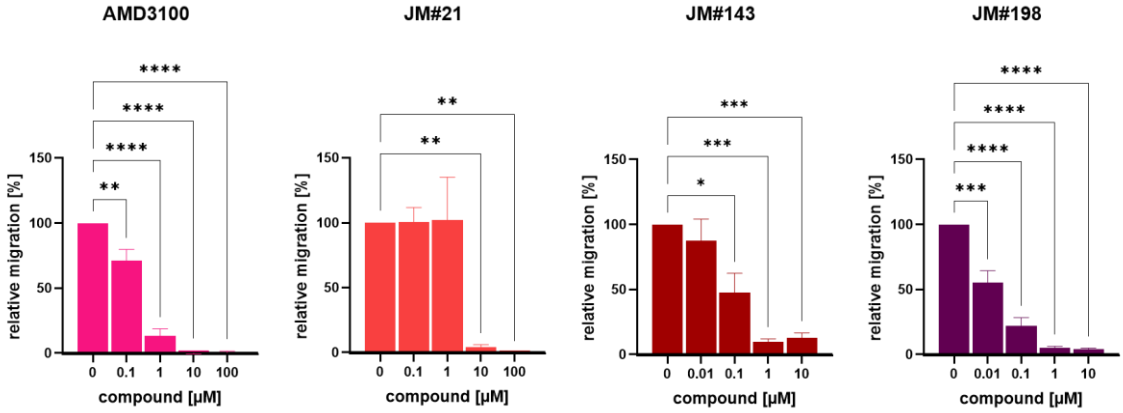


Figure 17. Advanced EPI-X4 derivatives inhibit CXCL12 induced migration of the murine T cell line BW5147. 75,000 BW5147 cells were applied to the upper compartment of a transwell assay system in the presence of serially diluted compounds. Same concentrations of compounds were applied to the lower compartment, which was filled up with assay buffer containing 100 ng/ml CXCL12 or dH_2O. Both compartments were combined and incubated for 4 hours at 37°C. Afterwards, migrated cells present in the lower compartment were quantified using CellTiter-Glo® viability assay. Shown data are derived from n=3 individual experiments, performed in triplicates ±SEM. Significant differences were calculated using One-way ANOVA, *=p<0.05, **=p<0.01, ***=p<0.001, ****=p<0.0001.

In summary, these data show that data obtained for EPI-X4 derivatives in immortalized cells can be confirmed in human primary CD4+ T cells, whereas cell line dependent differences on murine CXCR4 were observed which have to be considered for the use of mouse models.

3.3 CXCR4 antagonizing effect of optimized EPI-X4 derivatives in Mantle cell lymphoma and chronic lymphocytic leukemia.

Overactivation of the CXCL12/CXCR4 axis has been linked to several cancer types including non-Hodgkin Lymphoma[136–138,166–168]. CXCR4 has been shown to play an important role in disease progression by inducing cancer cell survival, growth, metastasis and resistance to classical chemotherapeutics[138,139,166,168–171,180,195,240]. Thus, CXCR4 is a promising drug target for cancer therapy[166,168,169,171,180,195]. For this reason, I aimed to test the efficacy of optimized EPI-X4 derivatives first in chronic lymphocytic leukemia (CLL) and Mantle cell lymphoma (MCL) cell lines (Mec-2 and HG3, and Maver-1 and Jeko-1, respectively) but also on splenocytes from a commonly used CLL mouse model, the transgenic T cell leukemia/lymphoma 1A mouse model (Eμ-TCL1 model).

3.3.1 EPI-X4 derivatives antagonize CXCL12/CXCR4 signaling on MCL and CLL cell lines.

CXCR4 expression on all cell lines was evaluated using the human anti-CXCR4 antibodies clones 12G5 and 1D9. The two tested CLL cell lines Mec-2 and HG-3 expressed lower levels of CXCR4 than the MCL cell lines (Figure 18). While the highest expression levels of CXCR4 were detected on the MCL cell line Jeko-1, the lowest CXCR4 intensity was observed on HG-3 cells. Binding potencies of EPI-X4, its advanced derivatives and respective controls were determined by performing the antibody competition assay using anti-CXCR4 antibody clone 12G5. On all cells, the compounds dose-dependently inhibited antibody binding (Figure 19a). Of note, IC_{50} values were only meaningful for MCL cell lines as the signal to noise ratio was too low for the herein tested CLL cells (see Supplement Figure 3 for JM#21).

IC_{50} values are summarized in Table 7. With the exception of Alb(409-423) and EPI-X4, all tested derivatives showed stronger binding affinity to CXCR4 than AMD3100 on MCL cells. The fatty acid coupled variants JM#143, JM#194 and JM#198 were the most active derivatives with IC_{50} values in the low nM range.

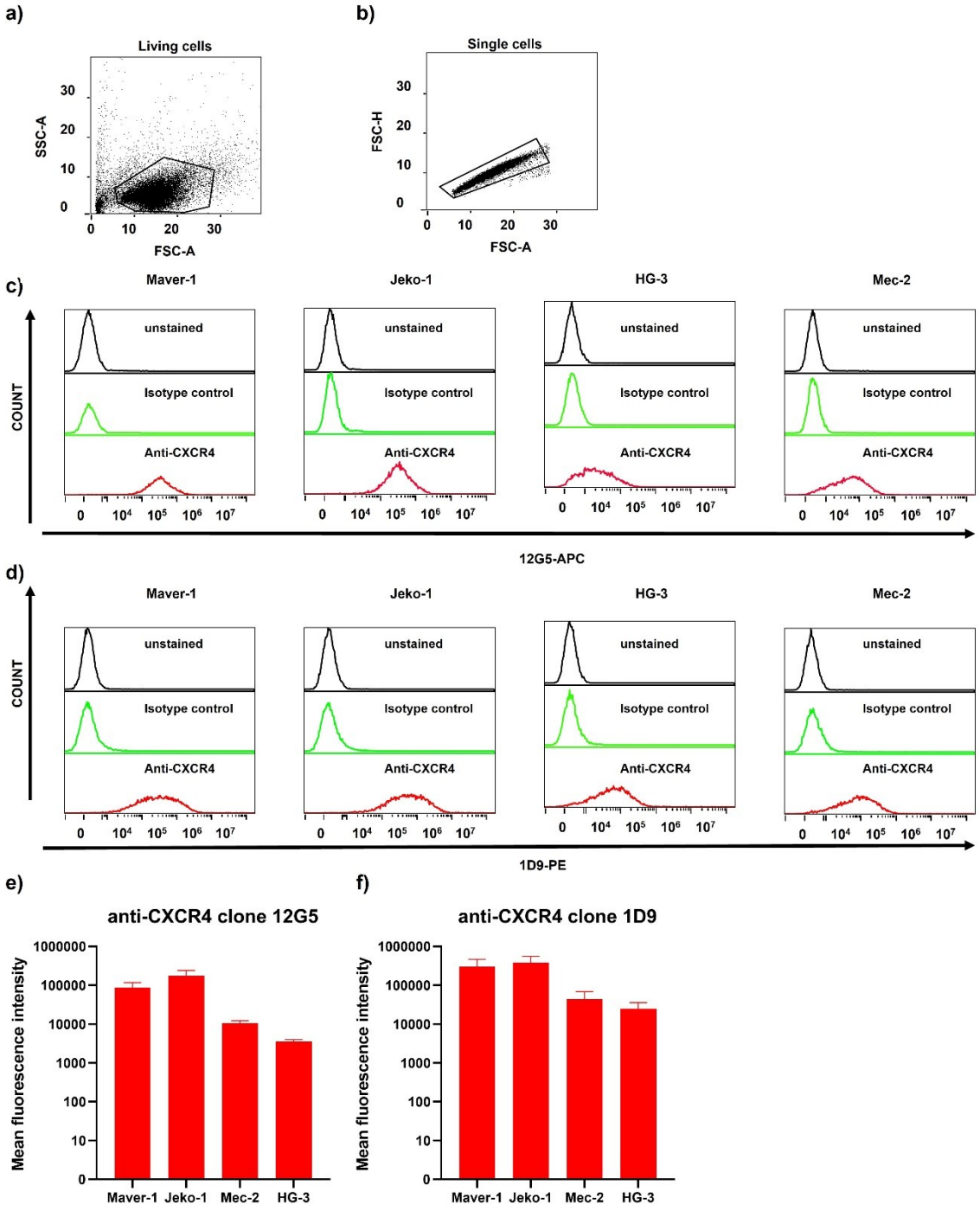


Figure 18. CXCR4 expression on human MCL and CLL cell lines. 100,000 cells were stained with human anti-CXCR4 antibodies clone 12G5 and 1D9 for one hour at 4°C before fixed with 2% PFA and analyzed by flow cytometry. Shown is one exemplary sample of the gating strategy, herein done for the MCL cell line Maver-1, to identify living single cells using FCS-A, SSC-A and FSC-H (a,b). Stacked histograms for the MCL cell lines Maver-1 and Jeko-1 as well as for the CLL cell lines HG-3 and Mec-2 were generated from unstained samples (black), isotype controls (green) and samples stained with specific anti-CXCR4 antibody (red) for 12G5-APC (c) and 1D9-PE (d). Summarized mean fluorescence intensity of n=3 individual experiments, performed in triplicates ± SEM are generated for clone 12G5 (e) and 1D9 (f).

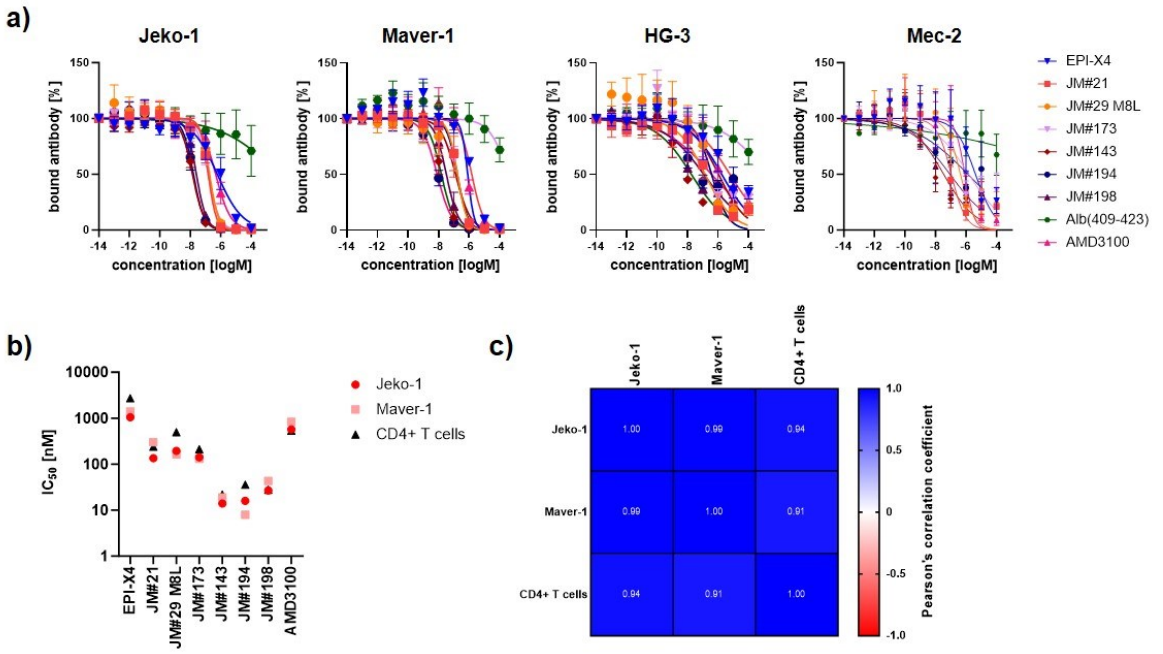


Figure 19. EPI-X4 derivatives bind to CXCR4 expressed on human MCL and CLL cell lines. Binding efficacy of compounds were analyzed using the 12G5 antibody competition assays. Shown are dose-response curves of all cell lines tested (a) whereof IC_{50} values were calculated using the non-linear regression model in GraphPad Prism. Obtained IC_{50} values were compared between Jeko-1, Maver-1 and human primary CD4+ T cells and illustrated as single dots for all derivatives tested (b) from which a correlation matrix was generated (c).

Most IC_{50} values are in the same range as those obtained for human primary CD4+ T cells (section 3.2.1, Figure 19b). Only JM#194 and JM#29 M8L showed greater binding potency to CXCR4 expressed on Maver-1 and Jeko-1 cells than on human primary CD4+ T cells. In general, there is a strong correlation between IC_{50} values obtained in MCL cell lines Maver-1 and Jeko-1 (r=0.99) as well as between primary CD4+ T cells and MCL cell lines (r≥0.91).

Table 7. IC_{50} values for the MCL cell lines Maver-1 and Jeko-1 obtained by antibody competition assay using anti-CXCR4 antibody clone 12G5.

Compound	Maver-1	Jeko-1
	IC_{50} ± SEM [nM]	
EPI-X4	1407 ± 209	1052 ± 598
JM#21	303 ± 210	136 ± 29
JM#29 M8L	163 ± 79	195 ± 44
JM#173	132 ± 61	142 ± 37
JM#143	19 ± 10	14 ± 3
JM#194	8 ± 2	16 ± 7
JM#198	43 ± 26	27 ± 8
Alb(409-423)	>100 000	>100 000
AMD3100	839 ± 95	575 ± 270

To test the responsiveness of the cell lines, intracellular Akt and Erk phosphorylation was induced by stimulation with 100 ng/ml CXCL12 as described before. Phosphorylation levels were plotted as n-fold induction compared to unstimulated cells as shown in Figure 20.

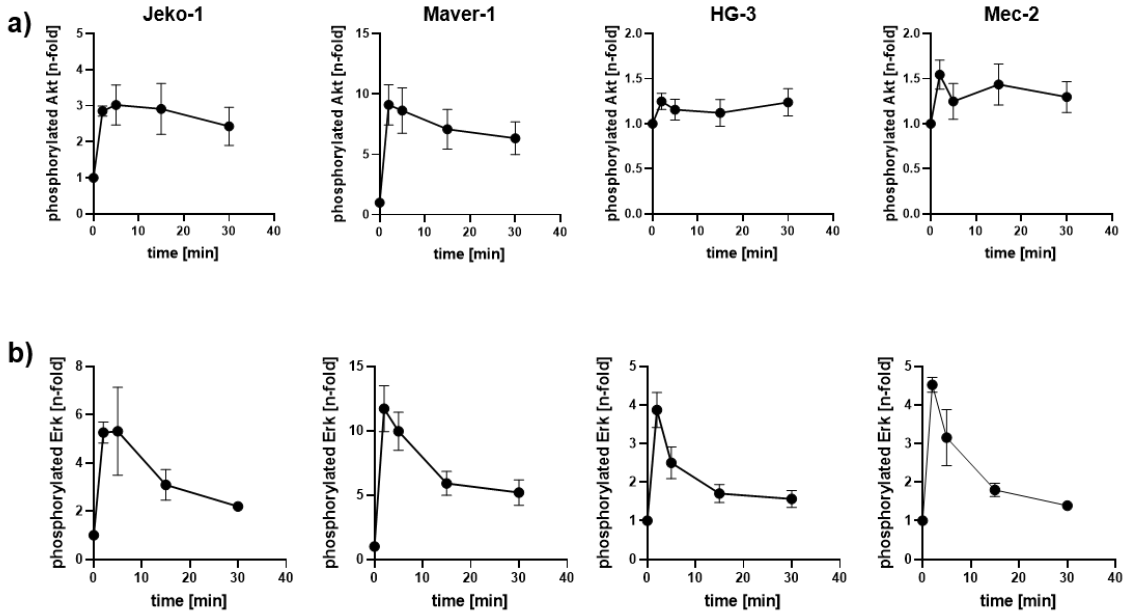


Figure 20. Levels of intracellular Akt and Erk phosphorylation in MCL and CLL cell lines after CXCL12 stimulation. MCL and CLL cells were stimulated with 100 ng/ml CXCL12 for indicated timepoints and subsequently stained for intracellular levels of pAkt (a) and pErk (b) which were measured by flow cytometry. Shown data are derived from n=3 individual experiments, measured at least in triplicates ± SEM. Values were normalized to the unstimulated control (t=0).

Interestingly, while increased phosphorylation levels of Erk 2 min after stimulation with CXCL12 were observed for all cell lines (Jeko-1 ~5-fold, Maver-1 ~12-fold, HG-3 ~4-fold and Mec-2 ~4.5-fold, respectively), high levels of Akt phosphorylation were only detected for the MCL cell lines Jeko-1 and Maver-1 (~3-fold and ~9-fold, respectively) but not in CLL cell lines HG-3 and Mec-2. Nevertheless, antagonistic activities of EPI-X4 and its advanced derivatives were evaluated on all cell lines. As shown in Figure 21a and b, all tested compounds dose-dependently inhibited CXCL12 induced Akt and Erk phosphorylation, with the exception of EPI-X4 and Alb(409-423), which did not reach 50% inhibition as expected from the previous experiments (see section 3.2.1 and section 3.2.2). For JM#29 M8L, an inhibition of pAkt below baseline was observed, probably due to inverse agonistic properties. Generally, EPI-X4 derivatives inhibited CXCL12 induced Akt and Erk phosphorylation more efficiently in the CLL cell lines Mec-2 and HG-3 than in MCL cell lines Maver-1 and Jeko-1 as summarized in Table 8 and Table 9, respectively. JM#198 was almost 10-fold more effective in inhibiting pAkt on Mec-2 (IC_{50} = 0.08 µM) compared to Jeko-1 (IC_{50} = 0.72 µM) (Table 8). Also, the Inhibition of pAkt and pErk by AMD3100 was around 40-fold less effective in Jeko-1 cells than in Mec-2 cells. Nevertheless, all fatty acid variants tested (JM#143, JM#194 and JM#198) were active on all cell lines tested with IC_{50} values below 1 µM. In general, the efficacy of EPI-X4 derivatives was lower in MCL cells than in CLL cells lines. Moreover, the efficacy in inhibiting pAkt and pErk in CLL cells

correlated very strong with the efficacy in CD4+ T cells (r=0.81-0.90), whereas a lower correlation (r=0.68-0.83) was observed between MCL cells and CD4+ T cells.

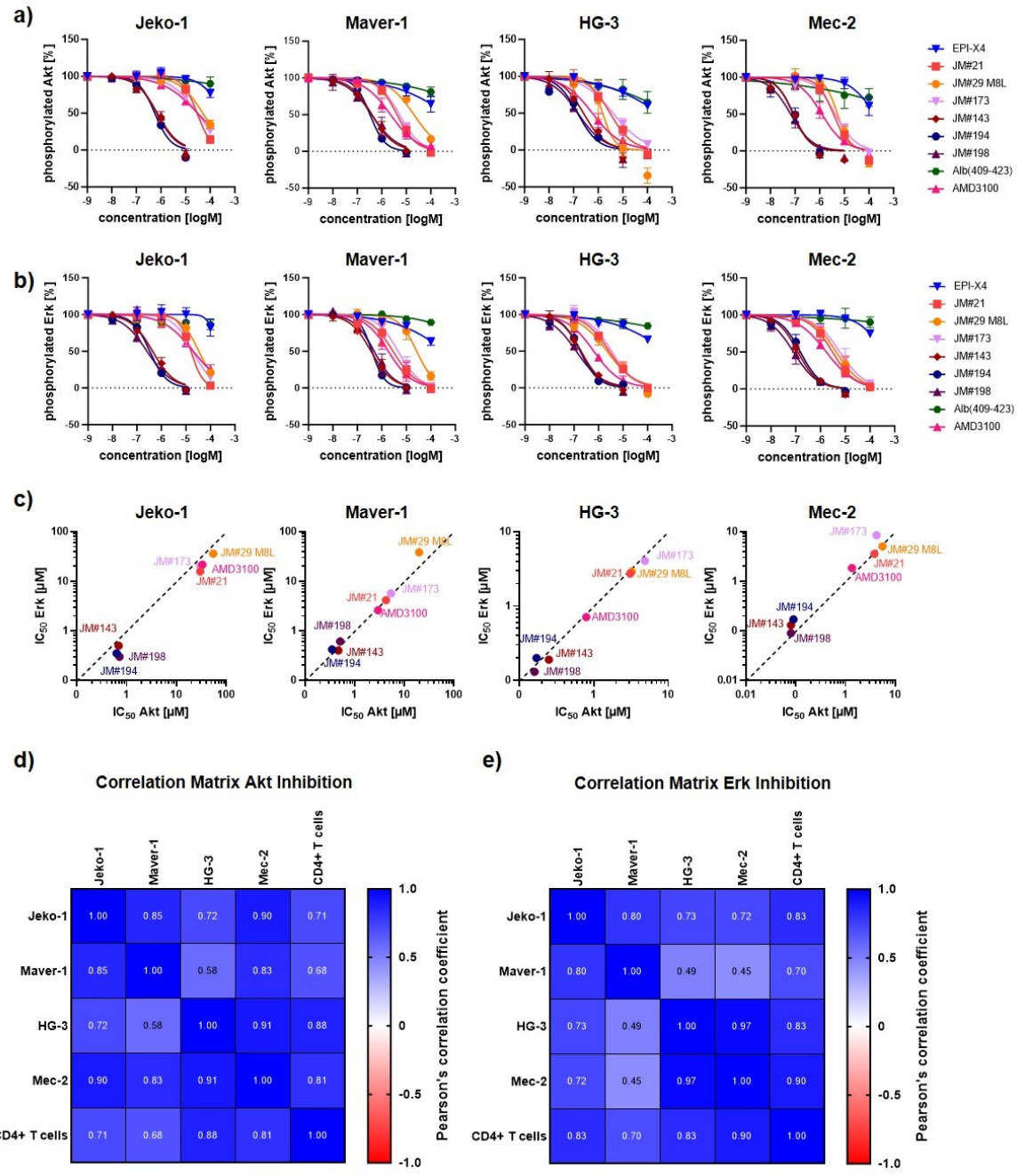


Figure 21. Advanced EPI-X4 derivatives antagonize CXCL12 induced Akt and Erk phosphorylation in MCL and CLL cell lines. Cells were pretreated with compounds for 10 min before stimulated with 100 ng/ml CXCL12 for 2 min. Cells were then stained for intracellular pAkt and pErk and analyzed by flow cytometry. (a,b) Shown are dose-response curves of pAkt and pErk, for all cell lines tested. Shown data are derived from n=3 independent experiments, performed at least in triplicates ± SEM. (c) IC_{50} values for the inhibition of pAkt and pErk were calculated using the non-linear regression model in GraphPad Prism and mean IC_{50} plotted for each cell line. Dotted lines indicate a perfect correlation with a Pearson correlation coefficient of r=1.0. (d,e) Correlation matrices for all IC_{50} values obtained for the inhibition of pAkt and pErk, respectively, for Jeko-1, Maver-1, HG-3, Mec-2 and CD4+ T cells.

Table 8. Summary of IC_{50} values for the inhibition of Akt phosphorylation.

Compound	Maver -1	Jeko-1	Mec-2	HG-3
	IC_{50} ± SEM [µM]			
EPI-X4	>100	>100	>100	>100
JM#21	4.29 ± 0.39	29.93 ± 6.14	3.83 ± 0.76	3.07 ± 0.57
JM#29 M8L	19.92 ± 3.64	54.59 ± 9.97	5.57 ± 1.88	3.24 ± 2.57
JM#173	5.40 ± 1.04	30.10 ± 2.05	4.21 ± 0.44	4.86 ± 1.92
JM#143	0.47 ± 0.16	0.69 ± 0.19	0.08 ± 0.01	0.25 ± 0.05
JM#194	0.35 ± 0.10	0.63 ± 0.14	0.09 ± 0.06	0.17 ± 0.07
JM#198	0.51 ± 0.28	0.72 ± 0.17	0.08 ± 0.03	0.16 ± 0.02
Alb(409-423)	>100	>100	>100	>100
AMD3100	2.96 ± 1.44	33.17 ± 9.15	1.35 ± 0.53	0.79 ± 0.33

Table 9. Overview of IC_{50} values for the inhibition of Erk phosphorylation.

Compound	Maver-1	Jeko-1	Mec-2	HG-3
	IC_{50} ± SEM [µM]			
EPI-X4	>100	>100	>100	>100
JM#21	4.16 ± 2.28	15.80 ± 2.46	3.59 ± 1.43	2.74 ± 0.20
JM#29 M8L	38.50 ± 21.67	36.07 ± 12.57	5.05 ± 1.60	2.91 ± 1.41
JM#173	5.68 ± 2.26	20.42 ± 5.69	8.51 ± 4.69	4.05 ± 1.54
JM#143	0.40 ± 0.13	0.50 ± 0.18	0.13 ± 0.03	0.19 ± 0.04
JM#194	0.42 ± 0.10	0.35 ± 0.06	0.17 ± 0.07	0.20 ± 0.07
JM#198	0.61 ± 0.27	0.30 ± 0.11	0.09 ± 0.04	0.13 ± 0.01
Alb(409-423)	>100	>100	>100	>100
AMD3100	2.61 ± 1.07	27.72 ± 4.49	1.85 ± 0.36	0.71 ± 0.11

Intracellular phosphorylation of Erk mediates chemotaxis and hence cell migration[241]. CXCL12 induced migration was evaluated on those cell lines with the highest response upon CXCL12 stimulation: Mec-2 and Maver-1. Cell migration towards CXCL12 was observed for both cell lines tested (see Figure 22) with a specific migration of approximately 15% for Mec-2 and 30% for Maver-1 cells.

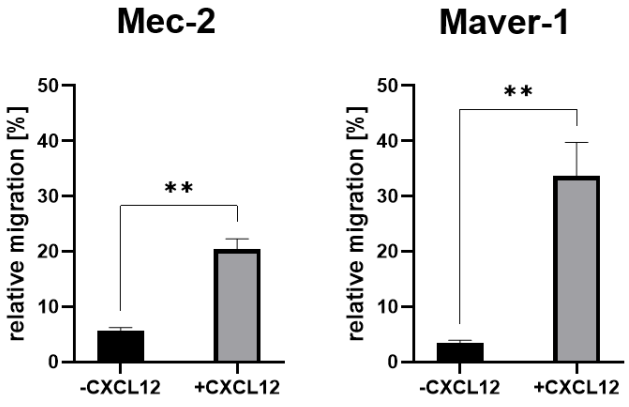


Figure 22. CXCL12 induces cell migration of Mec-2 and Maver-1. Cell migration towards a CXCL12 gradient was analyzed using a transwell migration system (pore size = 5 µm). For this, 75,000 cells were seeded into the upper chamber of the system and allowed to settle down for around 15 min. Meanwhile, the lower compartment was filled up with migration media containing 100 ng/ml CXCL12 or dH_2O as negative control. Both chambers were combined and incubated for 4 hours at 37°C. Afterwards, relative migration was determined by CellTiter Glo® viability assay. Shown data are derived from n=3 independent experiments, performed in triplicates ± SEM. Significance was calculated using an unpaired t-test, **=p< 0.01.

The efficacy to block CXCL12-induce cell migration was then tested for the most active derivatives JM#198 and JM#143 as well as AMD3100 and JM#21 in Mec-2 and Maver-1 cells. All tested derivatives inhibited CXCL12 induced cell migration in a dose-dependent

manner in both cell lines (Figure 23). The strongest inhibition was observed for the fatty acid coupled derivatives JM#143 and JM#198, as expected. Both showed an inhibition of over 50% at a concentration of 0.1 µM. In contrast, for AMD3100 and JM#21 higher concentrations were required to reach over 50% of inhibition. AMD3100 was more potent than JM#21 but less effective than JM#143 and JM#198.

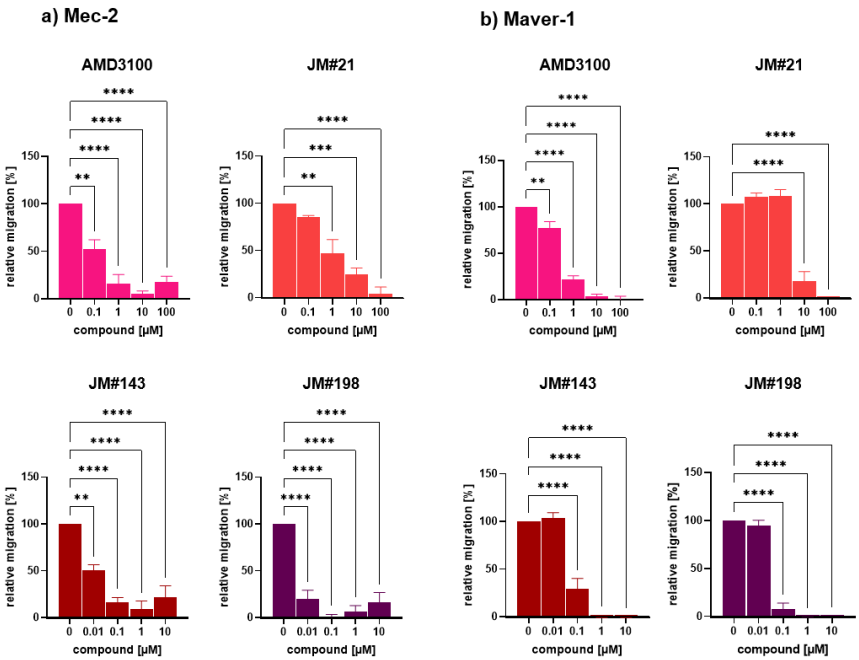


Figure 23. Advanced EPI-X4 derivatives block CXCL12 induced cell migration of Mec-2 and Maver-1 cells in a dose-dependent manner. 75,000 cells were seeded into the upper chamber of a transwell assay system along with different compound concentrations. Same compound concentrations were applied to the lower compartment which was filled up with migration media containing 100 ng/ml CXCL12 or dH2O as negative control. Both compartments were combined and migrated cells quantified after 4 h at 37°C using CellTiter-Glo®. Shown data are derived from n=3 individual experiments, performed in triplicates ±SEM. Significant differences were calculated using One-way ANOVA, *=p<0.05, **=p<0.01, ***=p<0.001, ****=p<0.0001.

3.3.2 Efficacy of EPI-X4 derivatives on splenocytes derived from the Eµ-TCL-1 mouse model.

Initially discovered as the causative agent for developing T-prolymphocytic leukemia (T-PLL), the overexpression of the TCL-1 gene is widely used in transgenic animal models to recapitulate different types of leukemia, either of T cell of B cell origin, including human CLL[242]. Thereby, this gene is overexpressed in B cells under the V_H-promoter-Ig_H-Eµ-enhancer (*TCL1*-tg)[243]. In order to study the CXCR4 antagonizing activity of the advanced EPI-X4 derivatives on murine primary cells I used splenocytes derived from six different syngeneic recipients which were transplanted with Eµ-TCL1 tumors. For this, I first determined the CXCR4 expression on all six donors (Figure 24). Interindividual differences in the CXCR4 expression levels were observed. The highest expression levels of CXCR4 were detected in mouse sample #5477, followed by #5253. Consequently, sample #5477 was

chosen to investigate the responsiveness upon CXCL12 stimulation by evaluating the intracellular phosphorylation status of Akt and Erk as described before.

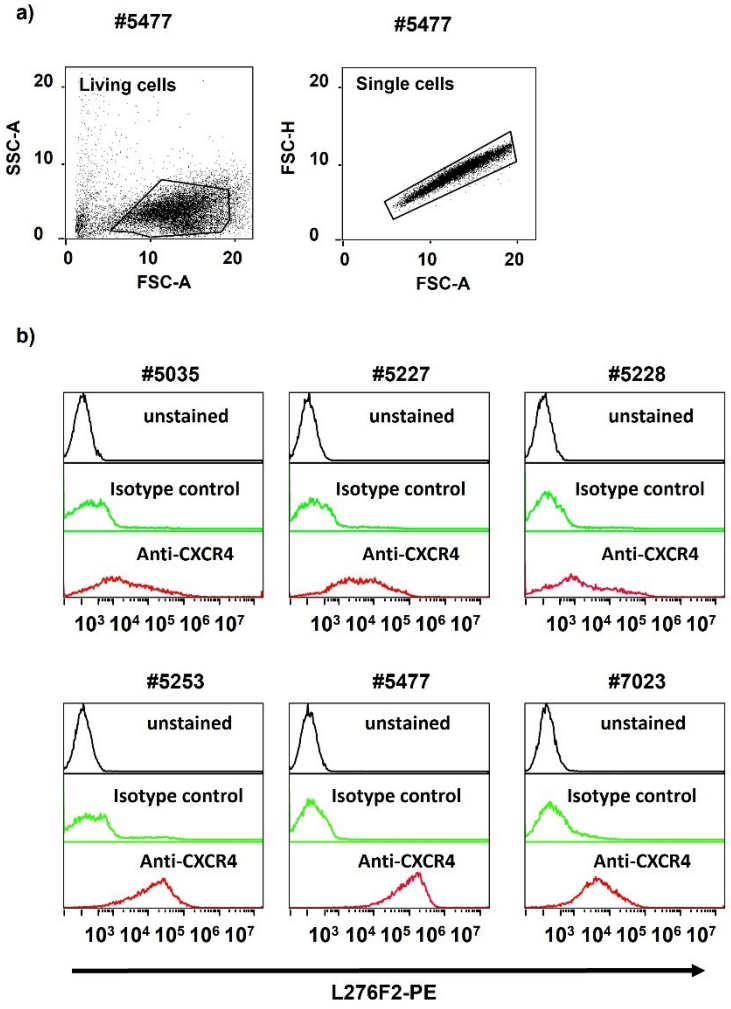


Figure 24. Detection of CXCR4 expression on splenocytes derived from the transgenic T cell leukemia/lymphoma 1A mouse model (Eμ-TCL1). Splenocytes were stained with the fluorescently labelled murine specific anti-CXCR4 antibody clone L276F2 for 1 hour at 4°C. Afterwards, unbound antibodies were removed, and cells subsequently fixed with 2% PFA prior analysis of fluorescence intensities using flow cytometry. Shown is the gating strategy to obtain living single cells using mouse sample #5477 (a) and representative stacked histograms of all samples tested (b) for unstained cells (black), cells stained with respective isotype control (green) and anti-CXCR4 antibody clone L276F2-PE (red).

Mean fluorescence intensities were then normalized to those obtained in unstimulated cells and plotted as n-fold induction over time. A CXCL12 induced increase in phosphorylated Akt and Erk was observed which peaks 2-5 min after stimulation with around 3-fold and approximately 7-fold, respectively (Figure 25a and b). Cells were then pretreated with different concentrations of the respective compounds for 10 min prior stimulation with 100 ng/ml CXCL12 for 2 min. As expected, neither Alb(409-423) nor EPI-X4 reached 50% inhibition even at the highest concentration tested (100 µM) which is in line with the results obtained in section 3.2.2 for murine B and T cells. While AMD3100 and JM#21 inhibited CXCL12 induced pAkt and pErk almost completely at 100 µM, JM#29 M8L reduced pAkt and pErk only by around 60% and 55%, respectively. JM#173 showed inhibitory activity of pAkt with around 75% inhibition at 100 µM but was less active in inhibiting pErk (35%), which was already observed for other murine cells tested in section 3.2.2. The fatty acid

derivative JM#143 inhibited pAkt and pErk levels by approximately 65% and 80%, respectively, at a concentration of 10 µM. Interestingly, while JM#198 led to an almost full inhibition of pAkt and pErk at 10 µM, JM#194 did not reach 50% of inhibition for both. Strong differences in antagonizing CXCL12 mediated signaling upon binding to mCXCR4 have already been observed for JM#194 in section 3.2.2 where 10 µM was also not sufficient in inhibiting pErk in BW5147 cells and less effective in A20 cells.

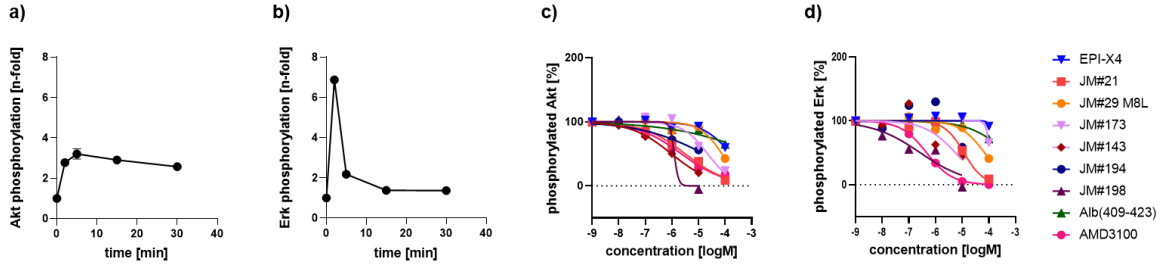


Figure 25. CXCL12 induced Akt and Erk phosphorylation in splenocytes derived from an Eµ-TCL1 mouse model is downregulated by advanced EPI-X4 derivatives in a dose-dependent manner. (a,b) Murine splenocytes were stimulated with 100 ng/ml CXCL12 for different time frames before intracellular levels of pAkt and pErk were analyzed using flow cytometry. Shown data are derived from n=1 experiment, performed at least in triplicates ±SEM. (c,d) Dose-response curves of pAkt and pErk, respectively, for splenocytes pretreated with different concentrations of compounds prior CXCL12 stimulation (100 ng/ml, 2 min). Analysis was done using flow cytometry. Shown data are derived from n=1 experiment, performed at least in duplicates.

Taken together, I showed that EPI-X4 derivatives efficiently target CXCR4 on MCL and CLL cells. Especially the fatty acid derivatives JM#143 and JM#198 were highly active on human CXCR4 and murine CXCR4 *in vitro* and are therefore promising candidates for further preclinical studies.

3.4 Further optimization strategies for EPI-X4 derivatives.

Although fatty acid coupled derivatives are very efficient in antagonizing CXCL12 mediated cell signaling and have improved systemic half-lives, the current lead derivative JM#198 is still not an ideal candidate for the treatment of chronic diseases, such as cancer, as its activity *in vivo* is still lost after 24 h[212]. I herein designed next-generation EPI-X4 derivatives using different optimization strategies: (1) coupling derivatives to the polymer polyethylene glycol (PEG) and albumin binders and (2) the attachment of dicarboxylic acids resulting in diacid variants of EPI-X4 and tested their efficacy and stability *in vitro* and *in vivo*.

3.4.1 PEGylation of JM#173 and JM#29.

Systemically applied peptides tend to be rapidly eliminated by the kidneys as already shown for JM#21[212]. Strategies to overcome this challenge are e.g. (1) conjugation to binders for albumin, the most prevalent plasma protein with a half-life of almost 3 weeks and (2) conjugation to polymers, e.g. polyethylene glycol (PEG). The concept and success of peptide modifications by PEG coupling is known for over 40 years. Long PEG chains protect conjugates from enzymatic degradation and renal excretion by increasing the hydrodynamic volume of the compounds by binding water molecules[244–246]. Indeed, it has been shown for JM#21 that conjugation to PEG_5 (PEG with a molar mass of 5 kDa) and PEG_{20} (molar mass of 20 kDa) results in prolonged plasma stability compared to the peptide alone[212,227]. In addition, coupling of JM#21 to the known albumin binder cholesterol via a PEG_5 linker showed increased plasma stability[212,227]. However, neither the PEG_{20} nor the Cholesterol coupled peptide remained active after 4 h *in vivo*[212]. In order to build up on these findings and further optimize EPI-X4 derivatives, I designed several conjugates using the most active N-terminal modified variants JM#29 and JM#173 (Table 10, Figure 26). The conjugates were synthesized by the group of Prof. Zelekin at Aarhus University. For conjugation, the reactive cysteine thiol group in the sequence of JM#29 or a C-terminally added cysteine thiol group in the sequence of JM#173 (JM#173-C) (highlighted in Figure 26a) have been used for the conjugation of PEG linkers (Figure 26b). As it is thought that homo- and heterodimerization of CXCR4 contributes to the differences in CXCR4 mediated signaling[247–249], peptide conjugates have been generated as monovalent and divalent molecules. Divalent molecules were equipped with two peptide copies equipped either on the same termini or opposite termini of the PEG, resulting in Y-shaped or telechelic variants, respectively. In addition, both peptides have been linked to cholesterol and trityl, to known albumin binders, via a PEG_5 linker (Figure 26b)[212,227,250].

Table 10. Peptide conjugates used and designed in this study.

Compound	Conjugate	Chemistry	Valency	Molecular weight [Da]
		JM#29 conjugated variants		
1	**MeO-Peg5kDa-JM#29**	maleimide	monomer	6673
2	**TrtS-Peg5kDa-JM#29**	maleimide	monomer	6598
3	**Chol-Peg5kDa-JM#29**	*bis*-sulfone	monomer	7000
4	**MeO-Peg20kDa-JM#29**	maleimide	monomer	21673
5	**JM#29-Peg20kDa-JM#29**	maleimide	telechelic dimer	23228
6	**MeO-Peg20kDa-bis-JM#29**	*bis*-sulfone	Y-shaped dimer	23228
		JM#173 conjugated variants		
7	**MeO-Peg5kDa-JM#173**	maleimide	monomer	6257
8	**TrtS-Peg5kDa-JM#173**	maleimide	monomer	6184
9	**Chol-Peg5kDa-JM#173**	*bis*-sulfone	monomer	6584
10	**MeO-Peg20kDa-JM#173**	maleimide	monomer	21257
11	**JM#173-Peg20kDa-JM#173**	maleimide	telechelic dimer	22396
12	**MeO-Peg20kDa-bis-JM#173**	*bis*-sulfone	Y-shpaed dimer	22436

MeO = methoxy-, TrtS =trityl-, Chol = cholesterol, Peg = polyethylene glycol

All generated compounds were tested for CXCR4 binding by performing the antibody competition assay as described before. IC_{50} values were obtained for each compound by performing the non-linear regression model using GraphPad Prism (Table 11).

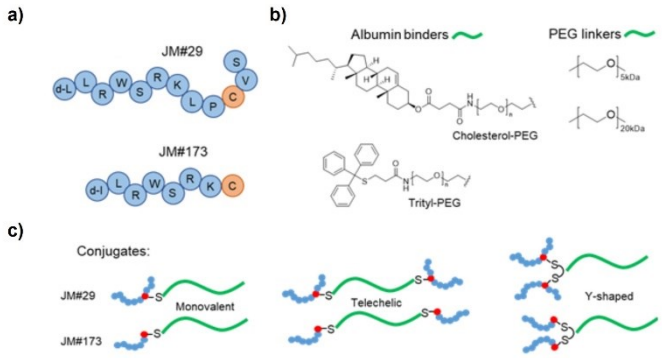


Figure 26. Schematic illustration of JM#29 and JM#173 conjugates designed in this study. a) Sequence of JM#29 and JM#173-C with the amino acid used for conjugation highlighted in orange b) Chemical structures of albumin binders cholesterol-poly(ethylene glycol) (PEG) and trityl-PEG (TrtS), both equipped with PEG_5 and synthetic PEG linkers (PEG_{20} and PEG_5) c) Schematic illustration of designed conjugates as monovalent or divalent variants (telechelic and Y-shaped). As author modified from Harms *et al.* (2023)[221] (CC BY-NC-ND 4.0, https://creativecommons.org/licenses/by-nc-nd/4.0/)

Although CXCR4 binding was detected for all compounds (Figure 27), conjugation with either TrtS-PEG or synthetic PEG linkers (both, PEG_{20} and PEG_5) led to a decreased binding activity demonstrated by higher IC_{50} values (Table 11), independent of the coupled peptide. Only the peptides conjugated to cholesterol-PEG remain as active as or slightly more active as the uncoupled peptide with IC_{50} values of 220 nM (**9**) and 227 nM (JM#173), and 238 nM (**3**) and 568 nM (JM#29), respectively. However, these variants were toxic at high concentrations (Figure 27c).

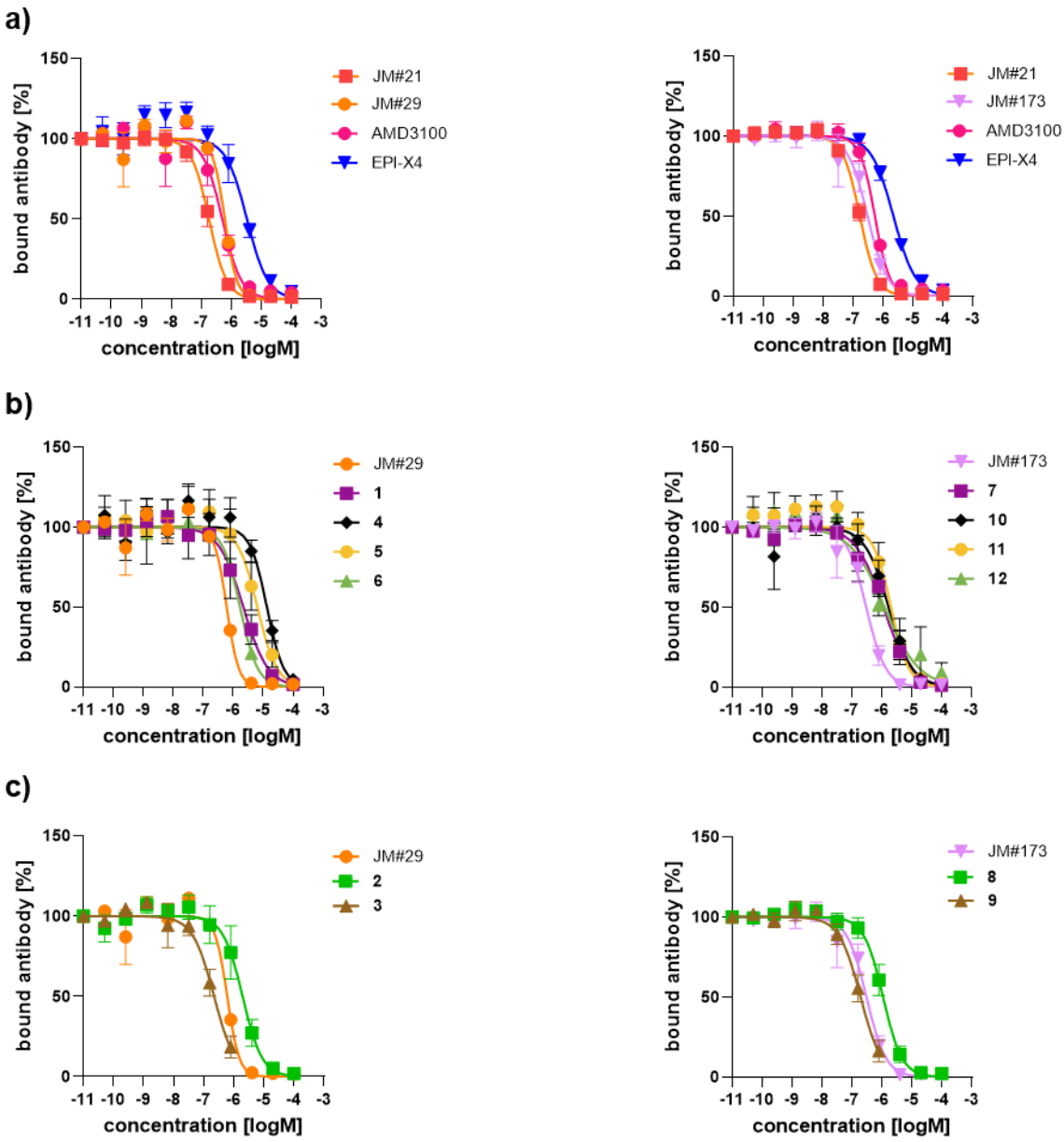


Figure 27. Polymer conjugates of JM#173 and JM#29 bind to CXCR4 with lower affinity than the unconjugated peptides. 50,000 SupT1 cells were seeded and pre-cooled at 4°C. Serially diluted compounds were applied to the cells together with a constant concentration of the APC-coupled CXCR4 antibody (clone 12G5) and incubated for 2 h at 4°C. Afterwards, unbound antibody was removed, and cells were analyzed using flow cytometry. Shown are dose-response curves for (a) controls and unconjugated peptides, (b) peptides conjugated to polyethylene glycol (PEG) and (c) peptides coupled to albumin binders. Shown data are derived from n=3 individual experiments ± SEM.

For both peptides, the Y-shaped PEGylated variants were 8-fold (**6**) or 2-fold (**12**) more active than their monovalent counterparts. Surprisingly, almost all conjugated peptides showed enhanced activities in the presence of plasma proteins (Supplement Figure 4, Table 11). The activity of the telechelic version of JM#29 (**5**) was approximately 10-fold enhanced in the presence of plasma proteins and thus as active as the unconjugated version. Also, its monovalent variant (**4**) showed an 8-fold increased activity in human plasma. The enhancing effect was slightly lower for the respective JM#173 conjugates with around 5-fold (**11**) and 3-fold (**10**) enhancement in the presence of plasma proteins.

In order to determine peptide stability in human plasma, I applied a previously described assay based on the antibody competition assay[212,220]. This has been shown to be not only a fast alternative to the time-consuming quantification of peptides present in human plasma by mass spectrometry but also to allow the evaluation of stability of e.g. albumin bound peptides or very large peptides like polymer-coupled ones[212,220,249]. Conjugates were spiked into 100% human plasma at a final concentration of 20 µM and incubated at 37°C. Aliquots were taken immediately (t=0), or after 2 h and 8 h, respectively, and stored at -80°C. To determine CXCR4 binding activities, aliquots were thawed in parallel and applied to the antibody competition assay. Remaining activity to compete with the antibody was determined based on the generated dose-response curves (Supplement Figure 5) and the corresponding area under the curves (AUCs) as described in section 2.2.7.1.

As expected from previously published data, JM#29, JM#173 and AMD3100 remained active after 2 and 8 hours of plasma incubation (Figure 28a and b) while EPI-X4 and JM#21 lost binding activity[212,219,220,227,251]. For the JM#29 conjugated variants, no loss of activity was observed, even after 8 hours of plasma incubation. Indeed, enhanced activity after plasma incubation was detected for all JM#29 conjugated variants with up about 3-fold increased activity compared to t=0 hours for the monovalent version equipped with a PEG_{20}. In contrast to that, all JM#173 coupled variants, except for variant **7**, lost activity over time (Figure 28, Table 11).

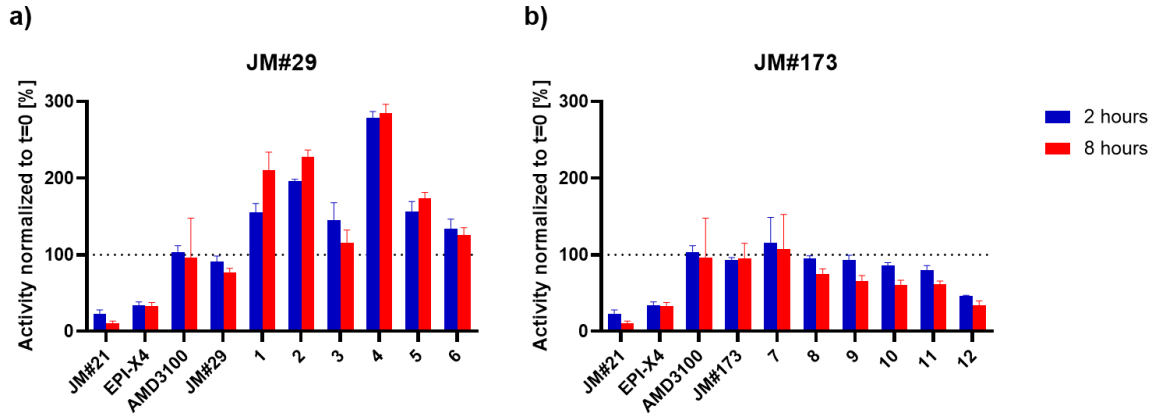


Figure 28. Activity of JM#29 and JM#173 conjugated variants upon incubation in human plasma. JM#29 (a) and JM#173 (b) conjugates were spiked into full human plasma reaching a final concentration of 20 µM. Mixtures were incubated at 37°C and aliquots taken at given time points. Activity of each aliquot was determined in parallel using the antibody competition assay. For this, aliquots were serially diluted and applied to SupT1 cells along with a constant concentration of the CXCR4 antibody (clone 12G5) as described before. Remaining activities were calculated based on the areas under the curve (AUCs) of the dose-response curves (AUC (t=0)/AUC(t=x)*100). Shown are remaining activities after 2 hours (blue) and 8 hours (red) determined by n=3 individual rounds of plasma incubation ±SEM.

Table 11. Overview of JM#29 and JM#173 conjugates designed in this study.

Compound	[a]IC_{50} [nM] ± SEM of 12G5 competition		[b]n-fold enhancement	[c]Remaining activity after plasma incubation [%]	
	Phosphate buffered saline (PBS)	Plasma		2 hours	8 hours
Controls					
EPI—X4	2800 ± 614	1049 ± 220	2.7	34 ± 2	33 ± 3
JM#21	189 ± 31	54 ± 9	3.5	23 ± 3	10 ± 2
JM#29	568 ± 42	151 ± 7	3.8	91 ± 4	77 ± 3
JM#173	227 ± 91	110 ± 17	2.1	94 ± 2	95 ± 11
AMD3100	487± 59	376 ± 49	1.3	104 ± 5	96 ± 30
JM#29 conjugated variants					
1	2217 ± 1166	948 ± 203	2.3	156 ± 6	210 ± 14
2	2106 ± 928	1012 ± 131	2.1	196 ± 2	228 ± 5
3	238 ± 71	583 ± 76	0.4	145 ± 13	116 ± 9
4	13234 ± 3164	1643 ± 114	8.1	279 ± 5	284 ± 7
5	7817 ± 4587	740 ± 109	10.6	156 ± 8	174 ± 4
6	1685 ± 104	285 ± 57	5.9	134 ± 7	126 ± 5
JM#173 conjugated variants					
7	1231 ± 416	1239 ± 220	1.0	115 ± 19	108 ± 26
8	1165 ± 320	436 ± 13	2.7	95 ± 2	74 ± 4
9	220 ± 81	416 ± 47	0.5	93 ± 4	65 ± 4
10	1850 ± 607	537 ± 45	3.4	86 ± 2	60 ± 4
11	2226 ± 677	416 ± 48	5.3	80 ± 3	62 ± 2
12	971 ± 182	212 ± 9	4.6	46± 1	34 ± 4

[a]IC_{50} values of n=3-6 individual experiments (±SEM) performed in singlicates of compounds spiked in PBS and 100% human plasma, respectively. [b]N-fold enhancement determined by IC_{50} values in PBS/ IC_{50} values in Plasma [c]Remaining activity was determined by antibody competition assay of compounds incubated in 100% human plasma and calculated by AUC (t=0)/AUC(t=x)*100.

Since cholesterol-PEG conjugated peptides were cytotoxic at high concentrations, they were excluded from further *in vivo* experiments. Retention of apparent peptide activities after 4 h of blood circulation was analyzed for the other Albumin binders (**2** and **8**) and the monovalent PEGylated variants (**4** and **10**) as they were the most active conjugates, as well as the telechelic PEGylated variants (**5** and **11**) which showed activity in the presence of plasma proteins. Additionally, remaining peptide activity after blood circulation was determined on the most stable JM#173 conjugate (**7**).

Handling of animals was performed by the Department of Nuclear Medicine (Ulm University Medical Center). Apparent peptide activity in plasma was analyzed by me. First, compounds were injected into the tail vein of SCID mice (700 µg compound in 100 µl NaCl). After 4 hours, mice were sacrificed, and blood obtained by heart punctuation (Figure 29a). Blood plasma was obtained by centrifugation and analyzed for apparent activity of contained peptides for their activity to compete with the 12G5 antibody for receptor binding as described above. Compared to the control plasma without compound, some of the tested compounds remained active after a circulation time of 4 h *in vivo* (Figure 29b and c). Whereas for compounds **7** and **10** no activity was retained after 4 h *in vivo*, both TrtS-PEGylated variants (**2** and **8**) remained slightly active. A slight reduction in antibody binding and thus remaining activity was also detected for both telechelic variants (**5** and **11**) as well

as for the monovalent variant of JM#29 (**4**). However, none of the tested variants showed sufficient *in vivo* stability and therefore further optimization is required in the future.

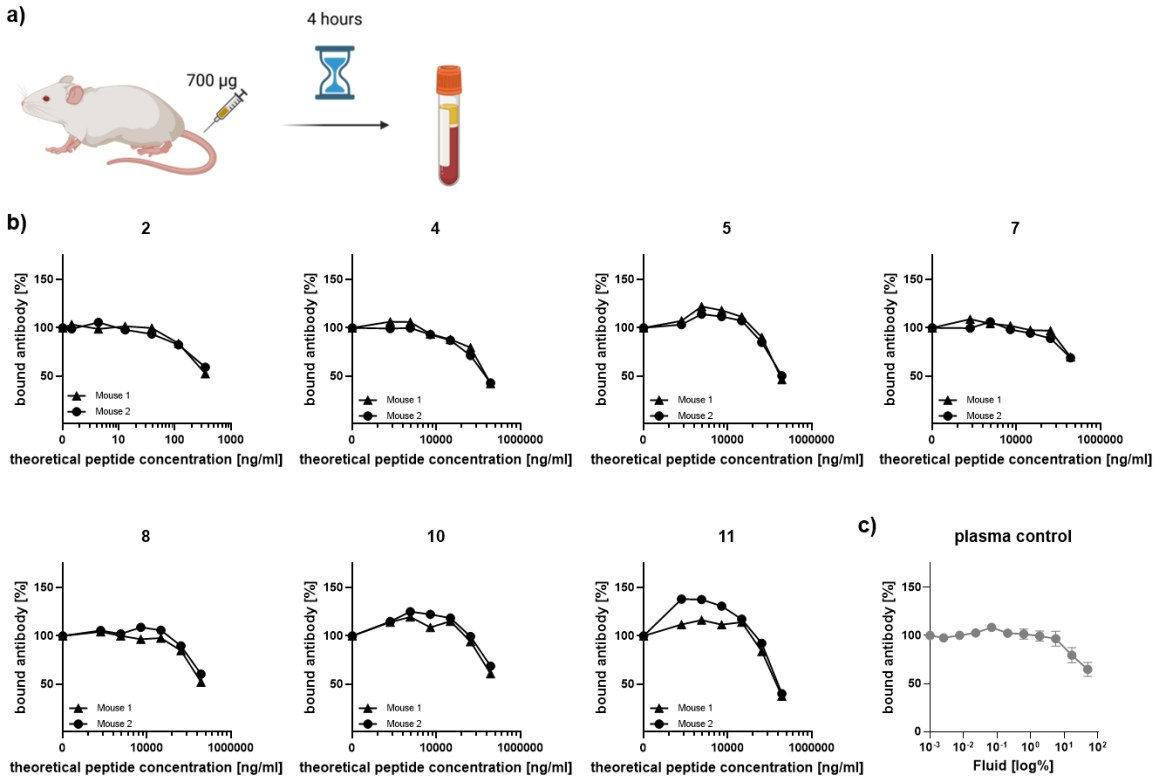


Figure 29. Peptide conjugates of JM#29 and JM#173 lose most of their activity after 4 hours of circulation *in vivo*. (a) 700 µg of conjugated peptides in 100 µl NaCl were injected into the tail vein of severe combined immune deficiency (SCID) mice. 4 hours later, mice were sacrificed, and blood collected by heart punctation. Plasma was obtained by centrifugation and stored at -80°C until remaining activity was determined in the antibody competition assay. For this, plasma was serially diluted in precooled PBS and applied to cells simultaneously with a constant concentration of CXCR4 antibody clone 12G5 as described above. Each data point is derived from one individual mouse measured in duplicates (b) or n=4 plasma controls (c) measured in duplicates ±SEM. Schematic in (a) created with BioRender.com, printed with the permission according to Biorender Academic License Terms (https://biorender.com/terms/).

3.4.2 Diacid variants

Another possible strategy to increase *in vivo* half-lives of therapeutics is their conjugation to long chain fatty acids. This has already been successfully done for EPI-X4 derivatives (JM#143, JM#194 and JM#198), and has also been applied to other therapeutics, which are already in clinical use[252]. For the GLP-1 analogue semaglutide, which has been approved in 2017 for subcutaneous application[253] and in 2019[254] as an oral drug, a long chain fatty diacid instead of a monoacid has been used for conjugation. Dicarboxylic fatty acids have a stronger affinity to human serum albumin[226] and thus, can result in longer circulation half-lives of conjugated peptides. Compared to its monoacid bound precursor Liraglutide, Semaglutide has a much longer *in vivo* half-life of 168 hours when applied subcutaneously[252] and can therefore be applied as a once-weekly administration [225,226].

Accordingly, I herein designed several optimized derivatives of JM#21 with or without protected N-terminus with a d-leucin. Long-chain fatty diacids of either 16 (C16) or 18 (C18) carbon atoms have been linked via the side chain of lysine in the peptides' sequences, either directly or via spacers: glutamic acid (Glu) or 8-amino-3,6-dioxaoctanic acid (2xOEG) (Table 12). EPI-X4 derivatives linked to monocarboxylic acids via a glutamic acid linker were shown to be more active than without linker, most likely to a lower steric hindrance by albumin[212,218]. All generated compounds were then tested for their binding affinity to CXCR4 and anti-CXCR4 activities in different assays and compared to the unconjugated JM#21 as well as to their monoacid counterparts JM#143 (C16), JM#194 (C16) and JM#198 (C18), respectively.

Table 12. Sequences of the diacid variants designed within this study.

Compound	Sequence
C16 diacid	
JM#226	ILRWSRK(-C16diacid)LPCVS
JM#227	ILRWSRK(-Glu-C16diacid)LPCVS
JM#244	ILRWSRK(-C16diacid)-NH_2
JM#246	ILRWSRK(-Glu-C16diacid)-NH_2
JM#248	(d-L)LRWSRK(-C16diacid)-NH_2
JM#250	(d-L)LRWSRK(-Glu-C16diacid)-NH_2
C18 diacid	
JM#228	ILRWSRK(-C18diacid)LPCVS
JM#229	ILRWSRK(-Glu-C18diacid)LPCVS
JM#230	ILRWSRK(-2xOEG-Glu-C18diacid)LPCVS
JM#245	ILRWSRK(-C18diacid)-NH_2
JM#247	ILRWSRK(-Glu-C18diacid)-NH_2
JM#249	(d-L)LRWSRK(-C18diacid)-NH_2
JM#251	(d-L)LRWSRK(-Glu-C18diacid)-NH_2

Glu = glutamic acid, NH2 = amidated C-terminus, OEG = oligo(ethylene glycol)

Binding to CXCR4 was analyzed by the 12G5 antibody competition assay as described before. As shown in Figure 30a, all tested compounds bind to CXCR4 with the exception of the inactive control Alb(409-423). While all tested monoacidic controls were as active as described before[197,212,219,220,227], the diacid variants were in general less active than their monoacidic counterparts. Stronger binding affinities were detected for the C16 variants compared to the C18 variants. The amidated and truncated versions of the C18 diacid variants (JM#245, JM#247, JM#249 and JM#251) revealed stronger binding affinity to CXCR4 than the C18 variants without N-terminal modifications (JM#228, JM#229, JM#230). For C18 diacid variants, stronger binding activity in the presence of glutamic acid linker was only detected between JM#228 (no linker) and JM#229 (glutamic acid linker). Introduction of the 2xOEG linker (JM#230) did not alter the binding activity compared to JM#229 (glutamic acid linker) but was slightly more active than the variant without any

linker (JM#228). No changes were observed for variants with the first amino acid replaced by d-L compared to the variants without this C-terminal substitution. Through their binding to CXCR4, EPI-X4 derivatives were shown to prevent the entry of X4-tropic HIV-1 into target cells[197,212,219,220,227]. In order to see whether the entry can be blocked by diacid variants of EPI-X4 their anti-HIV-1 activity was evaluated. For this TZM-bl reporter cells were used, which not only express the required co-receptor for viral entry (CXCR4) but also β-galactosidase, when infected by HIV-1. Cells were pretreated with serially diluted compounds for 10 min before inoculated with HIV-1. Three days post infection, cells were lysed, and the infection quantified by the conversion of the applied substrate by β-galactosidase. All tested compounds inhibited HIV-1 infections in a dose-dependent manner with the exception of Alb(409-423) (Figure 30b). Again, all diacid variants were less active than their monoacidic counterparts and the C16 diacid variants were more active than the C18 diacid variants. Here, no differences between the C16 diacid variants with (e.g. JM#227) or without the glutamic acid linker (e.g. JM#226) were detected. The same was shown for the C18 diacid variants JM#245 and JM#247. While the addition of a glutamic acid linker increases the activity in the non-truncated C18 diacid variant JM#229 in comparison to JM#228 (no linker), the activity of the truncated and amidated C18 diacid variant JM#251 (glutamic acid linker) is lower than in its counterpart without linker (JM#249).

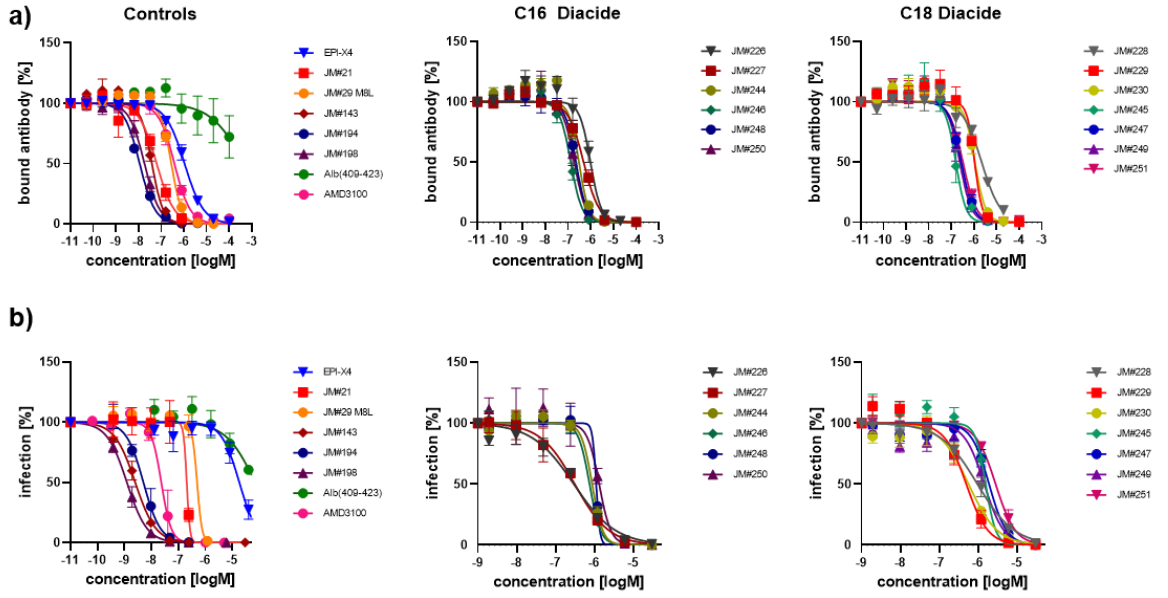


Figure 30. Diacid variants of EPI-X4 bind to CXCR4 and inhibit infections with human immunodeficiency virus-1 (HIV-1). (a) C16 and C18 diacid variants and respective controls were applied to SupT1 cells together with a constant concentration of APC-labelled CXCR4 antibody (clone 12G5). After 2 hours at 4°C, unbound antibodies were removed, and bound antibodies analyzes via flow cytometry. (b) Same variants were applied to the HIV-reporter cell line TZM-bl seeded the day before and pre-incubated for 10 min before inoculated with HIV-1 strain NL4-3. Three days post infection, a β-galactosidase assay was performed to determine infection rates. Signal from uninfected controls was subtracted and values normalized to the infected control without compound. Shown are data derived from at least n=3 individual experiments performed in triplicates ± SEM.

Afterwards, inhibitory activities of compounds were determined on intracellular Akt and Erk phosphorylation (Figure 31a and b, respectively). With the exception of Alb(409-423), all controls showed a dose-dependent reduction of CXCL12-induced pAkt and pErk levels. In agreement with binding activity and the inhibition of HIV-1 infections, all tested diacid variants were less active than their monoacidic counterparts. While a reduction of >50% was observed at a concentration of 1 µM for the monoacidic variants, the same concentrations did not reach 50% of inhibition for diacid variants. Indeed, while a concentration of 10 µM was sufficient to completely block CXCL12 mediated pAkt and pErk in the monoacid variants, some of the diacid variants e.g. JM#226 (C16) and JM#228 (C18) did not fully inhibit CXCL12 induced Akt and Erk phosphorylation. Higher antagonistic properties were detected for C16 diacid variants with the glutamic acid linker (JM#246 and JM#227) compared to their counterparts without glutamic acid linkers (JM#244 and JM#226). In contrast, for C18 diacid variants the glutamic acid linker increased antagonistic activities for JM#229 (glutamic acid linker) compared to JM#228 (no linker) for pErk and for JM#247 (glutamic acid linker) compared to JM#245 (no linker) for pAkt. A decreased activity was observed for the linker variants JM#247 (pErk) and JM#251 (pAkt and pErk) compared to their counterparts JM#245 and JM#249. Interestingly, while the addition of the 2xOEG linker in JM#230 did not affect both assays described above, it decreased the efficacy for antagonizing CXCL12 mediated Akt and Erk phosphorylation. Summarized, neither the C16 not the C18 diacid variants were as active as or more active than their monoacid counterparts JM#143, JM#194 and JM#198. Nevertheless, all diacid variants were more active than AMD3100 as well as JM#21 and JM#29 M8L. A decrease in activity for diacid compounds compared to monoacid compounds was already described before[226] and was thus partly expected.

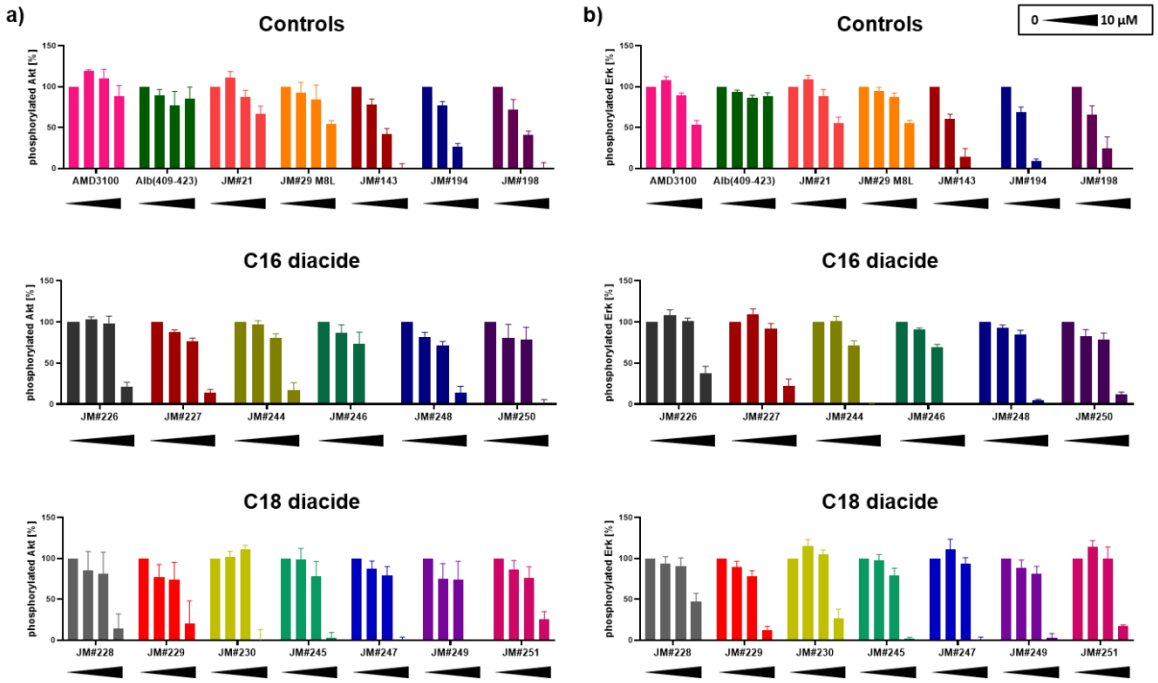


Figure 31. Diacid variants of EPI-X4 antagonize CXCL12 stimulated phosphorylation of Akt and Erk. SupT1 cells were pre-treated with diacid variants in different concentrations for 10 min. Afterwards, cells were stimulated with 100 ng/ml CXCL12 for 2 min before reaction was stopped by the addition of 10% PFA. Cells were permeabilized and stained for intracellular pAkt and pErk and analyzed via flow cytometry. Shown are the relative levels of phosphorylated Akt (a) and phosphorylated Erk (b) after background subtraction and normalization to cells stimulated with CXCL12 in the absence of any CXCR4 targeting compound. Data are derived from n=3 individual experiments, performed at least in triplicates, ± SEM.

In order to test the *ex vivo* stability of the variants, they were spiked into human plasma and their remaining activity was determined by the antibody competition assay as describe above (Supplement Figure 6). As depicted in Figure 32, all diacid variants are highly stable in human plasma with almost no detectable degradation. Only the C16 diacid variants JM#244 and JM#246 slightly lose their activity after 8 hours of plasma incubation (Table 13). In contrast to their monoacidic counterparts and except for JM#244 all diacid variants have reduced binding activities in the presence of plasma proteins. Nevertheless, truncated and amidated variants showed activity in the nM ranges (Table 13). However, all variants with a longer peptide sequence showed declined IC_{50} values independent of the use of the glutamic acid linker or not. Overall, the C16 diacid peptides were more active in the presence of plasma proteins than the C18 diacid variants, where only the two truncated and amidated variants without any linker, JM#245 and JM#249, showed activity below an IC_{50} value of 10 µM. Thus, especially for the C18 diacid variants, the use of a glutamic acid linker or the 2xOEG linker negatively influence the activity of the diacid variants. Nevertheless, the most stable C16 variants with activities in the nM range in the presence of plasma proteins were selected for the evaluation *in vivo*: JM#246, JM#248 and JM#250. In addition, both C18 diacid variants with an activity below 10 µM were tested: JM#245 and JM#249.

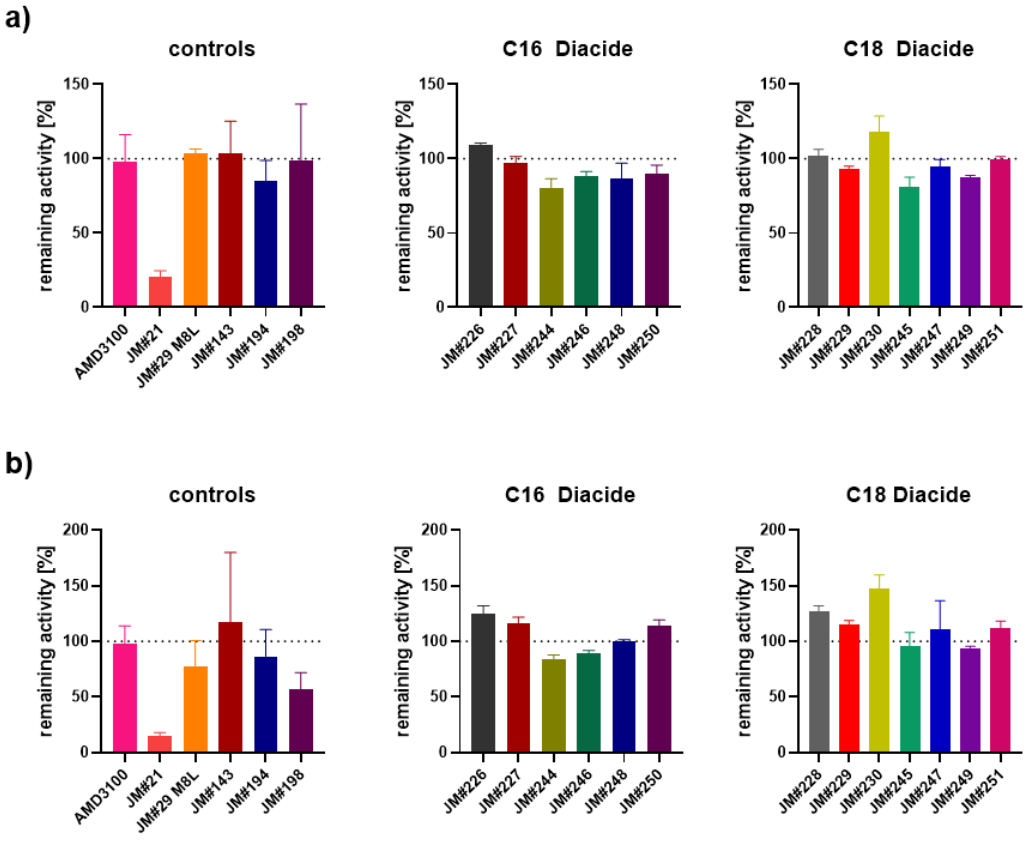


Figure 32. Activity of diacid variants after incubation in human blood plasma. Diacid variants of EPI-X4 and respective controls were spiked into full human plasma reaching a final concentration of 20 µM. Mixtures were incubated at 37°C and aliquots taken after given time points. Remaining activity of each aliquot was determined using the antibody competition assay. Shown are apparent activities after 2 h (a) and 8 h (b) derived from at least n=3 individual rounds of spiking ± SEM.

Prior the *in vivo* analyses, the toxicity of the diacid variants was evaluated *in vitro*. For this, cells were treated with different concentrations of diacid variants and respective controls for 24 h. Relative toxicity of the used compounds was then determined using flow cytometry and normalized to cells which were killed before at 65°C for 10 min. As illustrated in Figure 33, only JM#228 killed approximately 21% of the cells at the highest concentration tested (30 µM). Toxic effects have also been observed for the monoacid variants JM#143, JM#194 and JM#198 leading to a decrease of living cells of around 17%, 9% and 36%, respectively, at a concentration of 30 µM. Notably, none of the peptides revealed toxic effects at lower concentrations.

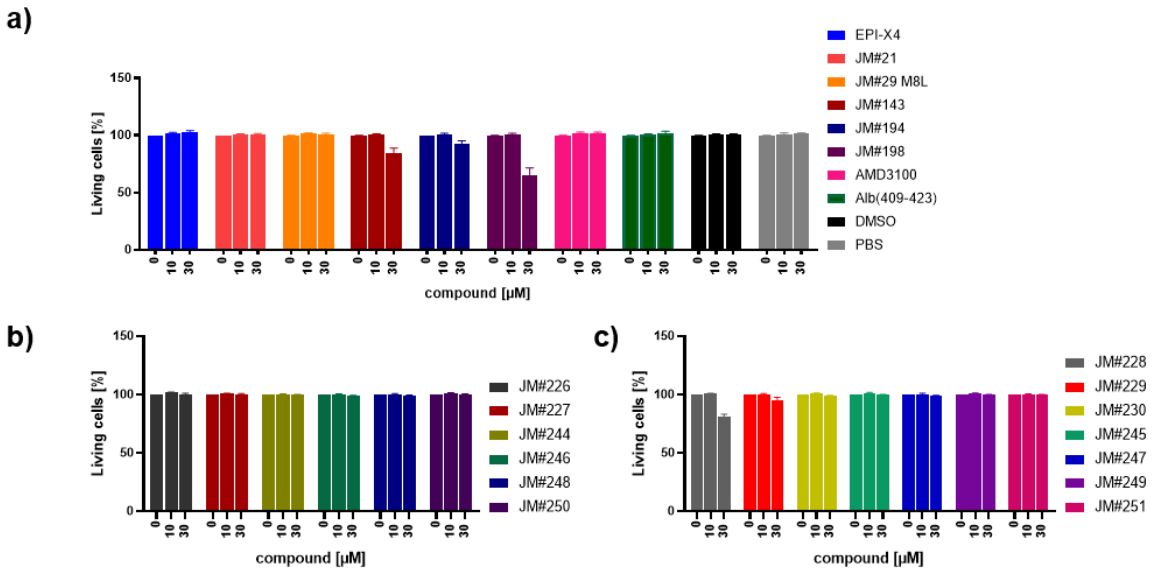


Figure 33. Most diacid variants are not toxic at concentrations > 10 µM. SupT1 cells were treated with different concentrations of diacid variants of EPI-X4 or respective controls for 24 h. The next day, compounds were removed, and death cells stained using a fixable viability stain and analyzed in flow cytometry. Shown are the percentage of living cells for controls (a), C16 diacid variants (b) and C18 diacid variants (c) determined from n=3 individual experiments, each performed in singlicates, ± SEM.

Table 13. Activities of diacid EPI-X4 variants.

Compound	12G5[a]		n-fold IC_{50} in plasma[b]	HIV-1 inhibition[c]	Activity after plasma incubation [% ± SEM]	
	in PBS	in Plasma				
	IC_{50} ± SEM [nM]			IC_{50} ± SEM [nM]	2 hours	8 hours
Controls						
EPI-X4	1103±217	n.d.	n.d.	19713±6862	n.d	n.d.
JM#21	55 ± 14	52 ± 15	1.0	153 ± 36	20±4	14 ± 3
JM#29 M8L	291 ± 59	120 ± 22	2.4	747 ± 196	103 ± 3	78 ± 23
JM#143	39 ± 4	2 ± 1	18.9	3 ± 1	104± 21	117±63
JM#194	11 ± 1	1 ± 0	13.8	6 ± 3	85 ± 14	86 ± 24
JM#198	19 ± 4	3 ± 2	6.4	1 ± 0	98 ± 38	56 ± 15
AMD3100	388 ± 100	541± 117	0.7	21 ± 11	98 ± 18	97 ± 16
Alb(409-423)	>100 000	n.d.	n.d.	>50 000	n.d.	n.d.
C16 diacid						
JM#226	959 ± 219	>10 000	n.d.	268 ± 52	109 ± 2	124 ± 8
JM#227	508 ± 118	9122± 1089	0.1	267 ± 58	97 ± 5	116 ± 5
JM#244	302 ± 39	126 ± 25	2.4	854 ± 135	80 ± 6	84 ± 4
JM#246	126 ± 22	270 ± 44	0.5	783 ± 137	88 ± 3	89 ± 3
JM#248	208 ± 21	220 ± 24	0.9	929 ± 102	87 ± 10	100 ± 1
JM#250	187 ± 36	774 ± 268	0.2	984 ± 296	90 ± 6	114 ± 5
C18 diacid						
JM#228	2164 ± 259	>10 000	n.d.	1012 ± 390	102 ± 4	127 ± 5
JM#229	1054 ± 66	>10 000	n.d.	533 ± 145	93 ± 1	115 ± 4
JM#230	1115 ± 180	>10 000	n.d.	491 ± 144	118 ±10	147±13
JM#245	178 ± 53	1301 ± 546	0.1	1553 ± 115	81 ± 7	96 ± 12
JM#247	290 ± 70	>10 000	n.d.	1777 ± 334	95 ± 5	110±26
JM#249	270 ± 63	1047 ± 212	0.3	1160 ± 312	87 ± 1	94 ± 2
JM#251	327 ± 48	>10 000	n.d.	2913 ± 480	99 ± 2	112 ± 6

[a]Competition with a 12G5 antibody, [b]n-fold enhancement determined by IC_{50} values in PBS/ IC_{50} values in Plasma, [c]Inhibition of HIV-1 infection. Data represent means of n=3 individual experiments ± SEM, n.d. = not determined

To test the bioavailability of selected diacid variants, 70 µg of the compound diluted in 100 µl saline were injected into the tail vein of a C57BL6 mice. After 4 hours, mice were sacrificed, and blood obtained by heart punctation. Obtained plasma were then analyzed by me using the antibody competition assay as described before. Unfortunately, most of the tested compounds did not show any binding activity after 4 hours *in vivo*. A reduction of antibody binding above the background control was only observed for JM#250 in both mice tested (Figure 34a and c). Overall, none of the designed diacid variants was superior in comparison to the current lead derivative JM#198.

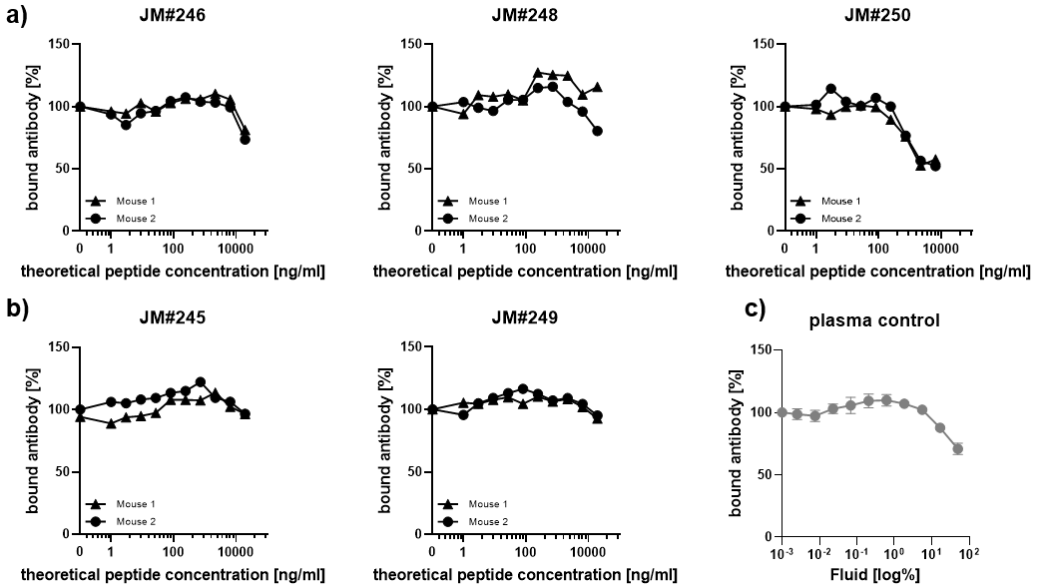


Figure 34. Most diacid variants lost their binding activity to CXCR4 after 4 h *in vivo.* 70 µg of compound was injected into the tail vein of C57BL6 mice. After 4 hours, mice were sacrificed, and blood obtained by heart punctation, and plasma collected after centrifugation and stored at -80°C. Remaining activity was determined by antibody competition assay. Shown are dose-response curves for C16 diacid variants (a), C18 diacid variants (b) and the plasma only control (c). Each datapoint represent mean values obtained from an individual mouse, or n=4 for plasma controls, measured at least in duplicates ± SEM.

3.5 Establishment of the HET-CAM model to determine peptide stability.

The hen's egg test – chorionallantoic membrane (HET-CAM) model is widely used in scientific research especially in the field of oncology including studying tumor growth and angiogenesis, but also for drug development especially in the evaluation of toxicity[255–258]. So far, to my knowledge, little is known about studying the stability of drugs *in vivo* using the HET-CAM model. In collaboration with the Department of Nuclear Medicine, Ulm University Medical Center, I herein established the HET-CAM model to determine plasma stability. For this purpose, we used chicken embryos which have reached at least development day 15, at which point the individual organ systems, such as the kidneys, are developed and discernible and blood volume is almost at maximum. Shortly, chicken eggs were incubated starting from embryo development day (EDD) 0 (Figure 36a) and the eggshell was opened on EDD2 (Figure 36b) and further incubated until EDD14. Then blood was taken from a prominent vessel of the CAM (Figure 36c), which is a highly vascularized membrane surrounding the chicken embryo within the hen egg[255], and blood plasma was obtained for further *ex vivo* analysis.

In order to see whether the enzymatic degradation of peptides is comparable between humans, mice and chicken blood plasma, I first analyzed the remaining activity of JM#21 after *ex vivo* incubation in plasma obtained from those different species. For this, JM#21 was spiked into 100 % of plasma and remaining peptide activity was determined using the antibody competition assay. Plasma samples were analyzed directly (0 min) and after 7.5 min, which is roughly the half-life of JM#21 in human plasma determined before[212,219]. As expected, spiking of JM#21 into human plasma led to a time dependent reduction of activity (Figure 35a) with IC_{50} values of 94 nM and 182 nM after 0 min and 7.5 min of plasma incubation, respectively. While the activity of JM#21 was lower in murine plasma (110 nM and 440 nM, respectively), it was as active in chicken plasma as in human plasma with IC_{50} values of 94 nM and 177 nM after 0 min and 7.5 min after plasma incubation, respectively. Indeed, the remaining activity of JM#21 was more equally between human plasma and chicken plasma with a remaining activity of around 60% in both species. In contrast to that, JM#21 lost its activity significantly faster in murine plasma, reflected by a remaining activity of only 30% after 7.5 min (Figure 35c). Interestingly, plasma derived from chicken embryos has a lower unspecific impact on antibody binding to CXCR4 than plasma derived from humans and mice (Figure 35b).

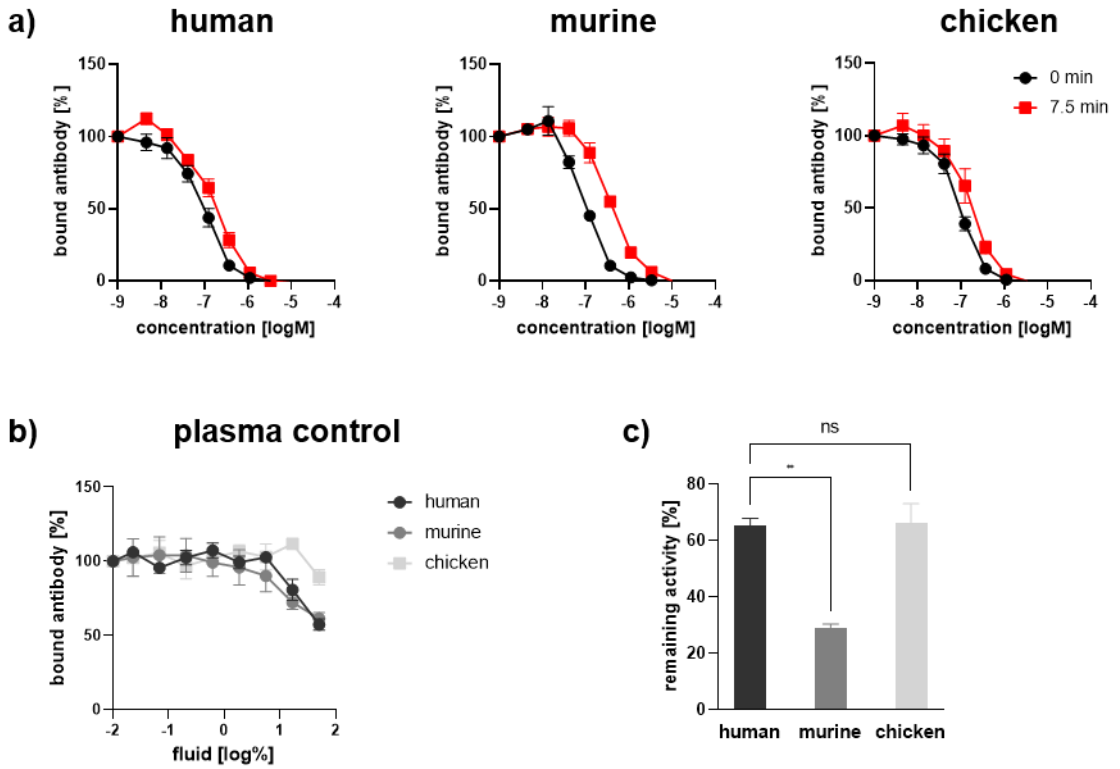


Figure 35. Activity of JM#21 after incubation in plasma derived from different species. JM#21 was spiked into plasma from mice, humans and chicken embryos reaching a final concentration of 20 µM. Plasma mixtures were incubated for 0 min and 7.5 min, and remaining activities determined using an antibody competition assay. Shown are dose-response curves for murine, human and chicken plasma spiked with JM#21 (a) or not (b). (c) Remaining activity was determined for each species by AUCs using GraphPad Prism and calculated with AUC(t=0)/AUC(t=x)*100. Significant differences were calculated using one-way ANOVA **=p<0.01, ns= not significant. Shown are data derived from n=3 individual rounds of spiking, measured in duplicates, ± SEM.

Next, I evaluated the bioavailability of the peptides after injection into the CAM of the chicken embryo. For this, peptides were injected into a prominent vessel of the CAM surrounding the chicken embryo at EED 15 or EED 16 (Figure 36d) and blood obtained after given timepoints. For comparative analysis, the same peptides at similar concentrations were injected into the tail vein of a C57BL6 mice as described before and blood obtained after given timepoints as well.

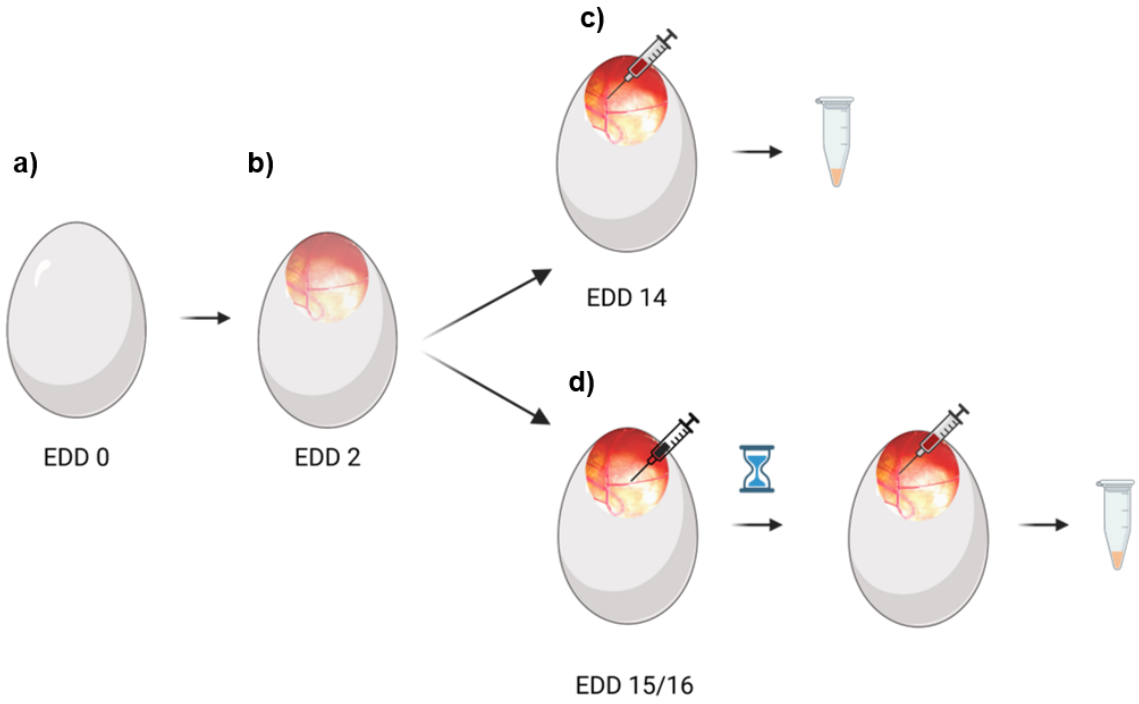


Figure 36. Schematic illustration of the hen's egg test – chorionallantoic membrane (HET-CAM) experiments performed in this study. (a) Chicken eggs were incubated starting from embryonic development day (EDD) 0 at 37.8°C and 65% relative humidity. (b) The eggshell was opened on EDD 2 and further incubated until (c) blood was taken on EDD 14 and plasma obtained for *ex vivo* analysis or (d) until EDD 15/16 where peptides were injected into a prominent vessel of the CAM. After given timepoints, blood was taken, and plasma obtained for the analysis of remaining activity using the antibody competition assay. Chicken egg handling was performed by Jessica Löffler and Gordon Winter (Department of Nuclear Medicine, Ulm University Medical Center). Figure was created with BioRender.com, printed with the permission according to Biorender Academic License Terms (https://biorender.com/terms/).

Remaining activity of the peptides in the obtained plasma was then analyzed using the antibody competition assay as described before. In accordance with already published data for mice[212], JM#21 strongly lost its activity already 10 min after the injection into the CAM (Figure 37a). While the bioavailability of JM#198 after 4 hours *in vivo* is comparable between mice and chicken embryos (Figure 37b and c) with remaining activities of 88% and 83%, respectively, differences were more pronounced after increasing circulation time. Eight hours post injection JM#198 remained an activity of 13.5% in mice and 41.5% in chicken embryos and 24 hours post injection in mice, JM#198 is almost inactive in the obtained plasma (1.8% remaining activity) while a remaining activity of 16% was still detectable in chicken plasma. Thus, JM#198 has a slightly longer circulation half-life in chicken embryos than in mice with half-lives of approximately 7 h and 5.5 h, respectively (Figure 37d). Overall, these data show, that the use of the chorioallantoic membrane surrounding the chicken embryo is a promising alternative to the mouse model for screening plasma stabilities of drugs.

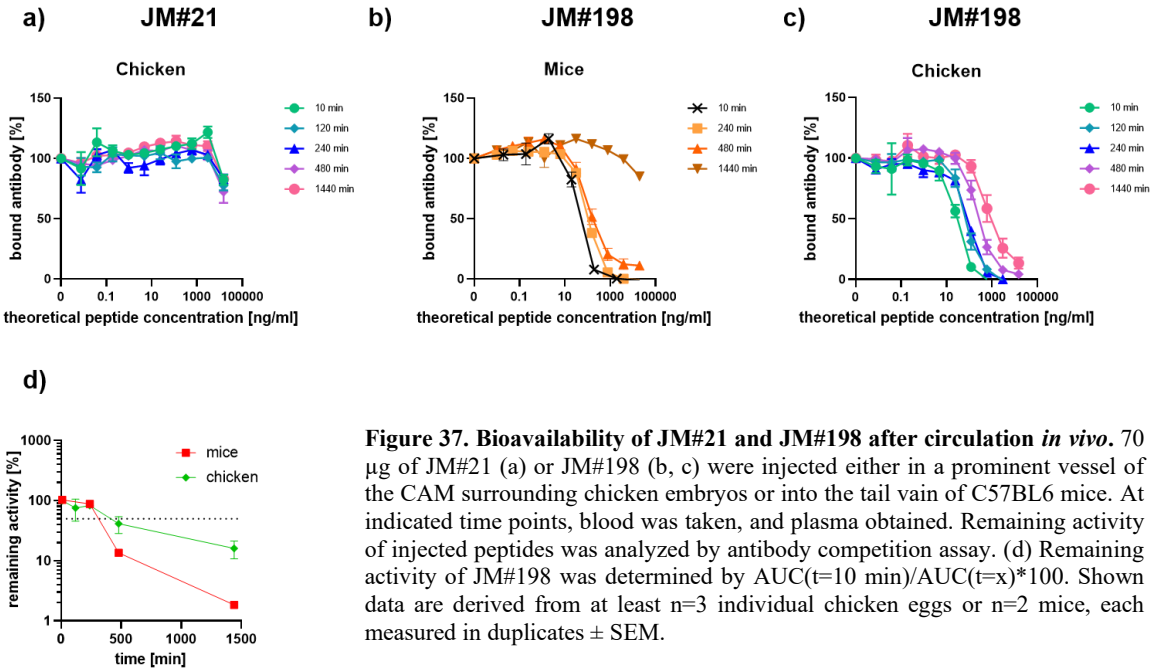


Figure 37. Bioavailability of JM#21 and JM#198 after circulation *in vivo*. 70 µg of JM#21 (a) or JM#198 (b, c) were injected either in a prominent vessel of the CAM surrounding chicken embryos or into the tail vain of C57BL6 mice. At indicated time points, blood was taken, and plasma obtained. Remaining activity of injected peptides was analyzed by antibody competition assay. (d) Remaining activity of JM#198 was determined by AUC(t=10 min)/AUC(t=x)*100. Shown data are derived from at least n=3 individual chicken eggs or n=2 mice, each measured in duplicates ± SEM.

4 Discussion

4.1 Pharmaceutical preparations of HSA do not contain EPI-X4.

EPI-X4, the natural antagonist of CXCR4, can be cleaved from its precursor human serum Albumin under acidic conditions by aspartic proteases like Cathepsin D and Cathepsin E[197]. Since it is the most abundant protein in the human plasma, loss of albumin or failure of albumin production through e.g. nephrotic syndromes or liver failures requires substitution by medicinal HSA to maintain its important function within the human body[198–203,205]. Medicinal HSA is obtained by purification of pooled human plasma using different fractionation processes and further stabilized by sodium caprylate and sodium acetyltryptophanate[200,201,205,206]. However, when administered intravenously, which is commonly done at doses of 20-100 g, side effects like anaphylactic reactions as well as complications in the renal, cardiac and respiratory system can occur but are very rare and only sporadic[259–262]. Until now, it has never been investigated whether these side effects could be related to EPI-X4, which might be generated during the production or storage of medical HSA and hence leading to an undesirable application into the human bloodstream. To answer this, I herein determined the presence of EPI-X4 in eight different medicinal HSA samples. In fact, none of the different samples contained detectable amounts of EPI-X4. Relevant concentrations of EPI-X4 were only detected after acidification and in the presence of aspartic proteases Cathepsin D and Cathepsin E. Based on these findings, it is assumed that EPI-X4 is not generated during the production or storage of medicinal HSA but can be generated within the human body under specific conditions. Therefore, it is unlikely that side effects are related to EPI-X4 in the HSA preparations. However, it has to be considered that EPI-X4 might be generated after administration and that the generation and degradation of EPI-X4 might be influenced by other drugs applied along with the HSA. In order to investigate this, information about patients have to be collected and analyzed for possible associations regarding the occurrence of side effects and their additionally applied medications. Overall, although not completely impossible, it is more likely, that the occurrence of side effects from medicinal HSA is more related to the patient's health status than the chemical properties of the HSA preparations.

4.2 EPI-X4 derivatives are antagonistically active on primary T cells.

CXCR4 is considered a promising drug and thus widely studied in the field of oncology. In addition, CXCR4 is expressed on immune cells and involved in (auto)immunological

diseases and contributes to the tumor microenvironment which facilitates the survival and growth of the tumor[59,62,63,66,81,263,264]. Since the endogenous peptide inhibitor of CXCR4 (EPI-X4) only has low activity, optimized derivatives were developed with improved CXCR4 antagonizing activity[75,212,218–221,227]. However, their efficacy in antagonizing CXCL12 mediated cell responses were mostly evaluated on SupT1 cells, a T-lymphoblastic cell line.

Immortalized cell lines are widely used in scientific research, e.g. for drug development, vaccine production and for studying biological processes. Compared to primary cells, they have the advantages to be less expensive, easy to handle and they can be propagated for a long time. However, it is important to consider that they might differ from primary cells not only phenotypically but also in their responsiveness to stimuli[265,266]. Indeed, differences in the efficacy of potential drugs have been determined for e.g. pentamidine. Whereas it was sufficiently active against melanoma cell lines, it was less potent in primary cell cultures[267]. Same was observed for bisphosphonates where cell lines were more sensitive to bisphosphonates than tumor-derived cells[268]. However, phenotypic differences were not only found between cancer cell lines and primary cancer cells, but also between malignant and healthy cells, on which CXCR4 is often overexpressed[68–73]. Thus, testing the efficacy of a drug on primary or malign cells is of high importance to estimate its therapeutic potential.

In my thesis, I studied the most promising previously developed EPI-X4 derivatives for their antagonistic efficacy on human primary CD4+ T cells which are important drivers of (auto)inflammatory diseases and contribute to the tumor microenvironment (TME). Indeed, I observed differences in the responsiveness to CXCL12 for immortalized cancer cell lines and primary CD4+ T cells.

In our previous studies it has been described that CXCL12 induces the phosphorylation of Erk in SupT1 cells by around 4-fold whereas an only barely induction for pAkt (~1.6x) was observed[212]. Here, I demonstrated that human primary CD4+ T cells were more responsive to CXCL12 reflected by an increase of pAkt and pErk of approximately 15-fold and 7-fold, respectively. These findings highlighted the differences between cell lines and primary cells as it is well-known that signaling pathways are altered in cancer cells. Indeed, overactivation and abnormal expression of pAkt and hence cancer cell proliferation and survival is a common molecular characteristic of human cancers, due to the expression of certain oncogenes and/or the loss of tumor suppressor genes, like PI3KCA (phosphatidylinositol-4,5-Bisphosphate 3-Kinase Catalytic Subunit Alpha) or Phosphatase and Tensin Homologe

(PTEN)[269]. Since it has been shown that cancer cells lacking PTEN expression, a negative regulator of the PI3K pathway, express constitutively activated Akt[270] and inactivating mutations of PTEN have been found in SupT1 cells[271], it is more likely that the herein showed differences in Akt phosphorylation are due to a constitutively activated pathway than an altered responsiveness to CXCL12. Although activating mutations of the Erk pathway are highly abundant in cancer cells, especially of its upstream molecules *ras* and *raf* [272], to my knowledge nothing is known about the mutation status of *ras* and *raf* in SupT1 cells. Due to the fact, that CXCL12 still stimulates pErk in SupT1 cells[212] but to a lower extend than in human primary CD4+ T cells, differences in phosphorylation levels of Erk between SupT1 cells and primary T cells are most likely due to a constitutively activated Erk signaling pathway and hence a reduced responsiveness to CXCL12.

Nevertheless, along with AMD3100, most tested advanced EPI-X4 derivatives were as active in competing with CXCR4 antibody clone 12G5 for receptor binding on CD4+ T cells as on SupT1 cells. Differences were only observed for the fatty acid coupled derivatives where the C16 variant JM#143 was around 5-fold more active in binding to CXCR4 expressed on CD4+ T cells than on SupT1 cells while its truncated version JM#194 were approximately 7-fold more active in competing for receptor binding on SupT1 cells than on CD4+ T cells. The C18 variants JM#198 was shown to bind stronger to CXCR4 expressed on SupT1 cells than on CD4+ T cells (56-fold) and showed also a slightly higher activity in antagonizing CXCL12 induced Erk phosphorylation on SupT1 cells than on CD4+ T cells (~2.5 fold). However, it can't be excluded that batch specific differences explain the observed differences in the binding activity. Although differences between human primary cells and cancer cell lines have been detected in their responsiveness to the stimuli CXCL12, no great difference in the efficacy of EPI-X4 derivatives have been detected and hence can be transferred to human primary CD4+ T cells demonstrating their potential therapeutic efficacy *in vivo*. However, dependent on their cancerous origin and CXCR4 expression levels, the efficacy might still differ between different cancer cell lines or primary cancer cells.

It might therefore be important to further evaluate their efficacy on other cancer types and, before applied clinically, also on freshly isolated patient cancer cells. Testing promising drug candidates for therapeutic potential is commonly done in animal models before conducting clinical trials in humans. This is of high impact since it has been shown that the efficacy of several drugs greatly differs between mice and humans. This was not only shown for CXCR4 antagonists like AMD3100 or FC-131[236–239], but also for other target specific drugs like

Maraviroc, a CCR5 antagonist[273], or betulinic acid derivatives, synthetic ligands of TGR5[274].

4.3 EPI-X4 derivatives are less efficient on murine cells than on human cells.

Although EPI-X4 and some derivatives have already been shown therapeutic potential in different mouse models[75,197,212,219], it is yet not known how efficient EPI-X4 and its optimized derivatives interact with murine CXCR4 (mCXCR4) compared to human CXCR4 (hCXCR4). Thus, testing these derivatives on murine cells is important, not only for the interpretation of the data but also for the correct estimation of the required applied concentrations of peptides *in vivo*. Although sharing a homology of 91%, the human CXCR4 antibody clone 12G5 is not able to bind to murine CXCR4 due to the differences in the amino acids shown to be crucial for antibody binding[235]. Even though the amino acids of CXCR4 involved in the binding of anti-CXCR4 clone 12G5 and EPI-X4 derivatives, respectively, are different, it is likely that binding of EPI-X4 derivatives to the receptor and thus antagonistic properties differs between humans and mice because EPI-X4 derivatives have been shown to compete with this antibody for receptor binding[220].

In order to clarify the efficacy of the current lead derivatives of EPI-X4 for their antagonizing properties on mCXCR4 I used the murine T lymphoblastic cell line (BW5147) and three murine cell lines of B cell origin at different developmental stages ranging from pro-B cell (Ba/F3) over pre-B cell (300-19) to mature B cell (A20). Interestingly, although CXCR4 expression was confirmed on all cell lines they differed in their responsiveness to murine CXCL12. This can be expected, since the responsiveness of B cells declines with their development resulting in the release of immature B cells from the bone marrow[275]. While the pro-B cell line Ba/F3 showed the best responsiveness to CXCL12 stimulation, the responsiveness of the pre-B cell line 300-19 was quite lower. Nevertheless, according to mature CD19+ B cells within the human blood, the mature murine B cell line A20 respond to CXCL12 in the same way: rapid phosphorylation of Erk but no alteration in cell migration[275].

Cell line dependent differences in inhibiting CXCL12 stimulated Akt and Erk phosphorylation were observed for all EPI-X4 derivatives tested as well as AMD3100. In addition, most of the compounds tested were less effective on mCXCR4 than on hCXCR4 expressed on CD4+ T cells. For example, the antagonistic activity of JM#21 in inhibiting CXCL12 stimulated Erk phosphorylation varied between the murine cell lines from about 8 µM for Ba/F3 and BW5147 cells up to 33 µM for A20 cells and thus less effective than on CD4+ T cells with an IC_{50} value of about 1 µM. While AMD3100 showed higher

antagonistic activity on mCXCR4 expressed on Ba/F3 and BW5147 cells (IC_{50}s of 1 µM and 2.7 µM, respectively) than on hCXCR4 expressed on CD4+ T cells (IC_{50} of 3 µM) it was less efficient on mCXCR4 expressed on A20 cells with an IC_{50} of around 8 µM. Especially, the amidated and truncated variants JM#173 and JM#194 were less effective on mCXCR4 than on hCXCR4. JM#173 showed antagonistic activity on mCXCR4 of roughly 100 µM or more while its IC_{50} value on CD4 + T cells was about 10 µM and thus 10x more active on hCXCR4 than on mCXCR4. Lower potency on mCXCR4 expressed on BW5147 cells (IC_{50} >10 µM), A20 cells (IC_{50} ~5 µM), Ba/F3 (IC_{50} µM) and hCXCR4 expressed on CD4+ T cells (IC_{50} 0.1 µM) was also observed for JM#194, the palmitic variant of JM#173. The most promising candidate is JM#198, a variant of JM#21 coupled to stearic acid via a glutamic acid linker, showed the strongest activity not only on hCXCR expressed on CD4+ T cells (IC_{50} 170 nM) but also on mCXCR4 expressed on A20 cells (IC_{50} 250 nM), Ba/F3 cells (IC_{50} 120 nM) and BW5147 cells (IC_{50} 1030 nM).

Overall, these data indicate that either other amino acids within the receptor are involved in ligand binding or differences in the amino acid composition of the receptor lead to conformational differences of the binding pocket which influences the binding of EPI-X4 derivatives. However, the amino acids within the receptor which have been shown so far to be crucial for the interaction with EPI-X4 and derivatives thereof[218] do not vary between human and mice, which I have shown by performing pairwise sequence alignment of human and murine CXCR4. In order to evaluate cell line specific differences in the amino acid composition of CXCR4 which might explain differences in the binding modes of EPI-X4 and derivatives thereof, additional sequence analysis followed by computational modelling is required.

In addition, it might be possible, that EPI-X4 derivatives also interact with other receptors, e.g. CXCR7. CXCR7 is another G-protein coupled receptor and functions as a scavenger receptor for CXCL12 thus activating intracellular signaling kinases like Erk and Akt[276–278]. Intriguingly, AMD3100, a small molecule inhibitor of CXCR4 has been shown to not only bind to CXCR4 but also to CXCR7[279]. While AMD3100 has antagonistic properties on CXCR4, it acts as an allosteric agonist on CXCR7 thereby activating the recruitment of β-arrestin to CXCR7 leading to opposite cellular effects[279]. Moreover, TC14012, another CXCR4 antagonist, has been shown to have agonistic effects on CXCR7 with increased recruitment of β-arrestin and activation of intracellular Erk[278]. However, to prove this hypothesis, expression levels of CXCR7 as well as assessment of β-arrestin recruitment to

murine CXCR7 and changes in intracellular signaling cascades and comparison with human CXCR7 are required.

Overall, these data indicate that especially the truncated and amidated variants of EPI-X4 are less effective on mCXCR4 than on hCXCR4 compared to their 12-mer counterparts and are therefore not suitable for murine applications. Nevertheless, they are highly active on hCXCR4 thus reflecting their therapeutic potential in humans. It should therefore be considered to evaluate their binding activity to CXCR4 of different species first *in silico* by using different modelling approaches and then *in vitro* using species specific cells. This additional pre-clinical evaluation may help to select the best animal model and thus reduce the number of animals during pre-clinical drug development.

4.4 Advanced EPI-X4 derivatives are promising drug candidates for advanced preclinical development for the treatment of Mantle cell lymphoma and chronic lymphocytic leukemia.

The CXCR4/CXCL12 axis is widely studied in the field of oncology in which it contributes to different steps of tumorigenesis[75–80,87–90]. Overexpression of CXCR4 has been found on many different cancer types and expression levels of CXCR4 and CXCL12 has been shown to correlate with the potential of tumors to metastasize[68–72,91–93]. Besides that, the CXCR4/CXCL12 axis also contributes to the tumor microenvironment (TME) which facilitates cancer progression through various pathways[81,95,96,280,281]. The TME varies between different cancer types but generally consists of immune cells, stromal cells as well as blood vessels and components of the extracellular matrix[94]. Within the TME, the CXCR4/CXCL12 axis contributes to cancer progression in two different ways: (1) CXCL12 is secreted by cancer cells which leads to the recruitment of immune cells and stromal cells to the TME and (2) through the interaction of CXCL12, secreted by cells of the TME, with CXCR4 expressed on cancer cells leading e.g. to the retention of the cancer cells within the protective niches[81,264].

Within the last decades, several new potential drugs have been developed which target specific interactions of the tumor cells with cells of the TME[94,282,283]. Many of them are currently evaluated in clinical trials or already approved for different types of cancer[283–285]. Within this study I focused on the inhibition of the CXCR4/CXCL12 pathways in mantle cell lymphoma (MCL) and chronic lymphocytic leukemia (CLL) which are both subtypes of non-Hodgkin lymphomas. Both diseases are highly heterogenous and the composition of the TME is relevant for disease progression[130,131,158,160,163,164,286]. Besides classical

chemotherapy, treatments for CLL and MCL patients often target not only the cancer cells themselves, but also the TME, using different kind of inhibitors[176,263,287–289]. However, so far, no CXCR4 antagonist is approved for the treatment of MCL and CLL.

Promising pre-clinical studies showed that CXCR4 antagonists have great therapeutic potential and are therefore under clinical investigation[139,169,185,195,290–292]. Within this study, I showed that the optimized derivatives of EPI-X4 inhibit CXCL12 induced signaling and cell migration of both, MCL and CLL cell lines. However, cell lines of the same disease did not only differ in their responsiveness to CXCL12 but also in the efficacy of the tested EPI-X4 derivatives which was especially shown for the two MCL cell lines. These data reflect the heterogeneity of the disease. Differences in the responsiveness to stimuli or potential drugs have been shown before for different types of cancer, e.g. breast cancer, but also for CLL and MCL cells[139,291,293].

The fatty acid variants JM#143, JM#198 and JM#194 were very active in antagonizing CXCL12 mediated cell responses of MCL and CLL cell lines. This is not only in line with the data published before but also those determined above on CD4+ T cells. However, in cells derived from the Eμ-TCL1 mouse model, the truncated variants JM#173 and JM#194 were less effective than in human CLL cell lines. This was indeed not surprisingly as it has been shown above that those variants were also less effective on murine cells as compared to human cells, strengthening the hypotheses that there are differences in the binding mode of EPI-X4 derivatives to CXCR4 of different species or having opposite effects on other receptors like CXCR7. Both hypotheses have still to be proven e.g. through computational modelling or differences in expression levels of CXCR7 and the induction of beta-arrestin recruitment to CXCR7.

Nevertheless, it will be interesting to show how the other derivatives may act *in vivo*, especially the fatty acid derivatives as they bind to albumin which is known to accumulate in cancerous tissue[224]. Therefore, it is planned to use the Eμ-TCL1 mouse model for the evaluation of the therapeutic efficacy of the most promising variant JM#198, a highly active derivative of EPI-X4. JM#198 is not only more active than AMD3100 but it is also protected from enzymatic degradation in blood plasma and has a relatively long systemic half-life[212].Therapeutic efficacy will be evaluated in comparison to the approved BTK inhibitor Ibrutinib, the BCL-2 inhibitor Venetoclax or in combination with these therapies. Especially the combinational treatment might be of interest as it has been shown in a phase I clinical trial that the combination of ibrutinib and ulocuplumab, a CXCR4 antibody, is effective and safe in Waldenström's macroglobulinemia patients[294]. Therefore, combinational treatment

of EPI-X4 derivatives with ibrutinib will also be considered and will be tested before on cell-based assays in the near future.

Moreover, in collaboration with the Institute of Immunology, Ulm University, the efficacy of the advanced derivatives will be tested on Eμ-TCL1 cells harboring knockouts of BTK and/or p53. His unpublished data indicate that knock-out of BTK and p53 strongly increase the expression of CXCR4 in Eμ-TCL1 cells leading to a stronger responsiveness to CXCL12. This is interesting as alterations within the encoding region of p53 are associated with a poorer overall survival of MCL and CLL patients[129–132,150], and p53 knock-out is linked to elevated CXCR4 expression in prostate cancer and breast cancer[295,296]. Moreover, inhibiting BTK, thus leading to the disruption of constitutively activated BCR signaling, has great therapeutic potential for CLL and MCL [297,298] associated with reduced CXCR4 surface expression and dose-dependent responsiveness to CXCL, leading to the egress of MCL and CLL cells into the circulation[175,299]. It will be interesting to see how these knock-out cells will influence the efficacy of the optimized EPI-X4 derivatives which will be evaluated in the near future. Since MCL and CLL are highly heterogenous diseases[129,131,181] the influence of both, p53 and BTK, in line with the efficacy of EPI-X4 derivatives might open a new treatment strategy in the field of personalized medicine overcoming resistances and failures in the current treatment options of both diseases.

4.5 *In* vivo stability of EPI-X4 derivatives – Evaluating the impact of PEGylation and Albumin-binding.

PEGylation of peptides is a common strategy to overcome the problem of rapid peptide elimination via the kidneys. Due to the fact that it binds water molecules, PEG increases the hydrodynamic volume of the conjugates thereby protecting them not only from enzymatic degradation but also from renal excretion[300–302]. This effect is known for more than 40 years and the first PEGylated drug was approved in 1990 for the treatment of severe combined immunodeficiency disease (SCID)[302]. Up to today, there are many more PEGylated drugs on the market for different diseases e.g. acute lymphoblastic leukemia and Hepatitis C[300]. Previous studies on JM#21 already showed, that coupling the peptide to PEG leads to the protection from enzymatic degradation and hence an increased stability in human plasma[227]. However, the increased stability was correlated with a loss of activity. In addition to these variants, several bivalent conjugates were designed leading to an increased antagonistic activity, however, these variants were not stable in blood plasma preventing their therapeutic use[227].

Within my study, I evaluated the efficacy of PEGylated variants of JM#29 and JM#173. Both are N-terminally modified variants of JM#21 with a length of 12 and 7 amino acids, respectively, and are stable in human plasma[212,221]. PEGylated variants of JM#29 and JM#173 showed a reduced binding affinity compared to their unconjugated counterparts. This effect has also been described for other drugs[227,301,303,304]. This is most likely caused by PEG shielding the peptide from binding to the CXCR4 binding pocket or by conformational changes resulting in a different binding mode. The dimeric PEGylated variants (telechelic and Y-shaped) of both peptides were as active or even more active as the monovalent version which has also been shown before for JM#21 PEGylated variants[227]. This indicates the importance of the design as either the shielding effect is reduced, or it sterically fits better into the binding pocket of CXCR4.

Only the JM#29 coupled variants remained completely active in human plasma while most of the JM#173 variants lost activity over time. This can be explained by the differences in the amino acid length which, in combination with the conjugated PEG may lead to sterically differences in the binding to CXCR4. However, this has to be further investigated using computational modelling to design new PEGylated variants which binds in the same way to CXCR4 as their unconjugated counterparts. It might be an option to design and evaluate PEGylated variants with an additional linker between the peptide and PEG to see if PEG sterically influences the binding mode of the peptide. In addition, for further variants it might be an option to test PEGs of higher molecular weight, e.g. PEG_{40}, since it has been shown that the molecular weight of PEG itself influences the clearance from the blood as well as the pharmacokinetic parameters. PEG of higher molecular weight has been shown to remain longer in the blood leading to a longer half-life of the conjugated cargo[305]. This is in line with my data showing that the monovalent PEG_{20} version remained longer active than the monovalent PEG_5 variant of JM#173. Since accumulation effects occurring more apparently with PEGs of increasing molecular weight[304], another option for further optimization strategy might be the use of branched low molecular weight PEGs, e.g. PEG_2. This would probably lead to enhanced bioavailability due to reduced accumulation effects without being eliminated by the kidneys due to the increased overall size of the drug. However, I would appreciate to first evaluate the best molecular weight of PEG either linear or branched using positron emission tomography as it was done before for radiolabeled JM#21[212] to evaluate their biodistribution and their possible elimination rates via the kidneys and accumulation effects.

Besides the use of PEG to increase systemic half-lives of drugs, another strategy to achieve this goal is the conjugation to serum albumin. Albumin is an excellent conjugation partner due to its long circulation half-life (almost 3 weeks in humans) thus preventing any conjugated cargo from renal elimination[222,224]. This has already been demonstrated for many drugs including several EPI-X4 derivatives, which bind to albumin through long fatty acid chains or cholesterol. In a previous study, cholesterol has been coupled to JM#21 with a PEG_5 linker resulting in almost complete resistance against human plasma while remaining as active as the unconjugated peptide[227]. Although both cholesterol coupled peptides studied herein showed high activity and *ex vivo* stability in human plasma, they were cytotoxic at high concentration which has already been described before for cholesterol-PEG_5-JM#21[227] and are therefore not suitable for *in viv*o use.

Additionally, both peptides, JM#29 and JM#173, have been coupled to trityl (TrtS), described to bind to albumin via the one of the two major binding sites namely Sudlow I thereby increasing the circulation half-live of a conjugated cargo to almost 15 h[250]. In my study both TrtS-coupled peptides showed a high affinity to CXCR4, even in the presence of plasma proteins, and remained highly active after incubation in human plasma. This indicates that their activities are not negatively influenced by binding to albumin and that they are not enzymatically degraded by plasma proteins. However, both variants lost their activity after 4 hours *in vivo* which is most likely due to liver accumulation, shown before for TrtS conjugates[250] or other mechanism of degradation through e.g. tissue specific enzymes. In order to further evaluate this, additional mouse experiments are required to analyze the biodistribution of the coupled peptides to see if they accumulate in specific tissues or if they are excreted via the kidneys.

Nevertheless, since albumin is known to accumulate in cancerous tissue, coupling EPI-X4 derivatives to albumin via specific albumin binders might still be a good method to increase circulation half-lives of the derivatives and should be further pursued.

4.6 Comparative analysis of newly generated diacid variants and monoacid versions: No clear advantages observed.

Increasing plasma half-lives through binding to albumin can not only be achieved by the use of albumin binders like TrtS and cholesterol, which bind to albumin either through the Sudlow site I [250] or unspecific[306], respectively, but also by coupling them to fatty acids as albumin has seven binding sites for fatty acids[307]. Peptide coupling to monocarboxylic acids has already been successfully applied not only to EPI-X4 derivatives but also to other

peptides which are currently under clinical investigations or already successfully approved[308–310]. Dicarboxylic acids, also termed diacid fatty acids, were shown having stronger binding affinity to albumin through the additional carboxylic group as compared to monoacidic fatty acids[226]. Prolonged half-lives of diacid coupled peptides in comparison to monoacid coupled peptides have been shown for the therapeutic GLP-1 receptor agonists Semaglutide and Liraglutide, and the insulin analogues Insulin degludec and Insulin determir, respectively[252].

I herein showed that EPI-X4 derivatives equipped with dicarboxylic acids of C16 or C18 length were less active in comparison to their monoacidic counterparts. Overall, the C16 diacid variants were more active than the C18 diacid variants. This was surprising, as for the monoacidic variants increasing antagonistic activity with increasing length of the coupled fatty acid side chain has been shown by me and others[212]. However, the loss of activity when fatty diacid acids of the same length as the monoacidic version are equipped has already been described during the discovery of semaglutide[226]. It has been shown that the use of longer-length diacid fatty acids leads to a higher efficacy when fatty acids of diacid moieties are used instead of monoacid moieties. This has been observed with Insulin degludec (C16 diacid) and Insulin determir (C14 monoacid) as well as Liraglutide (C16 monoacid) and Semaglutide (C18 monoacid)[226,311,312].

Even though all EPI-X4 diacid variants remained active after incubation in full human plasma, indicating that they are protected from enzymatic degradation, most of the *in vivo* tested variants almost completely lost their activity to bind to CXCR4 after 4 hours and thus were not superior to the current lead derivative JM#198. Although Insulin degludec is approved as a long-acting insulin analogue for subcutaneous injection it has to be mentioned that its half-life is around 3x lower in rats and ~5x lower in humans when administered intravenously[252]. It might be of importance to retest the herein generated diacid EPI-X4 variants for subcutaneous injection. In addition, Insulin degludec and Semaglutid, have longer amino acid sequences than the herein tested EPI-X4 derivatives, which might further influence distribution and half-lives of drugs. While insulin degludec consists of total 40 amino acids, divided into two different peptide backbones, the GLP-1 analogue semaglutide is 31 amino acids long[313,314].

For further optimization, a bigger structure-activity relationship should be considered creating new diacid variants with peptide backbones of longer length. Since I herein showed that EPI-X4 derivatives equipped with diacids of C16 length were more active than those coupled to diacids of C18 length it might also be feasible to include diacids of shorter length

(e.g.C14) and probably of longer length (e.g. C20) to see whether the length of the fatty diacid might influence the efficacy of the peptide backbone. In addition, the use of different linkers between the peptide and the fatty diacid should also be included. However, conducting a bigger structure activity relationship study would include the use of many mice to analyze the biodistribution and the half-lives *in vivo*. In order to overcome the problem of involving high numbers of animals in the field of drug development, I started to establish a new model to determine plasma stability *in vivo*.

4.7 HET-CAM model is a reliable alternative to determine peptide stability *in vivo.*

Every year, millions of animals are used for medicinal and scientific research including drug development[315,316]. However, the percentage of all new drug candidates making the transition from preclinical research to clinical trials and ultimately to the approval is only approximately 0.1%[317]. Due to this imbalance in human benefit and animal welfare, the use of animal models is critically discussed. Nowadays, many countries strictly regulate the use of animal models through animal testing guidelines and laws in accordance with the 3Rs concept[318]. The 3R principle was firstly introduced in 1959 by Russell and Burch aiming in the **r**eplacement, **r**eduction and **r**efinement of animal experiments by various methods[319]. In accordance with the 3R concept and in collaboration with the Department of Nuclear Medicine, Ulm University Medical Center, I started to test whether peptide stability and bioavailability can be evaluated in chicken embryos instead of mice using the hen's egg test – chorioallantoic membrane (HET-CAM).

The HET-CAM model has not only the advantage that before hatching it is not considered as an animal model and thus not restricted by the German Government, it is also a low-cost model which allows simple and quick evaluation of pharmacological substances[320]. It is nowadays widely used in scientific and pharmacological research mainly in oncological and toxicological studies but also for the evaluation of the biodistribution of drugs *in vivo*[256–258,320,321]. However, to my knowledge, it has never been considered as a model to study the stability of (peptide) drugs *in vivo*.

Within this study I evaluated the *ex vivo* stability of the EPI-X4 variant JM#21 by analyzing its proteolytic degradation in plasma derived from humans, mice and chicken embryos. This showed that the remaining activity and thus proteolytic degradation of JM#21 is more comparable between humans and chicken than humans and mice indicating that HET-CAM model mimics the proteolytic degradation of peptide drugs more efficiently than mice.

Moreover, the CAM studies showed that the remaining activity of JM#21 after circulation *in vivo* are in line with previously published data determined in mice[212] indicating comparable proteolytic elimination processes in mice and chicken embryos. Interestingly, JM#198 showed a higher remaining activity after circulation in chicken eggs than in mice. Since JM#198 binds to serum albumin through its fatty acid chain and is thus better shielded from proteolytic elimination, this is most likely due to differences in the half-lives of species-specific albumin, which is approximately one day for mice[322] and around 42 hours for newly hatched chicken[323]. However, this is still substantially lower than the half-life of albumin in humans, indicating that the systemic half-lives of EPI-X4 derivatives in humans might be higher.

Although little is known about the proteolytic activity of plasma in chicken embryos, especially in comparison to other species, the herein showed data that at least for the tested EPI-X4 derivatives degradation in plasma is similar between CAM and human and thus are very promising. Nevertheless, further peptides and other CXCR4 antagonists, e.g. JM#143 and AMD3100, of which *in vivo* data are already published, are planned to be evaluated soon to get a more robust overview about using the HET-CAM model in addition or instead of animals. In addition, biodistribution studies of EPI-X4 derivatives are planned as well, as molecules such as radioligands have been shown to have similar distribution within chicken embryos and mice[321,324]. Overall, the HET-CAM model is a reliable *in vivo* model that can be used as a bridge between *in vitro* testing and animal models for pre-screen the stability of peptides and drugs, thus reducing the number of animals in preclinical drug development.

4.8 Conclusion and future perspectives

Even though several new EPI-X4 derivatives within this study have been generated no one showed superior efficacy over the previously described 12-mer derivative coupled to a C18 fatty acid JM#198 [212]. The PEGylated variants of JM#29 and JM#173 did not only show reduced binding affinity to CXCR4 in comparison to their unconjugated counterparts, the unconjugated counterparts itself are less efficient in binding to CXCR4 than JM#198[212]. Moreover, EPI-X4 derivatives equipped with C16 or C18 dicarboxylic acids were not only less effective than their monoacidic counterparts, among them JM#198, but also less stable in vivo than JM#198. Thus, JM#198 is still the current lead derivative of EPI-X4. It is not only highly active *in vitro* by binding to CXCR4 on primary cells as well as cancer cell lines derived from mice and humans, thereby antagonizing CXCL12 mediated cellular responses indicating their therapeutic potential but also remains active after circulation and will

therefore be tested in the near future in a CLL mouse model. In order to generate new EPI-X4 derivatives with longer systemic half-lives than JM#198, a bigger structure activity relationship study is planned by generating e.g. diacid EPI-X4 variants with different linkers, different length of the peptides and fatty diacids as well as PEGylated variants using e.g. PEGs of different molecular weight. In addition, the generation of cyclic EPI-X4 variants might also be a strategy to improve the pharmacokinetic and pharmacodynamic as it has been shown before that cyclic peptides have improved pharmacokinetic and pharmacodynamic properties over linear peptides[325,326].

With the herein established HET-CAM model to determine plasma stability *in vivo* one now has the possibility to test a bigger panel of promising candidates *in vivo* without being restricted by animal testing guidelines and laws. In addition, the model offers the possibility to evaluate the biodistribution of peptides to reduce the number of animals in preclinical drug development as it was previously performed in mice.

5 Summary

The interaction between the C-X-C motif chemokine receptor 4 (CXCR4) and the C-X-C motif chemokine 12 (CXCL12) plays a pivotal role in development, immune function, and homeostasis. A dysfunctional CXCR4/CXCL12 axis is involved in many pathophysiological processes including (auto)inflammatory diseases and tumorigenesis making CXCR4 a promising drug target. However, so far, only one CXCR4 antagonist is approved by the Food and Drug Administration (FDA): AMD3100. The endogenous peptide inhibitor of CXCR5 (EPI-X4) can be cleaved under acidic conditions from its precursor molecule human serum albumin (HSA). HSA is the most abundant protein in the human plasma and responsible for many physiological functions including the transport of insoluble compounds, e.g. fatty acids. It is therefore therapeutically applied for the treatment of several diseases. Pharmaceutical HSA is generated from a large pool of healthy human plasma donors. In order to clarify whether EPI-X4 might be generated during generation processes or storage of pharmaceutical HSA I used the EPI-X4 specific sandwich enzyme-linked immunosorbent assay (ELISA) and showed that EPI-X4 is not present in pharmacological HSA preparations, ensuring that there is no contamination with EPI-X4 and thus no co-administration of this bioactive peptide during HSA infusion.

EPI-X4 is a promising drug candidate for CXCR4 because of its direct interaction with it thus leading to the prevention of CXCL12 mediated cellular effects. So far, several strategies have already been applied to increase activity, plasma stability and *in vivo* half-lives of EPI-X4 resulting in various optimized variants like fatty acid coupled ones and N-terminally modified variants of EPI-X4 for therapeutic use. However, all of them have been mainly investigated on cancer cell lines without confirmation on human primary cells and murine cells which is of great importance to mimic their potential efficacy in humans and animal models. Within this study I showed that EPI-X4 and its optimized derivatives are not only effective on immortalized cancer cell lines but also on human primary cells thereby indicating their potential efficacy in human patients.

Potential drug candidates are commonly tested in animal models, mainly rodents, before applied to humans. It is therefore of great interest to test them on murine cells as well for correct interpretation and estimation of required concentrations. I therefore tested EPI-X4 derivatives on different murine cells lines and showed that, besides similar expression levels of CXCR4, the efficacy of EPI-X4 derivatives differs between human CXCR4 (hCXCR4) and murine CXCR4 (mCXCR4). In particular, the N-terminally modified versions JM#173 and JM#194, which is additionally coupled to a C16 fatty acid, were less active on mCXCR4

than hCXCR4 indicating differences in ligand/receptor interactions which have to be considered during pre-clinical evaluations as well as the involvement of other receptors like the C-X-C motif chemokine receptor 7 (CXCR7).

Besides its physiological role, the CXCR4/CXCL12 axis is involved in tumorigenesis by overexpression of CXCR4 on cancer cells and contribution to the tumor microenvironment (TME). Blocking the CXCR4/CXCL12 axis is therefore of great therapeutic interest and makes CXCR4 an important target for drug development. Promising preclinical studies reflect the therapeutic potential of CXCR4 antagonists on mantle cell lymphoma (MCL) and chronic lymphocytic leukemia (CLL). This study showed the effectiveness of JM#198, a 12mer EPI-X4 variant conjugated to a C18 fatty acid, in antagonizing CXCL12-mediated responses *in vitro* and will soon be investigated *in vivo* using a CLL specific mouse model.

Even though several EPI-X4 derivatives have been developed with increased CXCR4 antagonizing activity and plasma stability, their short *in vivo* half-lives render them less than ideal for therapeutic applications. In this study I explored several drug development strategies to enhance these properties: (1) PEGylation (peptide coupling to poly(ethylene glycol)), and (2) Albumin conjugation, either through specific binders or diacid moiety fatty acids. While these strategies have historically succeeded in prolonging systemic half-lives of other drugs, leading to their clinical approval, they failed to produce derivatives with superior efficacy than the current lead compound JM#198. While these methodologies hold promise, they necessitate further refinement and optimization.

The pre-clinical evaluation of drugs *in vivo* traditionally hinges on animal models, predominantly rodents. Given the substantial number of drugs failing in these early stages the ethics surrounding animal model usage is increasingly debated. Aiming to strike a balance between human advantages and animal welfare, I introduced an alternative approach for assessing peptide stability through the hen's egg test- chorionallantoic membrane (HET-CAM) model. By examining the enzymatic degradation *ex vivo* with plasma from humans, mice, and chicken embryo sources, I showcased that the breakdown of EPI-X4 derivatives in chicken embryo plasma mirrors that in human plasma. Furthermore, the systemic half-lives of JM#21 and its fatty acid coupled version JM#198 as determined within this model closely resemble those observed in mice. This is significant as utilizing the HET-CAM model for preliminary drug screening could curtail the number of animals needed in pre-clinical assessments, aligning more closely with the 3R principle's aspirations to reduce, refine, and replace animal testing.

6 References

1. Loetscher, M., Geiser, T., O'Reilly, T., Zwahlen, R., Baggiolini, M. & Moser, B. Cloning of a human seven-transmembrane domain receptor, LESTR, that is highly expressed in leukocytes. (1994). *J. Biol. Chem.* **269**, 232–237.
2. Wu, B., Chien, E. Y. T., Mol, C. D., Fenalti, G., Liu, W., Katritch, V., Abagyan, R., Brooun, A., Wells, P., Bi, F. C., Hamel, D. J., Kuhn, P., Handel, T. M., Cherezov, V. & Stevens, R. C. Structures of the CXCR4 Chemokine GPCR with Small-Molecule and Cyclic Peptide Antagonists. (American Association for the Advancement of Science, 2010). *Science* **330**, 1066–1071 American Association for the Advancement of Science.
3. Tuteja, N. Signaling through G protein coupled receptors. (2009). *Plant Signal. Behav.* **4**, 942–947.
4. Bianchi, M. E. & Mezzapelle, R. The Chemokine Receptor CXCR4 in Cell Proliferation and Tissue Regeneration. (2020). *Front. Immunol.* **11**, 2109.
5. Murdoch, C., Monk, P. N. & Finn, A. Functional expression of chemokine receptor CXCR4 on human epithelial cells. (1999). *Immunology* **98**, 36–41.
6. Jordan, N. J., Kolios, G., Abbot, S. E., Sinai, M. A., Thompson, D. A., Petraki, K. & Westwick, J. Expression of functional CXCR4 chemokine receptors on human colonic epithelial cells. (1999). *J. Clin. Invest.* **104**, 1061–1069.
7. Philipp-Abbrederis, K., Herrmann, K., Knop, S., Schottelius, M., Eiber, M., Lückerath, K., Pietschmann, E., Habringer, S., Gerngroß, C., Franke, K., Rudelius, M., Schirbel, A., Lapa, C., Schwamborn, K., Steidle, S., Hartmann, E., Rosenwald, A., Kropf, S., Beer, A. J., Peschel, C., Einsele, H., Buck, A. K., Schwaiger, M., Götze, K., Wester, H. & Keller, U. *In vivo* molecular imaging of chemokine receptor CXCR 4 expression in patients with advanced multiple myeloma. (2015). *EMBO Mol. Med.* **7**, 477–487.
8. Teicher, B. A. & Fricker, S. P. CXCL12 (SDF-1)/CXCR4 Pathway in Cancer. (2010). *Clin. Cancer Res.* **16**, 2927–2931.
9. Shirozu, M., Nakano, T., Inazawa, J., Tashiro, K., Tada, H., Shinohara, T. & Honjo, T. Structure and Chromosomal Localization of the Human Stromal Cell-Derived Factor 1 (SDF1) Gene. (1995). *Genomics* **28**, 495–500.
10. De La Luz Sierra, M., Yang, F., Narazaki, M., Salvucci, O., Davis, D., Yarchoan, R., Zhang, H. H., Fales, H. & Tosato, G. Differential processing of stromal-derived factor-1α and stromal-derived factor-1β explains functional diversity. (2004). *Blood* **103**, 2452–2459.

11. Strieter, R. M. & Gomperts, B. N. CHEMOKINES, CXC | CXCL12 (SDF-1). in (2006) *Encyclopedia of Respiratory Medicine* 390–394 Elsevier.
12. Wescott, M. P., Kufareva, I., Paes, C., Goodman, J. R., Thaker, Y., Puffer, B. A., Berdougo, E., Rucker, J. B., Handel, T. M. & Doranz, B. J. Signal transmission through the CXC chemokine receptor 4 (CXCR4) transmembrane helices. (2016). *Proc. Natl. Acad. Sci.* **113**, 9928–9933.
13. Kofuku, Y., Yoshiura, C., Ueda, T., Terasawa, H., Hirai, T., Tominaga, S., Hirose, M., Maeda, Y., Takahashi, H., Terashima, Y., Matsushima, K. & Shimada, I. Structural Basis of the Interaction between Chemokine Stromal Cell-derived Factor-1/CXCL12 and Its G-protein-coupled Receptor CXCR4. (2009). *J. Biol. Chem.* **284**, 35240–35250.
14. Crump, M. P. Solution structure and basis for functional activity of stromal cell-derived factor-1; dissociation of CXCR4 activation from binding and inhibition of HIV-1. (1997). *EMBO J.* **16**, 6996–7007.
15. Busillo, J. M. & Benovic, J. L. Regulation of CXCR4 signaling. (2007). *Biochim. Biophys. Acta BBA - Biomembr.* **1768**, 952–963.
16. Pozzobon, T., Goldoni, G., Viola, A. & Molon, B. CXCR4 signaling in health and disease. (Elsevier B.V., 2016). *Immunol. Lett.* **177**, 6–15 Elsevier B.V.
17. Cheng, Z.-J., Zhao, J., Sun, Y., Hu, W., Wu, Y.-L., Cen, B., Wu, G.-X. & Pei, G. β-Arrestin Differentially Regulates the Chemokine Receptor CXCR4-mediated Signaling and Receptor Internalization, and This Implicates Multiple Interaction Sites between β-Arrestin and CXCR4. (2000). *J. Biol. Chem.* **275**, 2479–2485.
18. Zhuo, Y., Crecelius, J. M. & Marchese, A. G protein–coupled receptor kinase phosphorylation of distal C-tail sites specifies βarrestin1-mediated signaling by chemokine receptor CXCR4. (2022). *J. Biol. Chem.* **298**, 102351.
19. Busillo, J. M., Armando, S., Sengupta, R., Meucci, O., Bouvier, M. & Benovic, J. L. Site-specific Phosphorylation of CXCR4 Is Dynamically Regulated by Multiple Kinases and Results in Differential Modulation of CXCR4 Signaling. (2010). *J. Biol. Chem.* **285**, 7805–7817.
20. Britton, C., Poznansky, M. C. & Reeves, P. Polyfunctionality of the CXCR4/CXCL12 axis in health and disease: Implications for therapeutic interventions in cancer and immune-mediated diseases. (2021). *FASEB J.* **35**,.
21. García-Cuesta, E. M., Santiago, C. A., Vallejo-Díaz, J., Juarranz, Y., Rodríguez-Frade, J. M. & Mellado, M. The Role of the CXCL12/CXCR4/ACKR3 Axis in Autoimmune Diseases. (2019). *Front. Endocrinol.* **10**, 585.

22. Maghazachi, A. A. Role of the Heterotrimeric G Proteins in Stromal-Derived Factor-1α-Induced Natural Killer Cell Chemotaxis and Calcium Mobilization. (1997). *Biochem. Biophys. Res. Commun.* **236**, 270–274.
23. Tan, W., Martin, D. & Gutkind, J. S. The Gα13-Rho Signaling Axis Is Required for SDF-1-induced Migration through CXCR4. (2006). *J. Biol. Chem.* **281**, 39542–39549.
24. Orsini, M. J., Parent, J.-L., Mundell, S. J. & Benovic, J. L. Trafficking of the HIV Coreceptor CXCR4. (1999). *J. Biol. Chem.* **274**, 31076–31086.
25. Rigo, A., Ferrarini, I., Innamorati, G. & Vinante, F. A single amino acid substitution in CXCL12 confers functional selectivity at the beta-arrestin level. (2018). *Oncotarget* **9**, 28830–28841.
26. Sun, Y., Cheng, Z., Ma, L. & Pei, G. β-Arrestin2 Is Critically Involved in CXCR4-mediated Chemotaxis, and This Is Mediated by Its Enhancement of p38 MAPK Activation. (2002). *J. Biol. Chem.* **277**, 49212–49219.
27. Fong, A. M., Premont, R. T., Richardson, R. M., Yu, Y.-R. A., Lefkowitz, R. J. & Patel, D. D. Defective lymphocyte chemotaxis in β-arrestin2- and GRK6-deficient mice. (2002). *Proc. Natl. Acad. Sci.* **99**, 7478–7483.
28. Tachibana, K., Hirota, S., Iizasa, H., Yoshida, H., Kawabata, K., Kataoka, Y., Kitamura, Y., Matsushima, K., Yoshida, N., Nishikawa, S., Kishimoto, T. & Nagasawa, T. The chemokine receptor CXCR4 is essential for vascularization of the gastrointestinal tract. (1998). *Nature* **393**, 591–594.
29. Nagasawa, T., Hirota, S., Tachibana, K., Takakura, N., Nishikawa, S., Kitamura, Y., Yoshida, N., Kikutani, H. & Kishimoto, T. Defects of B-cell lymphopoiesis and bone-marrow myelopoiesis in mice lacking the CXC chemokine PBSF/SDF-1. (1996). *Nature* **382**, 635–638.
30. Zou, Y.-R., Kottmann, A. H., Kuroda, M., Taniuchi, I. & Littman, D. R. Function of the chemokine receptor CXCR4 in haematopoiesis and in cerebellar development. (1998). *Nature* **393**, 595–599.
31. Tissir, F., Wang, C.-E. & Goffinet, A. M. Expression of the chemokine receptor Cxcr4 mRNA during mouse brain development. (2004). *Dev. Brain Res.* **149**, 63–71.
32. Ivins, S., Chappell, J., Vernay, B., Suntharalingham, J., Martineau, A., Mohun, T. J. & Scambler, P. J. The CXCL12/CXCR4 Axis Plays a Critical Role in Coronary Artery Development. (2015). *Dev. Cell* **33**, 455–468.
33. Minami, H., Nagaharu, K., Nakamori, Y., Ohishi, K., Shimojo, N., Kageyama, Y., Matsumoto, T., Sugimoto, Y., Tawara, I., Masuya, M., Miwa, H. & Katayama, N.

CXCL12–CXCR4 Axis Is Required for Contact-Mediated Human B Lymphoid and Plasmacytoid Dendritic Cell Differentiation but Not T Lymphoid Generation. (2017). *J. Immunol.* **199**, 2343–2355.

34. McGrath, K. E., Koniski, A. D., Maltby, K. M., McGann, J. K. & Palis, J. Embryonic Expression and Function of the Chemokine SDF-1 and Its Receptor, CXCR4. (1999). *Dev. Biol.* **213**, 442–456.
35. Wu, X., Li, D.-J., Yuan, M.-M., Zhu, Y. & Wang, M.-Y. The Expression of CXCR4/CXCL12 in First-Trimester Human Trophoblast Cells1. (2004). *Biol. Reprod.* **70**, 1877–1885.
36. Doitsidou, M., Reichman-Fried, M., Stebler, J., Köprunner, M., Dörries, J., Meyer, D., Esguerra, C. V., Leung, T. & Raz, E. Guidance of Primordial Germ Cell Migration by the Chemokine SDF-1. (2002). *Cell* **111**, 647–659.
37. Tokoyoda, K., Egawa, T., Sugiyama, T., Choi, B.-I. & Nagasawa, T. Cellular Niches Controlling B Lymphocyte Behavior within Bone Marrow during Development. (2004). *Immunity* **20**, 707–718.
38. Sugiyama, T., Kohara, H., Noda, M. & Nagasawa, T. Maintenance of the Hematopoietic Stem Cell Pool by CXCL12-CXCR4 Chemokine Signaling in Bone Marrow Stromal Cell Niches. (2006). *Immunity* **25**, 977–988.
39. Singh, P., Mohammad, K. S. & Pelus, L. M. CXCR4 expression in the bone marrow microenvironment is required for hematopoietic stem and progenitor cell maintenance and early hematopoietic regeneration after myeloablation. (2020). *Stem Cells Dayt. Ohio* **38**, 849–859.
40. Porecha, N. K., English, K., Hangoc, G., Broxmeyer, H. E. & Christopherson, K. W. Enhanced Functional Response to CXCL12/SDF-1 Through Retroviral Overexpression of CXCR4 on M07e Cells: Implications for Hematopoietic Stem Cell Transplantation. (2006). *Stem Cells Dev.* **15**, 325–333.
41. Ramirez, P., Wagner, J. E., Defor, T. E., Eide, C. R., Miller, J. S., Weisdorf, D. J. & Brunstein, C. G. CXCR4 expression in CD34+ cells and unit predominance after double umbilical cord blood transplantation. (2013). *Leukemia* **27**, 1181–1183.
42. Kawabata, K., Ujikawa, M., Egawa, T., Kawamoto, H., Tachibana, K., Iizasa, H., Katsura, Y., Kishimoto, T. & Nagasawa, T. A cell-autonomous requirement for CXCR4 in long-term lymphoid and myeloid reconstitution. (1999). *Proc. Natl. Acad. Sci. U. S. A.* **96**, 5663–5667.

43. Suratt, B. T., Petty, J. M., Young, S. K., Malcolm, K. C., Lieber, J. G., Nick, J. A., Gonzalo, J.-A., Henson, P. M. & Worthen, G. S. Role of the CXCR4/SDF-1 chemokine axis in circulating neutrophil homeostasis. (2004). *Blood* **104**, 565–571.
44. Hampton, H. R., Bailey, J., Tomura, M., Brink, R. & Chtanova, T. Microbe-dependent lymphatic migration of neutrophils modulates lymphocyte proliferation in lymph nodes. (2015). *Nat. Commun.* **6**, 7139.
45. Kabashima, K., Shiraishi, N., Sugita, K., Mori, T., Onoue, A., Kobayashi, M., Sakabe, J.-I., Yoshiki, R., Tamamura, H., Fujii, N., Inaba, K. & Tokura, Y. CXCL12-CXCR4 engagement is required for migration of cutaneous dendritic cells. (2007). *Am. J. Pathol.* **171**, 1249–1257.
46. Döring, Y., Noels, H., van der Vorst, E. P. C., Neideck, C., Egea, V., Drechsler, M., Mandl, M., Pawig, L., Jansen, Y., Schröder, K., Bidzhekov, K., Megens, R. T. A., Theelen, W., Klinkhammer, B. M., Boor, P., Schurgers, L., van Gorp, R., Ries, C., Kusters, P. J. H., van der Wal, A., Hackeng, T. M., Gäbel, G., Brandes, R. P., Soehnlein, O., Lutgens, E., Vestweber, D., Teupser, D., Holdt, L. M., Rader, D. J., Saleheen, D. & Weber, C. Vascular CXCR4 Limits Atherosclerosis by Maintaining Arterial Integrity: Evidence From Mouse and Human Studies. (2017). *Circulation* **136**, 388–403.
47. Zernecke, A., Bot, I., Djalali-Talab, Y., Shagdarsuren, E., Bidzhekov, K., Meiler, S., Krohn, R., Schober, A., Sperandio, M., Soehnlein, O., Bornemann, J., Tacke, F., Biessen, E. A. & Weber, C. Protective Role of CXC Receptor 4/CXC Ligand 12 Unveils the Importance of Neutrophils in Atherosclerosis. (2008). *Circ. Res.* **102**, 209–217.
48. Molon, B., Gri, G., Bettella, M., Gómez-Moutón, C., Lanzavecchia, A., Martínez-A, C., Mañes, S. & Viola, A. T cell costimulation by chemokine receptors. (2005). *Nat. Immunol.* **6**, 465–471.
49. Contento, R. L., Molon, B., Boularan, C., Pozzan, T., Manes, S., Marullo, S. & Viola, A. CXCR4-CCR5: a couple modulating T cell functions. (2008). *Proc. Natl. Acad. Sci. U. S. A.* **105**, 10101–10106.
50. Nishimura, Y., Ii, M., Qin, G., Hamada, H., Asai, J., Takenaka, H., Sekiguchi, H., Renault, M.-A., Jujo, K., Katoh, N., Kishimoto, S., Ito, A., Kamide, C., Kenny, J., Millay, M., Misener, S., Thorne, T. & Losordo, D. W. CXCR4 Antagonist AMD3100 Accelerates Impaired Wound Healing in Diabetic Mice. (2012). *J. Invest. Dermatol.* **132**, 711–720.

51. Kitaori, T., Ito, H., Schwarz, E. M., Tsutsumi, R., Yoshitomi, H., Oishi, S., Nakano, M., Fujii, N., Nagasawa, T. & Nakamura, T. Stromal cell-derived factor 1/CXCR4 signaling is critical for the recruitment of mesenchymal stem cells to the fracture site during skeletal repair in a mouse model. (2009). *Arthritis Rheum.* **60**, 813–823.
52. Abbott, J. D., Huang, Y., Liu, D., Hickey, R., Krause, D. S. & Giordano, F. J. Stromal Cell–Derived Factor-1α Plays a Critical Role in Stem Cell Recruitment to the Heart After Myocardial Infarction but Is Not Sufficient to Induce Homing in the Absence of Injury. (2004). *Circulation* **110**, 3300–3305.
53. Walter, D. H., Haendeler, J., Reinhold, J., Rochwalsky, U., Seeger, F., Honold, J., Hoffmann, J., Urbich, C., Lehmann, R., Arenzana-Seisdesdos, F., Aicher, A., Heeschen, C., Fichtlscherer, S., Zeiher, A. M. & Dimmeler, S. Impaired CXCR4 Signaling Contributes to the Reduced Neovascularization Capacity of Endothelial Progenitor Cells From Patients With Coronary Artery Disease. (2005). *Circ. Res.* **97**, 1142–1151.
54. Zhang, H. & He, B. SDF1/CXCR4 axis plays a role in angiogenesis during the degeneration of intervertebral discs. (2019). *Mol. Med. Rep.*
55. Mirshahi, F., Pourtau, J., Li, H., Muraine, M., Trochon, V., Legrand, E., Vannier, J.-P., Soria, J., Vasse, M. & Soria, C. SDF-1 Activity on Microvascular Endothelial Cells. (2000). *Thromb. Res.* **99**, 587–594.
56. Lagane, B., Chow, K. Y. C., Balabanian, K., Levoye, A., Harriague, J., Planchenault, T., Baleux, F., Gunera-Saad, N., Arenzana-Seisdedos, F. & Bachelerie, F. CXCR4 dimerization and β-arrestin–mediated signaling account for the enhanced chemotaxis to CXCL12 in WHIM syndrome. (2008). *Blood* **112**, 34–44.
57. Majumdar, S. & Murphy, P. M. Adaptive Immunodeficiency in WHIM Syndrome. (2018). *Int. J. Mol. Sci.* **20**, 3.
58. Heusinkveld, L. E., Majumdar, S., Gao, J.-L., McDermott, D. H. & Murphy, P. M. WHIM Syndrome: from Pathogenesis Towards Personalized Medicine and Cure. (2019). *J. Clin. Immunol.* **39**, 532–556.
59. Zgraggen, S., Huggenberger, R., Kerl, K. & Detmar, M. An Important Role of the SDF-1/CXCR4 Axis in Chronic Skin Inflammation. (Public Library of Science, 2014). *PLoS ONE* **9**, e93665 Public Library of Science.
60. Hansen, I. B., Ellingsen, T., Hornung, N., Poulsen, J. H., Lottenburger, T. & Stengaard-Pedersen, K. Plasma level of CXC-chemokine CXCL12 is increased in rheumatoid

arthritis and is independent of disease activity and methotrexate treatment. (2006). *J. Rheumatol.* **33**, 1754–1759.

61. Nanki, T., Nagasaka, K., Hayashida, K., Saita, Y. & Miyasaka, N. Chemokines Regulate IL-6 and IL-8 Production by Fibroblast-Like Synoviocytes from Patients with Rheumatoid Arthritis. (2001). *J. Immunol.* **167**, 5381–5385.
62. Chung, S.-H., Seki, K., Choi, B.-I., Kimura, K. B., Ito, A., Fujikado, N., Saijo, S. & Iwakura, Y. CXC chemokine receptor 4 expressed in T cells plays an important role in the development of collagen-induced arthritis. (2010). *Arthritis Res. Ther.* **12**, R188.
63. Nagafuchi, Y., Shoda, H., Sumitomo, S., Nakachi, S., Kato, R., Tsuchida, Y., Tsuchiya, H., Sakurai, K., Hanata, N., Tateishi, S., Kanda, H., Ishigaki, K., Okada, Y., Suzuki, A., Kochi, Y., Fujio, K. & Yamamoto, K. Immunophenotyping of rheumatoid arthritis reveals a linkage between HLA-DRB1 genotype, CXCR4 expression on memory CD4+ T cells and disease activity. (2016). *Sci. Rep.* **6**, 29338.
64. Kanbe, K., Chiba, J., Inoue, Y., Taguchi, M. & Yabuki, A. SDF-1 and CXCR4 in synovium are associated with disease activity and bone and joint destruction in patients with rheumatoid arthritis treated with golimumab. (Taylor and Francis Ltd, 2016). *Mod. Rheumatol.* **26**, 46–50 Taylor and Francis Ltd.
65. Kanbe, K., Takagishi, K. & Chen, Q. Stimulation of matrix metalloprotease 3 release from human chondrocytes by the interaction of stromal cell-derived factor 1 and CXC chemokine receptor 4. (2002). *Arthritis Rheum.* **46**, 130–137.
66. Dotan, I., Werner, L., Vigodman, S., Weiss, S., Brazowski, E., Maharshak, N., Chen, O., Tulchinsky, H., Halpern, Z. & Guzner-Gur, H. CXCL12 Is a constitutive and inflammatory chemokine in the intestinal immune system: (2010). *Inflamm. Bowel Dis.* **16**, 583–592.
67. Werner, L., Elad, H., Brazowski, E., Tulchinsky, H., Vigodman, S., Kopylov, U., Halpern, Z., Guzner-Gur, H. & Dotan, I. Reciprocal regulation of CXCR4 and CXCR7 in intestinal mucosal homeostasis and inflammatory bowel disease. (2011). *J. Leukoc. Biol.* **90**, 583–590.
68. Lippitz, B. E. Cytokine patterns in patients with cancer: a systematic review. (2013). *Lancet Oncol.* **14**, e218–e228.
69. Zhao, H., Guo, L., Zhao, H., Zhao, J., Weng, H. & Zhao, B. CXCR4 over-expression and survival in cancer: a system review and meta-analysis. (2015). *Oncotarget* **6**, 5022–5040.

70. Darash-Yahana, M., Pikarsky, E., Abramovitch, R., Zeira, E., Pal, B., Karplus, R., Beider, K., Avniel, S., Kasem, S., Galun, E. & Peled, A. Role of high expression levels of CXCR4 in tumor growth, vascularization, and metastasis. (2004). *FASEB J.* **18**, 1240–1242.
71. Furusato, B., Mohamed, A., Uhlén, M. & Rhim, J. S. CXCR4 and cancer: CXCR4 and cancer. (2010). *Pathol. Int.* **60**, 497–505.
72. Balkwill, F. The significance of cancer cell expression of the chemokine receptor CXCR4. (2004). *Semin. Cancer Biol.* **14**, 171–179.
73. Pitt, L. A., Tikhonova, A. N., Hu, H., Trimarchi, T., King, B., Gong, Y., Sanchez-Martin, M., Tsirigos, A., Littman, D. R., Ferrando, A. A., Morrison, S. J., Fooksman, D. R., Aifantis, I. & Schwab, S. R. CXCL12-Producing Vascular Endothelial Niches Control Acute T Cell Leukemia Maintenance. (2015). *Cancer Cell* **27**, 755–768.
74. Pitot, H. C. The molecular biology of carcinogenesis. (1993). *Cancer* **72**, 962–970.
75. Kaiser, L. M., Harms, M., Sauter, D., Rawat, V. P. S., Glitscher, M., Hildt, E., Tews, D., Hunter, Z., Münch, J., Buske, C. & Roccaro, A. M. Targeting of CXCR4 by the Naturally Occurring CXCR4 Antagonist EPI-X4 in Waldenström's Macroglobulinemia. (2021). *Cancers* **13**, 826.
76. Kaiser, L. M., Hunter, Z. R., Treon, S. P. & Buske, C. CXCR4 in Waldenström's Macroglobulinema: chances and challenges. (2021). *Leukemia* **35**, 333–345.
77. Jiang, C., Ma, S., Hu, R., Wang, X., Li, M., Tian, F., Jiang, W., Zhu, L. & Bian, Z. Effect of CXCR4 on Apoptosis in Osteosarcoma Cells via the PI3K/Akt/NF-κβ Signaling Pathway. (2018). *Cell. Physiol. Biochem.* **46**, 2250–2260.
78. Smith, M. C. P., Luker, K. E., Garbow, J. R., Prior, J. L., Jackson, E., Piwnica-Worms, D. & Luker, G. D. CXCR4 Regulates Growth of Both Primary and Metastatic Breast Cancer. (2004). *Cancer Res.* **64**, 8604–8612.
79. Orimo, A., Gupta, P. B., Sgroi, D. C., Arenzana-Seisdedos, F., Delaunay, T., Naeem, R., Carey, V. J., Richardson, A. L. & Weinberg, R. A. Stromal Fibroblasts Present in Invasive Human Breast Carcinomas Promote Tumor Growth and Angiogenesis through Elevated SDF-1/CXCL12 Secretion. (2005). *Cell* **121**, 335–348.
80. Kojima, Y., Acar, A., Eaton, E. N., Mellody, K. T., Scheel, C., Ben-Porath, I., Onder, T. T., Wang, Z. C., Richardson, A. L., Weinberg, R. A. & Orimo, A. Autocrine TGF-β and stromal cell-derived factor-1 (SDF-1) signaling drives the evolution of tumor-promoting mammary stromal myofibroblasts. (2010). *Proc. Natl. Acad. Sci.* **107**, 20009–20014.

81. Mezzapelle, R., Leo, M., Caprioglio, F., Colley, L. S., Lamarca, A., Sabatino, L., Colantuoni, V., Crippa, M. P. & Bianchi, M. E. CXCR4/CXCL12 Activities in the Tumor Microenvironment and Implications for Tumor Immunotherapy. (2022). *Cancers* **14**, 2314.
82. Kalluri, R. & Weinberg, R. A. The basics of epithelial-mesenchymal transition. (2009). *J. Clin. Invest.* **119**, 1420–1428.
83. Roche, J. The Epithelial-to-Mesenchymal Transition in Cancer. (2018). *Cancers* **10**, 52.
84. Gloushankova, N. A., Zhitnyak, I. Y. & Rubtsova, S. N. Role of Epithelial-Mesenchymal Transition in Tumor Progression. (2018). *Biochem. Mosc.* **83**, 1469–1476.
85. Cheng, Y., Song, Y., Qu, J., Che, X., Song, N., Fan, Y., Wen, T., Xu, L., Gong, J., Wang, X., Zhang, C., Qu, X. & Liu, Y. The Chemokine Receptor CXCR4 and c-MET Cooperatively Promote Epithelial-Mesenchymal Transition in Gastric Cancer Cells. (2018). *Transl. Oncol.* **11**, 487–497.
86. Lin, Y., Ma, Q., Li, L. & Wang, H. The CXCL12–CXCR4 axis promotes migration, invasiveness, and EMT in human papillary thyroid carcinoma B-CPAP cells via NF-κB signaling. (2018). *Biochem. Cell Biol.* **96**, 619–626.
87. Gatti, M., Pattarozzi, A., Bajetto, A., Würth, R., Daga, A., Fiaschi, P., Zona, G., Florio, T. & Barbieri, F. Inhibition of CXCL12/CXCR4 autocrine/paracrine loop reduces viability of human glioblastoma stem-like cells affecting self-renewal activity. (2013). *Toxicology* **314**, 209–220.
88. Hermann, P. C., Huber, S. L., Herrler, T., Aicher, A., Ellwart, J. W., Guba, M., Bruns, C. J. & Heeschen, C. Distinct Populations of Cancer Stem Cells Determine Tumor Growth and Metastatic Activity in Human Pancreatic Cancer. (2007). *Cell Stem Cell* **1**, 313–323.
89. Mardani, A., Gheytanchi, E., Mousavie, S. H., Madjd Jabari, Z. & Shooshtarizadeh, T. Clinical Significance of Cancer Stem Cell Markers CD133 and CXCR4 in Osteosarcomas. (2020). *Asian Pac. J. Cancer Prev.* **21**, 67–73.
90. López-Gil, J. C., Martin-Hijano, L., Hermann, P. C. & Sainz, B. The CXCL12 Crossroads in Cancer Stem Cells and Their Niche. (2021). *Cancers* **13**, 469.
91. Iwasa, S., Yanagawa, T., Fan, J. & Katoh, R. Expression of CXCR4 and its ligand SDF-1 in intestinal-type gastric cancer is associated with lymph node and liver metastasis. (2009). *Anticancer Res.* **29**, 4751–4758.

92. Wang, M., Yang, X., Wei, M. & Wang, Z. The Role of CXCL12 Axis in Lung Metastasis of Colorectal Cancer. (2018). *J. Cancer* **9**, 3898–3903.
93. Zhang, J., Liu, C., Mo, X., Shi, H. & Li, S. Mechanisms by which CXCR4/CXCL12 cause metastatic behavior in pancreatic cancer. (2017). *Oncol. Lett.*
94. Anderson, N. M. & Simon, M. C. The tumor microenvironment. (2020). *Curr. Biol.* **30**, R921–R925.
95. Baghban, R., Roshangar, L., Jahanban-Esfahlan, R., Seidi, K., Ebrahimi-Kalan, A., Jaymand, M., Kolahian, S., Javaheri, T. & Zare, P. Tumor microenvironment complexity and therapeutic implications at a glance. (2020). *Cell Commun. Signal.* **18**, 59.
96. Labani-Motlagh, A., Ashja-Mahdavi, M. & Loskog, A. The Tumor Microenvironment: A Milieu Hindering and Obstructing Antitumor Immune Responses. (2020). *Front. Immunol.* **11**, 940.
97. Sant, M., Allemani, C., Tereanu, C., De Angelis, R., Capocaccia, R., Visser, O., Marcos-Gragera, R., Maynadié, M., Simonetti, A., Lutz, J.-M., Berrino, F., & and the HAEMACARE Working Group. Incidence of hematologic malignancies in Europe by morphologic subtype: results of the HAEMACARE project. (2010). *Blood* **116**, 3724–3734.
98. Tietsche de Moraes Hungria, V., Chiattone, C., Pavlovsky, M., Abenoza, L. M., Agreda, G. P., Armenta, J., Arrais, C., Avendaño Flores, O., Barroso, F., Basquiera, A. L., Cao, C., Cugliari, M. S., Enrico, A., Foggliatto, L. M., Galvez, K. M., Gomez, D., Gomez, A., de Iracema, D., Farias, D., Lopez, L., Mantilla, W. A., Martínez, D., Mela, M. J., Miguel, C. E., Ovilla, R., Palmer, L., Pavlovsky, C., Ramos, C., Remaggi, G., Santucci, R., Schusterschitz, S., Sossa, C. L., Tuna-Aguilar, E., Vela, J., Santos, T., de la Mora, O., Machnicki, G., Fernandez, M. & Barreyro, P. Epidemiology of Hematologic Malignancies in Real-World Settings: Findings From the Hemato-Oncology Latin America Observational Registry Study. (2019). *J. Glob. Oncol.* 1–19.
99. de Leval, L. & Jaffe, E. S. Lymphoma Classification. (2020). *Cancer J.* **26**, 176–185.
100. Singh, R., Shaik, S., Negi, B., Rajguru, J., Patil, P., Parihar, A. & Sharma, U. Non-Hodgkin's lymphoma: A review. (2020). *J. Fam. Med. Prim. Care* **9**, 1834.
101. Thandra, K. C., Barsouk, A., Saginala, K., Padala, S. A., Barsouk, A. & Rawla, P. Epidemiology of Non-Hodgkin's Lymphoma. (2021). *Med. Sci.* **9**, 5.
102. Coffey, J., Hodgson, D. C. & Gospodarowicz, M. K. Therapy of non-Hodgkin's lymphoma. (2003). *Eur. J. Nucl. Med. Mol. Imaging* **30**, S28–S36.

103. Harris, N. L., Jaffe, E. S., Diebold, J., Flandrin, G., Muller-Hermelink, H. K., Vardiman, J., Lister, T. A. & Bloomfield, C. D. The World Health Organization Classification of Neoplastic Diseases of the Hematopoietic and Lymphoid Tissues. (1999). *Ann. Oncol.* **10**, 1419–1432.
104. Bray, F., Ferlay, J., Soerjomataram, I., Siegel, R. L., Torre, L. A. & Jemal, A. Global cancer statistics 2018: GLOBOCAN estimates of incidence and mortality worldwide for 36 cancers in 185 countries. (2018). *CA. Cancer J. Clin.* **68**, 394–424.
105. Armitage, J. O., Gascoyne, R. D., Lunning, M. A. & Cavalli, F. Non-Hodgkin lymphoma. (2017). *The Lancet* **390**, 298–310.
106. Luo, J., Craver, A., Bahl, K., Stepniak, L., Moore, K., King, J., Zhang, Y. & Aschebrook-Kilfoy, B. Etiology of non-Hodgkin lymphoma: A review from epidemiologic studies. (2022). *J. Natl. Cancer Cent.* **2**, 226–234.
107. Shankland, K. R., Armitage, J. O. & Hancock, B. W. Non-Hodgkin lymphoma. (2012). *The Lancet* **380**, 848–857.
108. Oellerich, T., Brunnberg, U., Scheich, S. & Dreyling, M. Kapitel 28 Non-Hodgkin-Lymphome. in Serve, H. & Zurmeyer, D. (2022) *Therapie-Handbuch Onkologie und Hämatologie* 195–199 Elsevier GmbH.
109. Radkiewicz, C., Bruchfeld, J. B., Weibull, C. E., Jeppesen, M. L., Frederiksen, H., Lambe, M., Jakobsen, L., El-Galaly, T. C., Smedby, K. E. & Wästerlid, T. Sex differences in lymphoma incidence and mortality by subtype: A population-based study. (2023). *Am. J. Hematol.* **98**, 23–30.
110. Apor, E., O'Brien, J., Stephen, M. & Castillo, J. J. Systemic lupus erythematosus is associated with increased incidence of hematologic malignancies: A meta-analysis of prospective cohort studies. (2014). *Leuk. Res.* **38**, 1067–1071.
111. Opelz, G. & Henderson, R. Incidence of non-hodgkin lymphoma in kidney and heart transplant recipients. (1993). *The Lancet* **342**, 1514–1516.
112. Parker, A. S., Cerhan, J. R., Dick, F., Kemp, J., Habermann, T. M., Wallace, R. B., Sellers, T. A. & Folsom, A. R. Smoking and Risk of Non-Hodgkin Lymphoma Subtypes in a Cohort of Older Women. (2000). *Leuk. Lymphoma* **37**, 341–349.
113. Schöllkopf, C., Ekström Smedby, K., Hjalgrim, H., Rostgaard, K., Gadeberg, O., Roos, G., Porwit-MacDonald, A., Glimelius, B., Adami, H.-O. & Melbye, M. Cigarette Smoking and Risk of Non-Hodgkin's Lymphoma—A Population-Based Case-Control Study. (2005). *Cancer Epidemiol. Biomarkers Prev.* **14**, 1791–1796.

114. Geyer, S. M., Morton, L. M., Habermann, T. M., Allmer, C., Davis, S., Cozen, W., Severson, R. K., Lynch, C. F., Wang, S. S., Maurer, M. J., Hartge, P. & Cerhan, J. R. Smoking, alcohol use, obesity, and overall survival from non-Hodgkin lymphoma: A population-based study. (2010). *Cancer* **116**, 2993–3000.
115. Poiesz, B. J., Ruscetti, F. W., Gazdar, A. F., Bunn, P. A., Minna, J. D. & Gallo, R. C. Detection and isolation of type C retrovirus particles from fresh and cultured lymphocytes of a patient with cutaneous T-cell lymphoma. (1980). *Proc. Natl. Acad. Sci.* **77**, 7415–7419.
116. Wolf, T., Brodt, H.-R., Fichtlscherer, S., Mantzsch, K., Hoelzer, D., Helm, E., Mitrou, P. & Chow, K. U. Changing incidence and prognostic factors of survival in AIDS-related non-Hodgkin's lymphoma in the era of highly active antiretroviral therapy (HAART). (2005). *Leuk. Lymphoma* **46**, 207–215.
117. Biggar, R. J., Horm, J., Goedert, J. J. & Melbye, M. Cancer in a group at risk of acquired immunodeficiency syndrome (AIDS) through 1984. (1987). *Am. J. Epidemiol.* **126**, 578–586.
118. De Wolf-Peeters, C. & Pittaluga, S. Mantle-cell lymphoma. (1994). *Ann. Oncol.* **5**, S35–S37.
119. Lennert, K., Stein, H. & Kaiserling, E. Cytological and functional criteria for the classification of malignant lymphomata. (1975). *Br. J. Cancer. Suppl.* **2**, 29–43.
120. Cortelazzo, S., Ponzoni, M., Ferreri, A. J. M. & Dreyling, M. Mantle cell lymphoma. (2012). *Crit. Rev. Oncol. Hematol.* **82**, 78–101.
121. Dreyling, M., Geisler, C., Hermine, O., Kluin-Nelemans, H. C., Le Gouill, S., Rule, S., Shpilberg, O., Walewski, J. & Ladetto, M. Newly diagnosed and relapsed mantle cell lymphoma: ESMO Clinical Practice Guidelines for diagnosis, treatment and follow-up. (2014). *Ann. Oncol.* **25**, iii83–iii92.
122. Lynch, D. T., Koya, S., Acharya, U. & Kumar, A. Mantle Cell Lymphoma. in (2022) *StatPearls* Download on: March 1, 2023. Available from: http://www.ncbi.nlm.nih.gov/books/NBK536985/Treasure Island (FL): StatPearls Publishing.
123. Van Den Berghe, H., Parloir, C., David, G., Michaux, J. L. & Sokal, G. A new characteristic karyotypic anomaly in lymphoproliferative disorders. (1979). *Cancer* **44**, 188–195.
124. Hoster, E., Dreyling, M., Klapper, W., Gisselbrecht, C., van Hoof, A., Kluin-Nelemans, H. C., Pfreundschuh, M., Reiser, M., Metzner, B., Einsele, H., Peter, N., Jung, W.,

Wörmann, B., Ludwig, W.-D., Dührsen, U., Eimermacher, H., Wandt, H., Hasford, J., Hiddemann, W. & Unterhalt, M. A new prognostic index (MIPI) for patients with advanced-stage mantle cell lymphoma. (2008). *Blood* **111**, 558–565.

125. Geisler, C. H., Kolstad, A., Laurell, A., Räty, R., Jerkeman, M., Eriksson, M., Nordström, M., Kimby, E., Boesen, A. M., Nilsson-Ehle, H., Kuittinen, O., Lauritzsen, G. F., Ralfkiær, E., Ehinger, M., Sundström, C., Delabie, J., Karjalainen-Lindsberg, M.-L., Brown, P., Elonen, E., & for the Nordic Lymphoma Group. The Mantle Cell Lymphoma International Prognostic Index (MIPI) is superior to the International Prognostic Index (IPI) in predicting survival following intensive first-line immunochemotherapy and autologous stem cell transplantation (ASCT). (2010). *Blood* **115**, 1530–1533.
126. Lim, S. Y., Horsman, J. M. & Hancock, B. W. The Mantle Cell Lymphoma International Prognostic Index: Does it work in routine practice? (2010). *Oncol. Lett.* **1**, 187–188.
127. Vose, J. M. Mantle cell lymphoma: 2017 update on diagnosis, risk-stratification, and clinical management: Vose. (2017). *Am. J. Hematol.* **92**, 806–813.
128. Ginaldi, L., De Martinis, M., Matutes, E., Farahat, N., Morilla, R. & Catovsky, D. Levels of expression of CD19 and CD20 in chronic B cell leukaemias. (1998). *J. Clin. Pathol.* **51**, 364–369.
129. Eskelund, C. W., Dahl, C., Hansen, J. W., Westman, M., Kolstad, A., Pedersen, L. B., Montano-Almendras, C. P., Husby, S., Freiburghaus, C., Ek, S., Pedersen, A., Niemann, C., Räty, R., Brown, P., Geisler, C. H., Andersen, M. K., Guldberg, P., Jerkeman, M. & Grønbæk, K. TP53 mutations identify younger mantle cell lymphoma patients who do not benefit from intensive chemoimmunotherapy. (2017). *Blood* **130**, 1903–1910.
130. Delfau-Larue, M.-H., Klapper, W., Berger, F., Jardin, F., Briere, J., Salles, G., Casasnovas, O., Feugier, P., Haioun, C., Ribrag, V., Thieblemont, C., Unterhalt, M., Dreyling, M., Macintyre, E., Pott, C., Hermine, O. & Hoster, E. High-dose cytarabine does not overcome the adverse prognostic value of CDKN2A and TP53 deletions in mantle cell lymphoma. (2015). *Blood* **126**, 604–611.
131. Greiner, T. C., Dasgupta, C., Ho, V. V., Weisenburger, D. D., Smith, L. M., Lynch, J. C., Vose, J. M., Fu, K., Armitage, J. O., Braziel, R. M., Campo, E., Delabie, J., Gascoyne, R. D., Jaffe, E. S., Muller-Hermelink, H. K., Ott, G., Rosenwald, A., Staudt, L. M., Im, M. Y., Karaman, M. W., Pike, B. L., Chan, W. C. & Hacia, J. G. Mutation

and genomic deletion status of ataxia telangiectasia mutated (ATM) and p53 confer specific gene expression profiles in mantle cell lymphoma. (2006). *Proc. Natl. Acad. Sci. U. S. A.* **103**, 2352–2357.

132. Halldórsdóttir, A. M., Lundin, A., Murray, F., Mansouri, L., Knuutila, S., Sundström, C., Laurell, A., Ehrencrona, H., Sander, B. & Rosenquist, R. Impact of TP53 mutation and 17p deletion in mantle cell lymphoma. (2011). *Leukemia* **25**, 1904–1908.
133. Burger, J. A. & Ford, R. J. The microenvironment in mantle cell lymphoma: Cellular and molecular pathways and emerging targeted therapies. (2011). *Semin. Cancer Biol.* **21**, 308–312.
134. Efremov, D. G., Turkalj, S. & Laurenti, L. Mechanisms of B Cell Receptor Activation and Responses to B Cell Receptor Inhibitors in B Cell Malignancies. (2020). *Cancers* **12**, 1396.
135. Pighi, C., Gu, T.-L., Dalai, I., Barbi, S., Parolini, C., Bertolaso, A., Pedron, S., Parisi, A., Ren, J., Cecconi, D., Chilosi, M., Menestrina, F. & Zamò, A. Phospho-proteomic analysis of mantle cell lymphoma cells suggests a pro-survival role of B-cell receptor signaling. (2011). *Cell. Oncol. Dordr.* **34**, 141–153.
136. Juntikka, T., Vaittinen, S., Vahlberg, T., Jyrkkiö, S. & Minn, H. Somatostatin Receptors and Chemokine Receptor CXCR4 in Lymphomas: A Histopathological Review of Six Lymphoma Subtypes. (2021). *Front. Oncol.* **11**, 710900.
137. Trentin, L., Cabrelle, A., Facco, M., Carollo, D., Miorin, M., Tosoni, A., Pizzo, P., Binotto, G., Nicolardi, L., Zambello, R., Adami, F., Agostini, C. & Semenzato, G. Homeostatic chemokines drive migration of malignant B cells in patients with non-Hodgkin lymphomas. (2004). *Blood* **104**, 502–508.
138. Balsas, P., Palomero, J., Eguileor, Á., Rodríguez, M. L., Vegliante, M. C., Planas-Rigol, E., Sureda-Gómez, M., Cid, M. C., Campo, E. & Amador, V. SOX11 promotes tumor protective microenvironment interactions through CXCR4 and FAK regulation in mantle cell lymphoma. (2017). *Blood* **130**, 501–513.
139. Kurtova, A. V., Tamayo, A. T., Ford, R. J. & Burger, J. A. Mantle cell lymphoma cells express high levels of CXCR4, CXCR5, and VLA-4 (CD49d): Importance for interactions with the stromal microenvironment and specific targeting. (2009). *Blood* **113**, 4604–4613.
140. Kipps, T. J., Stevenson, F. K., Wu, C. J., Croce, C. M., Packham, G., Wierda, W. G., O'Brien, S., Gribben, J. & Rai, K. Chronic lymphocytic leukaemia. (2017). *Nat. Rev. Dis. Primer* **3**, 16096.

141. Morton, L. M., Wang, S. S., Devesa, S. S., Hartge, P., Weisenburger, D. D. & Linet, M. S. Lymphoma incidence patterns by WHO subtype in the United States, 1992-2001. (2006). *Blood* **107**, 265–276.
142. Li, Y., Wang, Y., Wang, Z., Yi, D. & Ma, S. Racial differences in three major NHL subtypes: Descriptive epidemiology. (2015). *Cancer Epidemiol.* **39**, 8–13.
143. Alaggio, R., Amador, C., Anagnostopoulos, I., Attygalle, A. D., Araujo, I. B. de O., Berti, E., Bhagat, G., Borges, A. M., Boyer, D., Calaminici, M., Chadburn, A., Chan, J. K. C., Cheuk, W., Chng, W.-J., Choi, J. K., Chuang, S.-S., Coupland, S. E., Czader, M., Dave, S. S., de Jong, D., Du, M.-Q., Elenitoba-Johnson, K. S., Ferry, J., Geyer, J., Gratzinger, D., Guitart, J., Gujral, S., Harris, M., Harrison, C. J., Hartmann, S., Hochhaus, A., Jansen, P. M., Karube, K., Kempf, W., Khoury, J., Kimura, H., Klapper, W., Kovach, A. E., Kumar, S., Lazar, A. J., Lazzi, S., Leoncini, L., Leung, N., Leventaki, V., Li, X.-Q., Lim, M. S., Liu, W.-P., Louissaint, A., Marcogliese, A., Medeiros, L. J., Michal, M., Miranda, R. N., Mitteldorf, C., Montes-Moreno, S., Morice, W., Nardi, V., Naresh, K. N., Natkunam, Y., Ng, S.-B., Oschlies, I., Ott, G., Parrens, M., Pulitzer, M., Rajkumar, S. V., Rawstron, A. C., Rech, K., Rosenwald, A., Said, J., Sarkozy, C., Sayed, S., Saygin, C., Schuh, A., Sewell, W., Siebert, R., Sohani, A. R., Tooze, R., Traverse-Glehen, A., Vega, F., Vergier, B., Wechalekar, A. D., Wood, B., Xerri, L. & Xiao, W. The 5th edition of the World Health Organization Classification of Haematolymphoid Tumours: Lymphoid Neoplasms. (2022). *Leukemia* **36**, 1720–1748.
144. Moreau, E. J., Matutes, E., A'Hern, R. P., Morilla, A. M., Morilla, R. M., Owusu-Ankomah, K. A., Seon, B. K. & Catovsky, D. Improvement of the Chronic Lymphocytic Leukemia Scoring System With the Monoclonal Antibody SN8(CD79b). (1997). *Am. J. Clin. Pathol.* **108**, 378–382.
145. Hanada, M., Delia, D., Aiello, A., Stadtmauer, E. & Reed, J. bcl-2 gene hypomethylation and high-level expression in B-cell chronic lymphocytic leukemia. (1993). *Blood* **82**, 1820–1828.
146. Rawstron, A. C., Kreuzer, K.-A., Soosapilla, A., Spacek, M., Stehlikova, O., Gambell, P., McIver-Brown, N., Villamor, N., Psarra, K., Arroz, M., Milani, R., de la Serna, J., Cedena, M. T., Jaksic, O., Nomdedeu, J., Moreno, C., Rigolin, G. M., Cuneo, A., Johansen, P., Johnsen, H. E., Rosenquist, R., Niemann, C. U., Kern, W., Westerman, D., Trneny, M., Mulligan, S., Doubek, M., Pospisilova, S., Hillmen, P., Oscier, D., Hallek, M., Ghia, P. & Montserrat, E. Reproducible diagnosis of chronic lymphocytic

leukemia by flow cytometry: An European Research Initiative on CLL (ERIC) & European Society for Clinical Cell Analysis (ESCCA) Harmonisation project: ERIC/ESCCA CONSENSUS: REPRODUCIBLE CLL DIAGNOSIS BY FLOW CYTOMETRY. (2018). *Cytometry B Clin. Cytom.* **94**, 121–128.

147. Källander, C. F. R., Simonsson, B., Hagberg, H. & Gronowitz, J. S. Serum deoxythymidine kinase gives prognostic information in chronic lymphocytic leukemia. (1984). *Cancer* **54**, 2450–2455.
148. Gronowitz, J. S., Källander, C. F. R., Diderholm, H., Hagberg, H. & Pettersson, U. Application of anin vitro assay for serum thymidine kinase: Results on viral disease and malignancies in humans. (1984). *Int. J. Cancer* **33**, 5–12.
149. Döhner, H., Stilgenbauer, S., Benner, A., Leupolt, E., Kröber, A., Bullinger, L., Döhner, K., Bentz, M. & Lichter, P. Genomic Aberrations and Survival in Chronic Lymphocytic Leukemia. (2000). *N. Engl. J. Med.* **343**, 1910–1916.
150. Dohner, H., Fischer, K., Bentz, M., Hansen, K., Benner, A., Cabot, G., Diehl, D., Schlenk, R., Coy, J. & Stilgenbauer, S. p53 gene deletion predicts for poor survival and non-response to therapy with purine analogs in chronic B-cell leukemias. (1995). *Blood* **85**, 1580–1589.
151. Rossi, D., Cerri, M., Deambrogi, C., Sozzi, E., Cresta, S., Rasi, S., De Paoli, L., Spina, V., Gattei, V., Capello, D., Forconi, F., Lauria, F. & Gaidano, G. The Prognostic Value of *TP53* Mutations in Chronic Lymphocytic Leukemia Is Independent of Del17p13: Implications for Overall Survival and Chemorefractoriness. (2009). *Clin. Cancer Res.* **15**, 995–1004.
152. Hamblin, T. J., Davis, Z., Gardiner, A., Oscier, D. G. & Stevenson, F. K. Unmutated Ig VH Genes Are Associated With a More Aggressive Form of Chronic Lymphocytic Leukemia. (1999). *Blood* **94**, 1848–1854.
153. Orchard, J. A., Ibbotson, R. E., Davis, Z., Wiestner, A., Rosenwald, A., Thomas, P. W., Hamblin, T. J., Staudt, L. M. & Oscier, D. G. ZAP-70 expression and prognosis in chronic lymphocytic leukaemia. (2004). *The Lancet* **363**, 105–111.
154. Damle, R. N., Wasil, T., Fais, F., Ghiotto, F., Valetto, A., Allen, S. L., Buchbinder, A., Budman, D., Dittmar, K., Kolitz, J., Lichtman, S. M., Schulman, P., Vinciguerra, V. P., Rai, K. R., Ferrarini, M. & Chiorazzi, N. Ig V Gene Mutation Status and CD38 Expression As Novel Prognostic Indicators in Chronic Lymphocytic Leukemia. (1999). *Blood* **94**, 1840–1847.

155. Wang, H., Kadlecek, T. A., Au-Yeung, B. B., Goodfellow, H. E. S., Hsu, L.-Y., Freedman, T. S. & Weiss, A. ZAP-70: an essential kinase in T-cell signaling. (2010). *Cold Spring Harb. Perspect. Biol.* **2**, a002279.

156. Reiners, K. S., Topolar, D., Henke, A., Simhadri, V. R., Kessler, J., Sauer, M., Bessler, M., Hansen, H. P., Tawadros, S., Herling, M., Krönke, M., Hallek, M. & Pogge von Strandmann, E. Soluble ligands for NK cell receptors promote evasion of chronic lymphocytic leukemia cells from NK cell anti-tumor activity. (2013). *Blood* **121**, 3658–3665.

157. McClanahan, F., Riches, J. C., Miller, S., Day, W. P., Kotsiou, E., Neuberg, D., Croce, C. M., Capasso, M. & Gribben, J. G. Mechanisms of PD-L1/PD-1–mediated CD8 T-cell dysfunction in the context of aging-related immune defects in the Eμ-TCL1 CLL mouse model. (2015). *Blood* **126**, 212–221.

158. Maffei, R., Bulgarelli, J., Fiorcari, S., Martinelli, S., Castelli, I., Valenti, V., Rossi, D., Bonacorsi, G., Zucchini, P., Potenza, L., Vallisa, D., Gattei, V., Poeta, G. D., Forconi, F., Gaidano, G., Narni, F., Luppi, M. & Marasca, R. Endothelin-1 Promotes Survival and Chemoresistance in Chronic Lymphocytic Leukemia B Cells through ETA Receptor. (2014). *PLoS ONE* **9**, e98818.

159. Kitada, S., Zapata, J. M., Andreeff, M. & Reed, J. C. Bryostatin and CD40-ligand enhance apoptosis resistance and induce expression of cell survival genes in B-cell chronic lymphocytic leukaemia: Apoptosis Resistance Induced by CD40L and Bryostatin in B-CLL. (1999). *Br. J. Haematol.* **106**, 995–1004.

160. Scielzo, C., Apollonio, B., Scarfò, L., Janus, A., Muzio, M., ten Hacken, E., Ghia, P. & Caligaris-Cappio, F. The functional in vitro response to CD40 ligation reflects a different clinical outcome in patients with chronic lymphocytic leukemia. (2011). *Leukemia* **25**, 1760–1767.

161. Sivina, M., Xiao, L., Kim, E., Vaca, A., Chen, S.-S., Keating, M. J., Ferrajoli, A., Estrov, Z., Jain, N., Wierda, W. G., Huang, X., Chiorazzi, N. & Burger, J. A. CXCL13 plasma levels function as a biomarker for disease activity in patients with chronic lymphocytic leukemia. (2021). *Leukemia* **35**, 1610–1620.

162. Bürkle, A., Niedermeier, M., Schmitt-Gräff, A., Wierda, W. G., Keating, M. J. & Burger, J. A. Overexpression of the CXCR5 chemokine receptor, and its ligand, CXCL13 in B-cell chronic lymphocytic leukemia. (2007). *Blood* **110**, 3316–3325.

163. Ticchioni, M., Essafi, M., Jeandel, P. Y., Davi, F., Cassuto, J. P., Deckert, M. & Bernard, A. Homeostatic chemokines increase survival of B-chronic lymphocytic

leukemia cells through inactivation of transcription factor FOXO3a. (2007). *Oncogene* **26**, 7081–7091.

164. Heinig, K., Gätjen, M., Grau, M., Stache, V., Anagnostopoulos, I., Gerlach, K., Niesner, R. A., Cseresnyes, Z., Hauser, A. E., Lenz, P., Hehlgans, T., Brink, R., Westermann, J., Dörken, B., Lipp, M., Lenz, G., Rehm, A. & Höpken, U. E. Access to Follicular Dendritic Cells Is a Pivotal Step in Murine Chronic Lymphocytic Leukemia B-cell Activation and Proliferation. (2014). *Cancer Discov.* **4**, 1448–1465.
165. ten Hacken, E. & Burger, J. A. Microenvironment interactions and B-cell receptor signaling in Chronic Lymphocytic Leukemia: Implications for disease pathogenesis and treatment. (2016). *Biochim. Biophys. Acta BBA - Mol. Cell Res.* **1863**, 401–413.
166. Möhle, R., Failenschmid, C., Bautz, F. & Kanz, L. Overexpression of the chemokine receptor CXCR4 in B cell chronic lymphocytic leukemia is associated with increased functional response to stromal cell-derived factor-1 (SDF-1). (1999). *Leukemia* **13**, 1954–1959.
167. Barretina, J., Juncà, J., Llano, A., Gutiérrez, A., Flores, A., Blanco, J., Clotet, B. & Esté, J. A. CXCR4 and SDF-1 expression in B-cell chronic lymphocytic leukemia and stage of the disease. (2003). *Ann. Hematol.* **82**, 500–505.
168. Kashyap, M. K., Amaya-Chanaga, C. I., Kumar, D., Simmons, B., Huser, N., Gu, Y., Hallin, M., Lindquist, K., Yafawi, R., Choi, M. Y., Amine, A.-A., Rassenti, L. Z., Zhang, C., Liu, S.-H., Smeal, T., Fantin, V. R., Kipps, T. J., Pernasetti, F. & Castro, J. E. Targeting the CXCR4 pathway using a novel anti-CXCR4 IgG1 antibody (PF-06747143) in chronic lymphocytic leukemia. (2017). *J. Hematol. Oncol.J Hematol Oncol* **10**, 112.
169. Burger, M., Hartmann, T., Krome, M., Rawluk, J., Tamamura, H., Fujii, N., Kipps, T. J. & Burger, J. A. Small peptide inhibitors of the CXCR4 chemokine receptor (CD184) antagonize the activation, migration, and antiapoptotic responses of CXCL12 in chronic lymphocytic leukemia B cells. (2005). *Blood* **106**, 1824–1830.
170. Białopiotrowicz, E., Górniak, P., Noyszewska-Kania, M., Puła, B., Makuch-Łasica, H., Nowak, G., Bluszcz, A., Szydłowski, M., Jabłonska, E., Piechna, K., Sewastianik, T., Polak, A., Lech-Marańda, E., Budziszewska, B. K., Wasylecka-Juszczyńska, M., Borg, K., Warzocha, K., Czardybon, W., Gałęzowski, M., Windak, R., Brzózka, K. & Juszczyński, P. Microenvironment-induced PIM kinases promote CXCR4-triggered mTOR pathway required for chronic lymphocytic leukaemia cell migration. (2018). *J. Cell. Mol. Med.* **22**, 3548–3559.

171. Burger, J. A., Burger, M. & Kipps, T. J. Chronic lymphocytic leukemia B cells express functional CXCR4 chemokine receptors that mediate spontaneous migration beneath bone marrow stromal cells. (1999). *Blood* **94**, 3658–3667.
172. Messmer, D., Fecteau, J.-F., O'Hayre, M., Bharati, I. S., Handel, T. M. & Kipps, T. J. Chronic lymphocytic leukemia cells receive RAF-dependent survival signals in response to CXCL12 that are sensitive to inhibition by sorafenib. (2011). *Blood* **117**, 882–889.
173. Laboratory of Biotechnology (MedBiotech), Rabat Medical and Pharmacy School, Mohammed V University in Rabat, Rabat, Morocco, Arrouchi, H., Lakhlili, W. & Ibrahimi, A. A review on PIM kinases in tumors. (2019). *Bioinformation* **15**, 40–45.
174. Decker, S., Finter, J., Forde, A. J., Kissel, S., Schwaller, J., Mack, T. S., Kuhn, A., Gray, N., Follo, M., Jumaa, H., Burger, M., Zirlik, K., Pfeifer, D., Miduturu, C. V., Eibel, H., Veelken, H. & Dierks, C. PIM Kinases Are Essential for Chronic Lymphocytic Leukemia Cell Survival (PIM2/3) and CXCR4-Mediated Microenvironmental Interactions (PIM1). (2014). *Mol. Cancer Ther.* **13**, 1231–1245.
175. Chen, S.-S., Chang, B. Y., Chang, S., Tong, T., Ham, S., Sherry, B., Burger, J. A., Rai, K. R. & Chiorazzi, N. BTK inhibition results in impaired CXCR4 chemokine receptor surface expression, signaling and function in chronic lymphocytic leukemia. (2016). *Leukemia* **30**, 833–843.
176. Palma, M., Mulder, T. A. & Österborg, A. BTK Inhibitors in Chronic Lymphocytic Leukemia: Biological Activity and Immune Effects. (2021). *Front. Immunol.* **12**, 686768.
177. Vlad, A., Deglesne, P.-A., Letestu, R., Saint-Georges, S., Chevallier, N., Baran-Marszak, F., Varin-Blank, N., Ajchenbaum-Cymbalista, F. & Ledoux, D. Down-regulation of CXCR4 and CD62L in Chronic Lymphocytic Leukemia Cells Is Triggered by B-Cell Receptor Ligation and Associated with Progressive Disease. (2009). *Cancer Res.* **69**, 6387–6395.
178. Quiroga, M. P., Balakrishnan, K., Kurtova, A. V., Sivina, M., Keating, M. J., Wierda, W. G., Gandhi, V. & Burger, J. A. B-cell antigen receptor signaling enhances chronic lymphocytic leukemia cell migration and survival: specific targeting with a novel spleen tyrosine kinase inhibitor, R406. (2009). *Blood* **114**, 1029–1037.
179. Niedermeier, M., Hennessy, B. T., Knight, Z. A., Henneberg, M., Hu, J., Kurtova, A. V., Wierda, W. G., Keating, M. J., Shokat, K. M. & Burger, J. A. Isoform-selective phosphoinositide 3'-kinase inhibitors inhibit CXCR4 signaling and overcome stromal

cell-mediated drug resistance in chronic lymphocytic leukemia: a novel therapeutic approach. (2009). *Blood* **113**, 5549–5557.

180. Burger, J. A., Tsukada, N., Burger, M., Zvaifler, N. J., Dell'Aquila, M. & Kipps, T. J. Blood-derived nurse-like cells protect chronic lymphocytic leukemia B cells from spontaneous apoptosis through stromal cell–derived factor-1. (2000). *Blood* **96**, 2655–2663.
181. Mukkamalla, S. K. R., Taneja, A., Malipeddi, D. & Master, S. R. Chronic Lymphocytic Leukemia. in (2022) *StatPearls* Download on: March 8, 2023. Available from: http://www.ncbi.nlm.nih.gov/books/NBK470433/Treasure Island (FL): StatPearls Publishing.
182. LiverTox: Clinical and Research Information on Drug-Induced Liver Injury [Internet]. Bethesda (MD): National Institute of Diabetes and Digestive and Kidney Diseases; 2012-. Chlorambucil. [Updated 2017 Oct 5]. Available from: https://www.ncbi.nlm.nih.gov/books/NBK548207/.
183. O'Brien, S., del Giglio, A. & Keating, M. Advances in the biology and treatment of B-cell chronic lymphocytic leukemia. (1995). *Blood* **85**, 307–318.
184. Lee, H.-Z., Miller, B. W., Kwitkowski, V. E., Ricci, S., DelValle, P., Saber, H., Grillo, J., Bullock, J., Florian, J., Mehrotra, N., Ko, C.-W., Nie, L., Shapiro, M., Tolnay, M., Kane, R. C., Kaminskas, E., Justice, R., Farrell, A. T. & Pazdur, R. U.S. Food and Drug Administration Approval: Obinutuzumab in Combination with Chlorambucil for the Treatment of Previously Untreated Chronic Lymphocytic Leukemia. (2014). *Clin. Cancer Res.* **20**, 3902–3907.
185. Zhao, R., Liu, J., Li, Z., Zhang, W., Wang, F. & Zhang, B. Recent Advances in CXCL12/CXCR4 Antagonists and Nano-Based Drug Delivery Systems for Cancer Therapy. (2022). *Pharmaceutics* **14**, 1541.
186. Taromi, S., Kayser, G., Catusse, J., von Elverfeldt, D., Reichardt, W., Braun, F., Weber, W. A., Zeiser, R. & Burger, M. CXCR4 antagonists suppress small cell lung cancer progression. (2016). *Oncotarget* **7**, 85185–85195.
187. Uy, G. L., Rettig, M. P., Motabi, I. H., McFarland, K., Trinkaus, K. M., Hladnik, L. M., Kulkarni, S., Abboud, C. N., Cashen, A. F., Stockerl-Goldstein, K. E., Vij, R., Westervelt, P. & DiPersio, J. F. A phase 1/2 study of chemosensitization with the CXCR4 antagonist plerixafor in relapsed or refractory acute myeloid leukemia. (2012). *Blood* **119**, 3917–3924.

188. Choueiri, T. K., Atkins, M. B., Rose, T. L., Alter, R. S., Ju, Y., Niland, K., Wang, Y., Arbeit, R., Parasuraman, S., Gan, L. & McDermott, D. F. A phase 1b trial of the CXCR4 inhibitor mavorixafor and nivolumab in advanced renal cell carcinoma patients with no prior response to nivolumab monotherapy. (2021). *Invest. New Drugs* **39**, 1019–1027.

189. Andtbacka, R. H. I., Wang, Y., Pierce, R. H., Campbell, J. S., Yushak, M., Milhem, M., Ross, M., Niland, K., Arbeit, R. D., Parasuraman, S., Bickley, K., Yeung, C. C., Aicher, L. D., Smythe, K. S. & Gan, L. Mavorixafor, an Orally Bioavailable CXCR4 Antagonist, Increases Immune Cell Infiltration and Inflammatory Status of Tumor Microenvironment in Patients with Melanoma. (2022). *Cancer Res. Commun.* **2**, 904–913.

190. Dale, D. C., Firkin, F., Bolyard, A. A., Kelley, M., Makaryan, V., Gorelick, K. J., Ebrahim, T., Garg, V., Tang, W., Jiang, H., Skerlj, R. & Beaussant Cohen, S. Results of a phase 2 trial of an oral CXCR4 antagonist, mavorixafor, for treatment of WHIM syndrome. (American Society of Hematology, 2020). *Blood* **136**, 2994–3003 American Society of Hematology.

191. Zhou, W., Guo, S., Liu, M., Burow, M. E. & Wang, G. Targeting CXCL12/CXCR4 Axis in Tumor Immunotherapy. (2019). *Curr. Med. Chem.* **26**, 3026–3041.

192. Leo, M. & Sabatino, L. Targeting CXCR4 and CD47 Receptors: An Overview of New and Old Molecules for a Biological Personalized Anticancer Therapy. (2022). *Int. J. Mol. Sci.* **23**, 12499.

193. De Clercq, E. Mozobil® (Plerixafor, AMD3100), 10 years after its approval by the US Food and Drug Administration. (2019). *Antivir. Chem. Chemother.* **27**,.

194. Lefort, S., Thuleau, A., Kieffer, Y., Sirven, P., Bieche, I., Marangoni, E., Vincent-Salomon, A. & Mechta-Grigoriou, F. CXCR4 inhibitors could benefit to HER2 but not to triple-negative breast cancer patients. (2017). *Oncogene* **36**, 1211–1222.

195. Kim, Y.-R. & Eom, K.-S. Simultaneous Inhibition of CXCR4 and VLA-4 Exhibits Combinatorial Effect in Overcoming Stroma-Mediated Chemotherapy Resistance in Mantle Cell Lymphoma Cells. (2014). *Immune Netw.* **14**, 296–306.

196. Stamatopoulos, B., Meuleman, N., De Bruyn, C., Pieters, K., Mineur, P., Le Roy, C., Saint-Georges, S., Varin-Blank, N., Cymbalista, F., Bron, D. & Lagneaux, L. AMD3100 disrupts the cross-talk between chronic lymphocytic leukemia cells and a mesenchymal stromal or nurse-like cell-based microenvironment: pre-clinical evidence

for its association with chronic lymphocytic leukemia treatments. (2012). *Haematologica* **97**, 608–615.

197. Zirafi, O., Kim, K.-A., Ständker, L., Mohr, K. B., Sauter, D., Heigele, A., Kluge, S. F., Wiercinska, E., Chudziak, D., Richter, R., Moepps, B., Gierschik, P., Vas, V., Geiger, H., Lamla, M., Weil, T., Burster, T., Zgraja, A., Daubeuf, F., Frossard, N., Hachet-Haas, M., Heunisch, F., Reichetzeder, C., Galzi, J.-L., Pérez-Castells, J., Canales-Mayordomo, A., Jiménez-Barbero, J., Giménez-Gallego, G., Schneider, M., Shorter, J., Telenti, A., Hocher, B., Forssmann, W.-G., Bonig, H., Kirchhoff, F. & Münch, J. Discovery and Characterization of an Endogenous CXCR4 Antagonist. (2015). *Cell Rep.* **11**, 737–747.
198. Mendez, C. M., McClain, C. J. & Marsano, L. S. Albumin therapy in clinical practice. (2005). *Nutr. Clin. Pract.* **20**, 314–320.
199. Doweiko, J. P. & Nompleggi, D. J. Role of albumin in human physiology and pathophysiology. (1991). *J. Parenter. Enter. Nutr.* **15**, 207–211.
200. Harm, S., Schildböck, C. & Hartmann, J. Removal of stabilizers from human serum albumin by adsorbents and dialysis used in blood purification. (2018). *PLoS ONE* **13**,.
201. Raoufinia, R., Mota, A., Keyhanvar, N., Safari, F., Shamekhi, S. & Abdolalizadeh, J. Overview of albumin and its purification methods. (2016). *Adv. Pharm. Bull.* **6**, 495–507.
202. Fanali, G., di Masi, A., Trezza, V., Marino, M., Fasano, M. & Ascenzi, P. Human serum albumin: From bench to bedside. (Elsevier Ltd, 2012). *Mol. Aspects Med.* **33**, 209–290 Elsevier Ltd.
203. Tsutsumi, T., Nakao, K., Mitsuoka, S., Hamasaki, K., Tsuruta, S., Shima, M., Nakata, K., Tamaoki, T. & Nagataki, S. Regulation of albumin and α-fetoprotein gene expression by colloid osmotic pressure in human hepatoma cells. (1993). *Gastroenterology* **104**, 256–262.
204. Pietrangelo, A. & Shafritz, D. A. Homeostatic regulation of hepatocyte nuclear transcription factor 1 expression in cultured hepatoma cells. (1994). *Proc. Natl. Acad. Sci. U. S. A.* **91**, 182–186.
205. Matejtschuk, P., Dash, C. H. & Gascoigne, E. W. Production of human albumin solution: a continually developing colloid. (2000). *Br J Anaesth* **85**, 887–95.
206. Yu, M. W. & Finlayson, J. S. Stabilization of Human Albumin by Caprylate and Acetyltryptophanate. (1984). *Vox Sang.* **47**, 28–40.

207. Walenbergh, S. M. A., Houben, T., Rensen, S. S., Bieghs, V., Hendrikx, T., van Gorp, P. J., Oligschlaeger, Y., Jeurissen, M. L. J., Gijbels, M. J. J., Buurman, W. A., Vreugdenhil, A. C. E., Greve, J. W. M., Plat, J., Hofker, M. H., Kalhan, S., Pihlajamäki, J., Lindsey, P., Koek, G. H. & Shiri-Sverdlov, R. Plasma cathepsin D correlates with histological classifications of fatty liver disease in adults and responds to intervention. (2016). *Sci. Rep.* **6**, 38278.

208. Morikawa, W., Yamamoto, K., Ishikawa, S., Takemoto, S., Ono, M., Fukushi, J., Naito, S., Nozaki, C., Iwanaga, S. & Kuwano, M. Angiostatin Generation by Cathepsin D Secreted by Human Prostate Carcinoma Cells. (2000). *J. Biol. Chem.* **275**, 38912–38920.

209. Gorodkiewicz, E., Guszcz, T., Roszkowska-Jakimiec, W. & Kozłowski, R. Cathepsin D serum and urine concentration in superficial and invasive transitional bladder cancer as determined by surface plasmon resonance imaging. (2014). *Oncol. Lett.* **8**, 1323–1327.

210. Kaiser, T., Kamal, H., Rank, A., Kolb, H.-J., Holler, E., Ganser, A., Hertenstein, B., Mischak, H. & Weissinger, E. M. Proteomics applied to the clinical follow-up of patients after allogeneic hematopoietic stem cell transplantation. (2004). *Blood* **104**, 340–349.

211. Mohr, K. B., Zirafi, O., Hennies, M., Wiese, S., Kirchhoff, F. & Münch, J. Sandwich enzyme-linked immunosorbent assay for the quantification of human serum albumin fragment 408-423 in bodily fluids. (Academic Press Inc., 2015). *Anal. Biochem.* **476**, 29–35 Academic Press Inc.

212. Harms, M. Endogenous CXCR4 antagonists: role in HIV-1 transmission and therapy of CXCR4-linked diseases. (2022) Available from: http://dx.doi.org/10.18725/OPARU-41859Universität Ulm.

213. Yamamoto, H., Yamada, T. & Itoh, Y. Probable Involvement of Cathepsin D in the Degradation of ℓ2-Microglobulin in Acidic Urine.

214. Pardesi, S. R., Dandekar, S. P., Jamdar, S. N. & Harikumar, P. Identification and purification of an aspartic proteinase from human semen. (2004). *Indian J. Clin. Biochem.* **19**, 84–90.

215. El Messaoudi, K., Thiry, L., Van Tieghem, N., Liesnard, C., Englert, Y., Moguilevsky, N. & Bollen, A. HIV-1 infectivity and host range modification by cathepsin D present in human vaginal secretions: (1999). *AIDS* **13**, 333–339.

216. El Messaoudi, K., Thiry, L. F., Liesnard, C., Van Tieghem, N., Bollen, A. & Moguilevsky, N. A Human Milk Factor Susceptible to Cathepsin D Inhibitors Enhances Human Immunodeficiency Virus Type 1 Infectivity and Allows Virus Entry into a Mammary Epithelial Cell Line. (2000). *J. Virol.* **74**, 1004–1007.
217. Zhu, J. & Dingess, K. A. The Functional Power of the Human Milk Proteome. (2019). *Nutrients* **11**, 1834.
218. Sokkar, P., Harms, M., Stürzel, C., Gilg, A., Kizilsavas, G., Raasholm, M., Preising, N., Wagner, M., Kirchhoff, F., Ständker, L., Weidinger, G., Mayer, B., Münch, J. & Sanchez-Garcia, E. Computational modeling and experimental validation of the EPI-X4/CXCR4 complex allows rational design of small peptide antagonists. (Springer US, 2021). *Commun. Biol.* **4**, 1–13 Springer US.
219. Harms, M., Habib, M. M. W., Nemska, S., Nicolò, A., Gilg, A., Preising, N., Sokkar, P., Carmignani, S., Raasholm, M., Weidinger, G., Kizilsavas, G., Wagner, M., Ständker, L., Abadi, A. H., Jumaa, H., Kirchhoff, F., Frossard, N., Sanchez-Garcia, E. & Münch, J. An optimized derivative of an endogenous CXCR4 antagonist prevents atopic dermatitis and airway inflammation. (2021). *Acta Pharm. Sin. B* **11**, 2694–2708.
220. Harms, M., Gilg, A., Ständker, L., Beer, A. J., Mayer, B., Rasche, V., Gruber, C. W. & Münch, J. Microtiter plate-based antibody-competition assay to determine binding affinities and plasma/blood stability of CXCR4 ligands. (2020). *Sci. Rep.* **10**, 1–10.
221. Harms, M., Fabech Hansson, R., Gilg, A., Almeida-Hernández, Y., Löffler, J., Rodríguez-Alfonso, A., Habib, M. M. W., Albers, D., Ahmed, N. S., Abadi, A. H., Winter, G., Rasche, V., Beer, A. J., Weidinger, G., Preising, N., Ständker, L., Wiese, S., Sanchez-Garcia, E., Zelikin, A. N. & Münch, J. Development of N-Terminally Modified Variants of the CXCR4-Antagonistic Peptide EPI-X4 for Enhanced Plasma Stability. (2023). *J. Med. Chem.* **66**, 15189–15204.
222. Pollaro, L. & Heinis, C. Strategies to prolong the plasma residence time of peptidedrugs. (2010). *MedChemComm* **1**, 319–324.
223. Elimination Pathways of Fusion Protein and Peptide Drugs. (2020). *Biointerface Res. Appl. Chem.* **11**, 9139–9147.
224. Spada, A., Emami, J., Tuszynski, J. A. & Lavasanifar, A. The Uniqueness of Albumin as a Carrier in Nanodrug Delivery. (2021). *Mol. Pharm.* **18**, 1862–1894.
225. Knudsen, L. B. Inventing Liraglutide, a Glucagon-Like Peptide-1 Analogue, for the Treatment of Diabetes and Obesity. (American Chemical Society, 2019). *ACS Pharmacol. Transl. Sci.* **2**, 468–484 American Chemical Society.

226. Lau, J., Bloch, P., Schäffer, L., Pettersson, I., Spetzler, J., Kofoed, J., Madsen, K., Knudsen, L. B., McGuire, J., Steensgaard, D. B., Strauss, H. M., Gram, D. X., Knudsen, S. M., Nielsen, F. S., Thygesen, P., Reedtz-Runge, S. & Kruse, T. Discovery of the Once-Weekly Glucagon-Like Peptide-1 (GLP-1) Analogue Semaglutide. (American Chemical Society, 2015). *J. Med. Chem.* **58**, 7370–7380 American Chemical Society.
227. Harms, M., Hansson, R. F., Carmali, S., Almeida-Hernández, Y., Sanchez-Garcia, E., Münch, J. & Zelikin, A. N. Dimerization of the Peptide CXCR4-Antagonist on Macromolecular and Supramolecular Protraction Arms Affords Increased Potency and Enhanced Plasma Stability. (2022). *Bioconjug. Chem.* **33**, 594–607.
228. Graham, F. L., Smiley, J., Russell, W. C. & Nairn, R. Characteristics of a human cell line transformed by DNA from human adenovirus type 5. (J Gen Virol, 1977). *J. Gen. Virol.* **36**, 59–74 J Gen Virol.
229. Wei, X., Decker, J. M., Liu, H., Zhang, Z., Arani, R. B., Kilby, J. M., Saag, M. S., Wu, X., Shaw, G. M. & Kappes, J. C. Emergence of Resistant Human Immunodeficiency Virus Type 1 in Patients Receiving Fusion Inhibitor (T-20) Monotherapy. (Antimicrob Agents Chemother, 2002). *Antimicrob. Agents Chemother.* **46**, 1896–1905 Antimicrob Agents Chemother.
230. Gilg, A., Harms, M., Olari, L. R., Urbanowitz, A. K., Bonig, H. & Münch, J. Absence of the CXCR4 antagonist EPI-X4 from pharmaceutical human serum albumin preparations. (BioMed Central, 2021). *J. Transl. Med.* **19**, 1–5 BioMed Central.
231. Speiser, D. E., Chijioke, O., Schaeuble, K. & Münz, C. CD4+ T cells in cancer. (2023). *Nat. Cancer* **4**, 317–329.
232. Hirahara, K. & Nakayama, T. CD4 + T-cell subsets in inflammatory diseases: beyond the T h 1/T h 2 paradigm. (2016). *Int. Immunol.* **28**, 163–171.
233. Yang, W., Yu, T. & Cong, Y. CD4+ T cell metabolism, gut microbiota, and autoimmune diseases: implication in precision medicine of autoimmune diseases. (2022). *Precis. Clin. Med.* **5**, pbac018.
234. Muscate, F., Woestemeier, A. & Gagliani, N. Functional heterogeneity of CD4+ T cells in liver inflammation. (2021). *Semin. Immunopathol.* **43**, 549–561.
235. Brelot, A., Heveker, N., Adema, K., Hosie, M. J., Willett, B. & Alizon, M. Effect of Mutations in the Second Extracellular Loop of CXCR4 on Its Utilization by Human and Feline Immunodeficiency Viruses. (1999). *J. Virol.* **73**, 2576–2586.

236. Hatse, S., Princen, K., Bridger, G., De Clercq, E. & Schols, D. Chemokine receptor inhibition by AMD3100 is strictly confined to CXCR4. (2002). *FEBS Lett.* **527**, 255–262.

237. Schottelius, M., Ludescher, M., Richter, F., Kapp, T. G., Kessler, H. & Wester, H.-J. Validation of [125I]CPCR4.3 as an investigative tool for the sensitive and specific detection of hCXCR4 and mCXCR4 expression in vitro and in vivo. (2019). *EJNMMI Res.* **9**, 75.

238. Jacobson, O., Weiss, I. D., Szajek, L., Farber, J. M. & Kiesewetter, D. O. 64Cu-AMD3100—A novel imaging agent for targeting chemokine receptor CXCR4. (2009). *Bioorg. Med. Chem.* **17**, 1486–1493.

239. Luyten, K., Van Loy, T., Cawthorne, C., Deroose, C. M., Schols, D., Bormans, G. & Cleeren, F. D-Peptide-Based Probe for CXCR4-Targeted Molecular Imaging and Radionuclide Therapy. (2021). *Pharmaceutics* **13**, 1619.

240. Chen, Z., Teo, A. E. & McCarty, N. ROS-Induced CXCR4 Signaling Regulates Mantle Cell Lymphoma (MCL) Cell Survival and Drug Resistance in the Bone Marrow Microenvironment via Autophagy. (2016). *Clin. Cancer Res. Off. J. Am. Assoc. Cancer Res.* **22**, 187–199.

241. Lin, C.-H., Shih, C.-H., Tseng, C.-C., Yu, C.-C., Tsai, Y.-J., Bien, M.-Y. & Chen, B.-C. CXCL12 Induces Connective Tissue Growth Factor Expression in Human Lung Fibroblasts through the Rac1/ERK, JNK, and AP-1 Pathways. (2014). *PLoS ONE* **9**, e104746.

242. Bresin, A., D'Abundo, L., Narducci, M. G., Fiorenza, M. T., Croce, C. M., Negrini, M. & Russo, G. TCL1 transgenic mouse model as a tool for the study of therapeutic targets and microenvironment in human B-cell chronic lymphocytic leukemia. (2016). *Cell Death Dis.* **7**, e2071.

243. Bichi, R., Shinton, S. A., Martin, E. S., Koval, A., Calin, G. A., Cesari, R., Russo, G., Hardy, R. R. & Croce, C. M. Human chronic lymphocytic leukemia modeled in mouse by targeted TCL1 expression. (2002). *Proc. Natl. Acad. Sci. U. S. A.* **99**, 6955–6960.

244. Kozlowski, A. & Milton Harris, J. Improvements in protein PEGylation: pegylated interferons for treatment of hepatitis C. (2001). *J. Controlled Release* **72**, 217–224.

245. Dong, X., Al-Jumaily, A. & Escobar, I. Investigation of the Use of a Bio-Derived Solvent for Non-Solvent-Induced Phase Separation (NIPS) Fabrication of Polysulfone Membranes. (2018). *Membranes* **8**, 23.

246. Matyjaszewski, K. & Möller, M. *Polymer science: a comprehensive reference*. (2012) Amsterdam: Elsevier.

247. Décaillot, F. M., Kazmi, M. A., Lin, Y., Ray-Saha, S., Sakmar, T. P. & Sachdev, P. CXCR7/CXCR4 Heterodimer Constitutively Recruits β-Arrestin to Enhance Cell Migration. (2011). *J. Biol. Chem.* **286**, 32188–32197.

248. Wang, J., He, L., Combs, C. A., Roderiquez, G. & Norcross, M. A. Dimerization of CXCR4 in living malignant cells: control of cell migration by a synthetic peptide that reduces homologous CXCR4 interactions. (2006). *Mol. Cancer Ther.* **5**, 2474–2483.

249. Rodríguez, D. & Gutiérrez-de-Terán, H. Characterization of the homodimerization interface and functional hotspots of the CXCR4 chemokine receptor. (John Wiley & Sons, Ltd, 2012). *Proteins Struct. Funct. Bioinforma.* **80**, 1919–1928 John Wiley & Sons, Ltd.

250. Jarlstad Olesen, M. T., Walther, R., Poier, P. P., Dagnæs-Hansen, F. & Zelikin, A. N. Molecular, Macromolecular, and Supramolecular Glucuronide Prodrugs: Lead Identified for Anticancer Prodrug Monotherapy. (2020). *Angew. Chem.* **132**, 7460–7466.

251. Rodríguez-Alfonso, A., Heck, A., Ruiz-Blanco, Y. B., Gilg, A., Ständker, L., Kuan, S. L., Weil, T., Sanchez-Garcia, E., Wiese, S., Münch, J. & Harms, M. Advanced EPI-X4 Derivatives Covalently Bind Human Serum Albumin Resulting in Prolonged Plasma Stability. (2022). *Int. J. Mol. Sci.* **23**, 15029.

252. Kurtzhals, P., Østergaard, S., Nishimura, E. & Kjeldsen, T. Derivatization with fatty acids in peptide and protein drug discovery. (2023). *Nat. Rev. Drug Discov.* **22**, 59–80.

253. Novo Nordisk. Company Announcements: Ozempic® (semaglutide) approved in the US. 2017. Download on: July 28, 2023. Available from: https://www.novonordisk.com/content/nncorp/global/en/news-and-media/news-and-ir-materials/news-details.html?id=356.

254. Novo Nordisk. Company Announcements: Rybelsus® (semaglutide tablets), the first GLP-1 in a tablet approved in the US. 2019. Download on: July 28, 2023. Available from: https://www.novonordisk.com/content/nncorp/global/en/news-and-media/news-and-ir-materials/news-details.html?id=356.

255. Nowak-Sliwinska, P., Segura, T. & Iruela-Arispe, M. L. The chicken chorioallantoic membrane model in biology, medicine and bioengineering. (2014). *Angiogenesis* **17**, 779–804.

256. Gebhardt, D. O. E. & Van Logten, M. J. The chick embryo test as used in the study of the toxicity of certain dithiocarbamates. (1968). *Toxicol. Appl. Pharmacol.* **13**, 316–324.

257. Kue, C. S., Tan, K. Y., Lam, M. L. & Lee, H. B. Chick embryo chorioallantoic membrane (CAM): an alternative predictive model in acute toxicological studies for anti-cancer drugs. (2015). *Exp. Anim.* **64**, 129–138.

258. Maugeri, A., Lombardo, G. E., Navarra, M., Cirmi, S. & Rapisarda, A. The chorioallantoic membrane: A novel approach to extrapolate data from a well-established method. (2022). *J. Appl. Toxicol.* **42**, 995–1003.

259. Shimode, N., Yasuoka, H., Kinoshita, M., Hirashima, K., Tsujimoto, S., Tashiro, C. & Kokubunji, A. Severe anaphylaxis after albumin infusion in a patient with ahaptoglobinemia. (2006). *Anesthesiology* **105**, 425–426.

260. Morishita, K., Shimada, E., Watanabe, Y. & Kimura, H. Anaphylactic transfusion reactions associated with anti-haptoglobin in a patient with ahaptoglobinemia. (2000). *Transfusion (Paris)* **40**, 120–121.

261. Rozich, J. D. & Paul, R. V. Acute renal failure precipitated by elevated colloid osmotic pressure. (1989). *Am. J. Med.* **87**, 358–360.

262. Kovalik, S. G., Ledgerwood, A. M., Lucas, C. E. & Higgins, R. F. The cardiac effect of altered calcium homeostasis after albumin resuscitation. (1981). *J. Trauma* **21**, 275–279.

263. Aue, G., Sun, C., Liu, D., Park, J.-H., Pittaluga, S., Tian, X., Lee, E., Soto, S., Valdez, J., Maric, I., Stetler-Stevenson, M., Yuan, C., Nakamura, Y., Muranski, P. & Wiestner, A. Activation of Th1 Immunity within the Tumor Microenvironment Is Associated with Clinical Response to Lenalidomide in Chronic Lymphocytic Leukemia. (2018). *J. Immunol. Baltim. Md 1950* **201**, 1967–1974.

264. Wald, O., Izhar, U., Amir, G., Avniel, S., Bar-Shavit, Y., Wald, H., Weiss, I. D., Galun, E. & Peled, A. CD4+CXCR4highCD69+ T Cells Accumulate in Lung Adenocarcinoma. (2006). *J. Immunol.* **177**, 6983–6990.

265. Kaur, G. & Dufour, J. M. Cell lines: Valuable tools or useless artifacts. (2012). *Spermatogenesis* **2**, 1–5.

266. Cree, I. A., Glaysher, S. & Harvey, A. L. Efficacy of anti-cancer agents in cell lines versus human primary tumour tissue. (2010). *Curr. Opin. Pharmacol.* **10**, 375–379.

267. Smith, J., Stewart, B. J., Glaysher, S., Peregrin, K., Knight, L. A., Weber, D. J. & Cree, I. A. The effect of pentamidine on melanoma ex vivo. (2010). *Anticancer. Drugs* **21**, 181–185.

268. Knight, L. A., Conroy, M., Fernando, A., Polak, M., Kurbacher, C. M. & Cree, I. A. Pilot studies of the effect of zoledronic acid (Zometa®) on tumor-derived cells ex vivo in the ATP-based tumor chemosensitivity assay. (2005). *Anticancer. Drugs* **16**, 969–976.

269. Song, M., Bode, A. M., Dong, Z. & Lee, M.-H. AKT as a Therapeutic Target for Cancer. (2019). *Cancer Res.* **79**, 1019–1031.

270. Chen, X., Thakkar, H., Tyan, F., Gim, S., Robinson, H., Lee, C., Pandey, S. K., Nwokorie, C., Onwudiwe, N. & Srivastava, R. K. Constitutively active Akt is an important regulator of TRAIL sensitivity in prostate cancer. (2001). *Oncogene* **20**, 6073–6083.

271. Zuurbier, L., Petricoin, E. F., Vuerhard, M. J., Calvert, V., Kooi, C., Buijs-Gladdines, J. G. C. A. M., Smits, W. K., Sonneveld, E., Veerman, A. J. P., Kamps, W. A., Horstmann, M., Pieters, R. & Meijerink, J. P. P. The significance of PTEN and AKT aberrations in pediatric T-cell acute lymphoblastic leukemia. (2012). *Haematologica* **97**, 1405–1413.

272. Guo, Y., Pan, W., Liu, S., Shen, Z., Xu, Y. & Hu, L. ERK/MAPK signalling pathway and tumorigenesis (Review). (2020). *Exp. Ther. Med.*

273. Saita, Y., Kondo, M. & Shimizu, Y. Species selectivity of small-molecular antagonists for the CCR5 chemokine receptor. (2007). *Int. Immunopharmacol.* **7**, 1528–1534.

274. Guo, S., Zhao, T., Yun, Y. & Xie, X. Recent progress in assays for GPCR drug discovery. (2022). *Am. J. Physiol. Cell Physiol.* **323**, C583–C594.

275. Palmesino, E., Moepps, B., Gierschik, P. & Thelen, M. Differences in CXCR4-mediated signaling in B cells. (2006). *Immunobiology* **211**, 377–389.

276. Tripathi, V., Kumar, R., Dinda, A. K., Kaur, J. & Luthra, K. CXCL12–CXCR7 Signaling Activates ERK and Akt Pathways in Human Choriocarcinoma Cells. (2014). *Cell Commun. Adhes.* **21**, 221–228.

277. Kumar, R., Tripathi, V., Ahmad, M., Nath, N., Mir, R. A., Chauhan, S. S. & Luthra, K. CXCR7 mediated Giα independent activation of ERK and Akt promotes cell survival and chemotaxis in T cells. (2012). *Cell. Immunol.* **272**, 230–241.

278. Gravel, S., Malouf, C., Boulais, P. E., Berchiche, Y. A., Oishi, S., Fujii, N., Leduc, R., Sinnett, D. & Heveker, N. The Peptidomimetic CXCR4 Antagonist TC14012 Recruits β-Arrestin to CXCR7. (2010). *J. Biol. Chem.* **285**, 37939–37943.
279. Kalatskaya, I., Berchiche, Y. A., Gravel, S., Limberg, B. J., Rosenbaum, J. S. & Heveker, N. AMD3100 Is a CXCR7 Ligand with Allosteric Agonist Properties. (Mol Pharmacol, 2009). *Mol. Pharmacol.* **75**, 1240–1247 Mol Pharmacol.
280. Guo, F., Wang, Y., Liu, J., Mok, S. C., Xue, F. & Zhang, W. CXCL12/CXCR4: a symbiotic bridge linking cancer cells and their stromal neighbors in oncogenic communication networks. (2016). *Oncogene* **35**, 816–826.
281. Burger, J. A. & Kipps, T. J. CXCR4: a key receptor in the crosstalk between tumor cells and their microenvironment. (2006). *Blood* **107**, 1761–1767.
282. Tiwari, A., Trivedi, R. & Lin, S.-Y. Tumor microenvironment: barrier or opportunity towards effective cancer therapy. (2022). *J. Biomed. Sci.* **29**, 83.
283. Bejarano, L., Jordão, M. J. C. & Joyce, J. A. Therapeutic Targeting of the Tumor Microenvironment. (2021). *Cancer Discov.* **11**, 933–959.
284. Wang, Q., Shao, X., Zhang, Y., Zhu, M., Wang, F. X. C., Mu, J., Li, J., Yao, H. & Chen, K. Role of tumor microenvironment in cancer progression and therapeutic strategy. (2023). *Cancer Med.* **12**, 11149–11165.
285. Xiao, Y. & Yu, D. Tumor microenvironment as a therapeutic target in cancer. (2021). *Pharmacol. Ther.* **221**, 107753.
286. Guièze, R. & Wu, C. J. Genomic and epigenomic heterogeneity in chronic lymphocytic leukemia. (2015). *Blood* **126**, 445–453.
287. McCay, J. & Gribben, J. G. The role of BTK inhibitors on the tumor microenvironment in CLL. (2022). *Leuk. Lymphoma* **63**, 2023–2032.
288. Messex, J. K. & Liou, G.-Y. Targeting BTK Signaling in the Microenvironment of Solid Tumors as a Feasible Cancer Therapy Option. (2021). *Cancers* **13**, 2198.
289. Eyre, T. A., Cheah, C. Y. & Wang, M. L. Therapeutic options for relapsed/refractory mantle cell lymphoma. (2022). *Blood* **139**, 666–677.
290. Liu, S.-H., Gu, Y., Pascual, B., Yan, Z., Hallin, M., Zhang, C., Fan, C., Wang, W., Lam, J., Spilker, M. E., Yafawi, R., Blasi, E., Simmons, B., Huser, N., Ho, W.-H., Lindquist, K., Tran, T.-T., Kudaravalli, J., Ma, J.-T., Jimenez, G., Barman, I., Brown, C., Chin, S. M., Costa, M. J., Shelton, D., Smeal, T., Fantin, V. R. & Pernasetti, F. A novel CXCR4 antagonist IgG1 antibody (PF-06747143) for the treatment of hematologic malignancies. (2017). *Blood Adv.* **1**, 1088–1100.

291. Beider, K., Ribakovsky, E., Abraham, M., Wald, H., Weiss, L., Rosenberg, E., Galun, E., Avigdor, A., Eizenberg, O., Peled, A. & Nagler, A. Targeting the CD20 and CXCR4 Pathways in Non-Hodgkin Lymphoma with Rituximab and High-Affinity CXCR4 Antagonist BKT140. (2013). *Clin. Cancer Res.* **19**, 3495–3507.
292. O'Callaghan, K., Lee, L., Nguyen, N., Hsieh, M.-Y., Kaneider, N. C., Klein, A. K., Sprague, K., Van Etten, R. A., Kuliopulos, A. & Covic, L. Targeting CXCR4 with cell-penetrating pepducins in lymphoma and lymphocytic leukemia. (2012). *Blood* **119**, 1717–1725.
293. Jamaludin, S., Azimi, I., Davis, F., Peters, A., Gonda, T., Thompson, E., Roberts-Thomson, S. & Monteith, G. Assessment of CXC ligand 12-mediated calcium signalling and its regulators in basal-like breast cancer cells. (2018). *Oncol. Lett.*
294. Treon, S. P., Meid, K., Hunter, Z. R., Flynn, C. A., Sarosiek, S. R., Leventoff, C. R., White, T. P., Cao, Y., Roccaro, A. M., Sacco, A., Demos, M. G., Guerrera, M. L., Kofides, A., Liu, X., Xu, L., Patterson, C. J., Munshi, M., Tsakmaklis, N., Yang, G., Ghobrial, I. M., Branagan, A. R. & Castillo, J. J. Phase 1 study of ibrutinib and the CXCR4 antagonist ulocuplumab in CXCR4-mutated Waldenström macroglobulinemia. (2021). *Blood* **138**, 1535–1539.
295. Mehta, S. A., Christopherson, K. W., Bhat-Nakshatri, P., Goulet, R. J., Broxmeyer, H. E., Kopelovich, L. & Nakshatri, H. Negative regulation of chemokine receptor CXCR4 by tumor suppressor p53 in breast cancer cells: implications of p53 mutation or isoform expression on breast cancer cell invasion. (2007). *Oncogene* **26**, 3329–3337.
296. Li, Q., Wang, M., Zeng, L., Guo, W., Xu, Y., Li, C., Lai, Y., Ye, L. & Peng, X. Deletion of Wild-type p53 Facilitates Bone Metastatic Function by Blocking the AIP4 Mediated Ligand-Induced Degradation of CXCR4. (2021). *Front. Pharmacol.* **12**, 792293.
297. St-Pierre, F. & Ma, S. Use of BTK Inhibitors in Chronic Lymphocytic Leukemia/Small Lymphocytic Lymphoma (CLL/SLL): A Practical Guidance. (2022). *Blood Lymphat. Cancer Targets Ther.* **12**, 81–98.
298. Bernard, S., Danglade, D., Gardano, L., Laguillier, C., Lazarian, G., Roger, C., Thieblemont, C., Marzec, J., Gribben, J., Cymbalista, F., Varin-Blank, N., Ledoux, D. & Baran-Marszak, F. Inhibitors of BCR signalling interrupt the survival signal mediated by the micro-environment in mantle cell lymphoma: BCR inhibition in MCL. (2015). *Int. J. Cancer* **136**, 2761–2774.
299. Chang, B. Y., Francesco, M., De Rooij, M. F. M., Magadala, P., Steggerda, S. M., Huang, M. M., Kuil, A., Herman, S. E. M., Chang, S., Pals, S. T., Wilson, W., Wiestner,

A., Spaargaren, M., Buggy, J. J. & Elias, L. Egress of CD19(+)CD5(+) cells into peripheral blood following treatment with the Bruton tyrosine kinase inhibitor ibrutinib in mantle cell lymphoma patients. (2013). *Blood* **122**, 2412–2424.

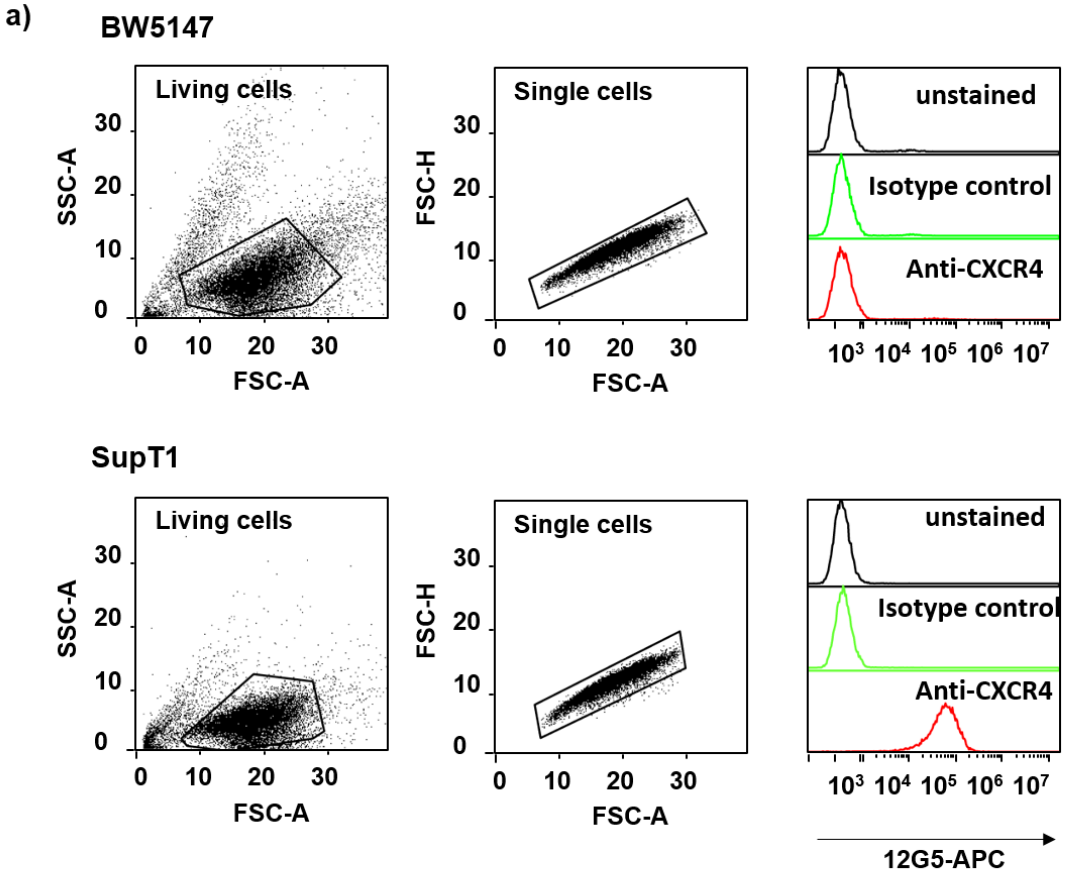
300. Veronese, F. M. & Mero, A. The Impact of PEGylation on Biological Therapies: (2008). *BioDrugs* **22**, 315–329.
301. McDonnell, T., Ioannou, Y. & Rahman, A. PEGylated drugs in rheumatology--why develop them and do they work? (2014). *Rheumatology* **53**, 391–396.
302. Awwad, S., Ginn, C. & Brocchini, S. The case for protein PEGylation. in (2018) *Engineering of Biomaterials for Drug Delivery Systems* 27–49 Elsevier.
303. Ocłoń, E., Solomon, G., Hayouka, Z., Salame, T. M., Goffin, V. & Gertler, A. Novel reagents for human prolactin research: large-scale preparation and characterization of prolactin receptor extracellular domain, non-pegylated and pegylated prolactin and prolactin receptor antagonist. (2018). *Protein Eng. Des. Sel.* **31**, 7–16.
304. Bailon, P., Palleroni, A., Schaffer, C. A., Spence, C. L., Fung, W.-J., Porter, J. E., Ehrlich, G. K., Pan, W., Xu, Z.-X., Modi, M. W., Farid, A., Berthold, W. & Graves, M. Rational Design of a Potent, Long-Lasting Form of Interferon: A 40 kDa Branched Polyethylene Glycol-Conjugated Interferon α-2a for the Treatment of Hepatitis C. (2001). *Bioconjug. Chem.* **12**, 195–202.
305. Yamaoka, T., Tabata, Y. & Ikada, Y. Distribution and Tissue Uptake of Poly(ethylene glycol) with Different Molecular Weights after Intravenous Administration to Mice. (1994). *J. Pharm. Sci.* **83**, 601–606.
306. Sankaranarayanan, S., de la Llera-Moya, M., Drazul-Schrader, D., Phillips, M. C., Kellner-Weibel, G. & Rothblat, G. H. Serum albumin acts as a shuttle to enhance cholesterol efflux from cells. (2013). *J. Lipid Res.* **54**, 671–676.
307. Van Der Vusse, G. J. Albumin as Fatty Acid Transporter. (2009). *Drug Metab. Pharmacokinet.* **24**, 300–307.
308. Keating, G. M. Insulin Detemir: A Review of its Use in the Management of Diabetes Mellitus. (2012). *Drugs* **72**, 2255–2287.
309. Drucker, D. J., Dritselis, A. & Kirkpatrick, P. Liraglutide. (2010). *Nat. Rev. Drug Discov.* **9**, 267–268.
310. US National Library of Medicine. ClinicalTrial.gov. (2022). Available from: https://clinicaltrials.gov/study/NCT05035095.

311. Zabeen, B., Ahmed, B., Islam, N., Tayyeb, S., Nahar, J. & Azad, K. Comparison of efficacy of detemir and degludec insulin in the management of children and adolescents with type 1 diabetes. (2022). *J. Diabetol.* **13**, 62.
312. Davies, M. J., Gross, J. L., Ono, Y., Sasaki, T., Bantwal, G., Gall, M. A., Niemeyer, M., Seino, H., & BEGIN BB T1 Study Group. Efficacy and safety of insulin degludec given as part of basal-bolus treatment with mealtime insulin aspart in type 1 diabetes: a 26-week randomized, open-label, treat-to-target non-inferiority trial. (2014). *Diabetes Obes. Metab.* **16**, 922–930.
313. Knudsen, L. B. & Lau, J. The Discovery and Development of Liraglutide and Semaglutide. (2019). *Front. Endocrinol.* **10**, 155.
314. Tennagels, N. & Werner, U. The metabolic and mitogenic properties of basal insulin analogues. (2013). *Arch. Physiol. Biochem.* **119**, 1–14.
315. Domínguez-Oliva, A., Hernández-Ávalos, I., Martínez-Burnes, J., Olmos-Hernández, A., Verduzco-Mendoza, A. & Mota-Rojas, D. The Importance of Animal Models in Biomedical Research: Current Insights and Applications. (2023). *Animals* **13**, 1223.
316. Sántha, M. Biologia futura: animal testing in drug development—the past, the present and the future. (2020). *Biol. Futura* **71**, 443–452.
317. Seyhan, A. A. Lost in translation: the valley of death across preclinical and clinical divide – identification of problems and overcoming obstacles. (2019). *Transl. Med. Commun.* **4**, 18.
318. Sneddon, L. U., Halsey, L. G. & Bury, N. R. Considering aspects of the 3Rs principles within experimental animal biology. (2017). *J. Exp. Biol.* **220**, 3007–3016.
319. Russell, W. M. S. & Burch, R. L. *The principles of humane experimental technique*. (1992) Potters Bar, Herts: Universities Federation for Animal Welfare.
320. Winter, G., Koch, A. B. F., Löffler, J., Lindén, M., Solbach, C., Abaei, A., Li, H., Glatting, G., Beer, A. J. & Rasche, V. Multi-Modal PET and MR Imaging in the Hen's Egg Test-Chorioallantoic Membrane (HET-CAM) Model for Initial In Vivo Testing of Target-Specific Radioligands. (2020). *Cancers* **12**, 1248.
321. Löffler, J., Hamp, C., Scheidhauer, E., Di Carlo, D., Solbach, C., Abaei, A., Hao, L., Glatting, G., Beer, A. J., Rasche, V. & Winter, G. Comparison of Quantification of Target-Specific Accumulation of [18F]F-siPSMA-14 in the HET-CAM Model and in Mice Using PET/MRI. (2021). *Cancers* **13**, 4007.
322. Nguyen, A., Reyes, A. E., Zhang, M., McDonald, P., Wong, W. L. T., Damico, L. A. & Dennis, M. S. The pharmacokinetics of an albumin-binding Fab (AB.Fab) can be

modulated as a function of affinity for albumin. (Protein Eng Des Sel, 2006). *Protein Eng. Des. Sel.* **19**, 291–297 Protein Eng Des Sel.

323. Patterson, R., Youngner, J. S., Weigle, W. O. & Dixon, F. J. The metabolism of serum proteins in the hen and chick and secretion of serum proteins by the ovary of the hen. (1962). *J. Gen. Physiol.* **45**, 501–513.
324. Haller, S., Ametamey, S. M., Schibli, R. & Müller, C. Investigation of the chick embryo as a potential alternative to the mouse for evaluation of radiopharmaceuticals. (2015). *Nucl. Med. Biol.* **42**, 226–233.
325. Galsky, M. D., Vogelzang, N. J., Conkling, P., Raddad, E., Polzer, J., Roberson, S., Stille, J. R., Saleh, M. & Thornton, D. A Phase I Trial of LY2510924, a CXCR4 Peptide Antagonist, in Patients with Advanced Cancer. (2014). *Clin. Cancer Res.* **20**, 3581–3588.
326. Di Maro, S., Trotta, A. M., Brancaccio, D., Di Leva, F. S., La Pietra, V., Ieranò, C., Napolitano, M., Portella, L., D'Alterio, C., Siciliano, R. A., Sementa, D., Tomassi, S., Carotenuto, A., Novellino, E., Scala, S. & Marinelli, L. Exploring the N-Terminal Region of C-X-C Motif Chemokine 12 (CXCL12): Identification of Plasma-Stable Cyclic Peptides As Novel, Potent C-X-C Chemokine Receptor Type 4 (CXCR4) Antagonists. (2016). *J. Med. Chem.* **59**, 8369–8380.

7 Supplementary Information



b)

```
CXCR4_HUMAN       1 ME--GISIYTSDNYTEEMGSGDYDSMKEPCFREENANFNKIFLPTIYSII     48
                    ||  .:||||||||:||:|||||||.||||||:|.:|||:|||||||.||
CXCR4_MOUSE       1 MEPISVSIYTSDNYSEEVGSGDYDSNKEPCFRDENVHFNRIFLPTIYFII     50

CXCR4_HUMAN      49 FLTGIVGNGLVILVMGYQKKLRSMTDKYRLHLSVADLLFVITLPFWAVDA     98
                    ||||||||||||||||||||||||||||||||||||||||||||||||||||
CXCR4_MOUSE      51 FLTGIVGNGLVILVMGYQKKLRSMTDKYRLHLSVADLLFVITLPFWAVDA    100

CXCR4_HUMAN      99 VANWYFGNFLCKAVHVIYTVNLYSSVLILAFISLDRYLAIVHATNSQRPR    148
                    :|:||||.|||||||:||||||||||||||||||||||||||||||||||||
CXCR4_MOUSE     101 MADWYFGKFLCKAVHIIYTVNLYSSVLILAFISLDRYLAIVHATNSQRPR    150

CXCR4_HUMAN     149 KLLAEKVVYVGVWIPALLLTIPDFIFANV-----SEADDRYICDRFYPND    193
                    |||||||.|||||||||||||||||||:|     |:.||||||||.||:.
CXCR4_MOUSE     151 KLLAEKAVYVGVWIPALLLTIPDFIFADVSQGDISQGDDRYICDRLYPDS    200

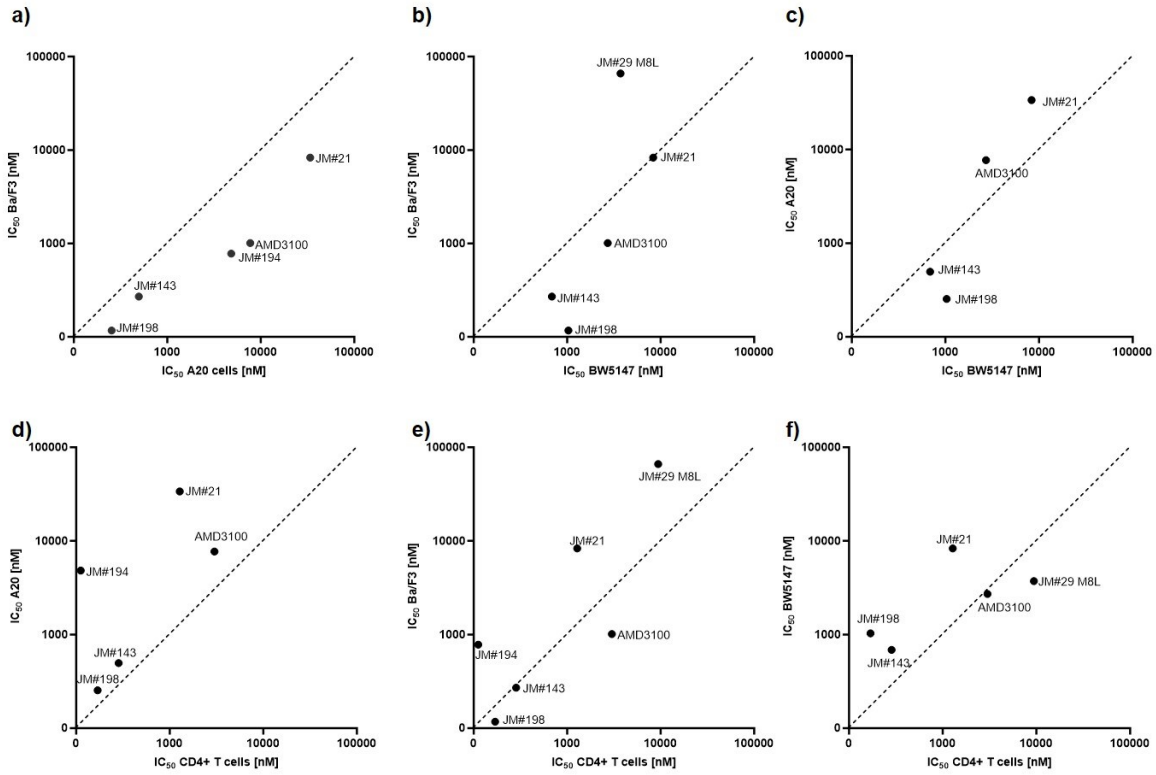
CXCR4_HUMAN     194 LWVVVFQFQHIMVGLILPGIVILSCYCIIISKLSHSKGHQKRKALKTTVI    243
                    ||:||||||||||||||||||||||||||||||||||||||||||||||||||
CXCR4_MOUSE     201 LWMVVFQFQHIMVGLILPGIVILSCYCIIISKLSHSKGHQKRKALKTTVI    250

CXCR4_HUMAN     244 LILAFFACWLPYYIGISIDSFILLEIIKQGCEFENTVHKWISITEALAFF    293
                    |||||||||||||:||||||||||.:|||||:||:.||||||||||||||
CXCR4_MOUSE     251 LILAFFACWLPYYVGISIDSFILLGVIKQGCDFESIVHKWISITEALAFF    300

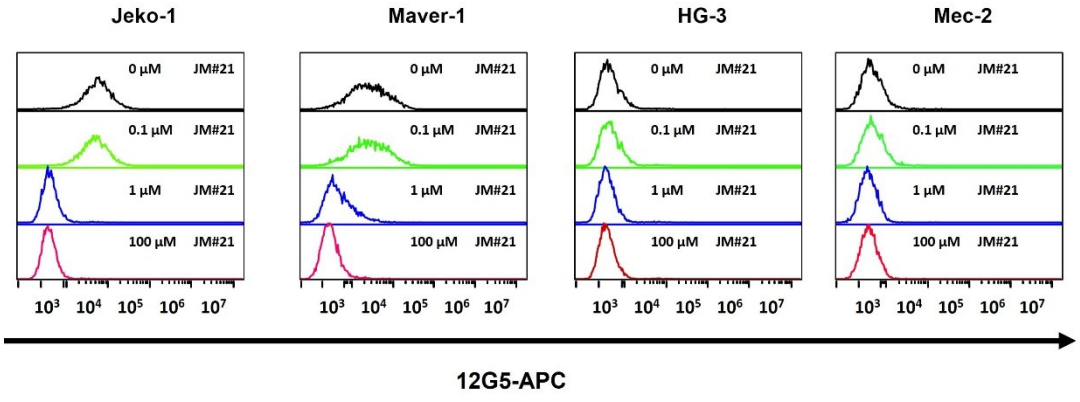
CXCR4_HUMAN     294 HCCLNPILYAFLGAKFKTSAQHALTSVSRGSSLKILSKGKRGGHSSVSTE    343
                    ||||||||||||||||:||||||.|:||||||||||||||||||||||||||
CXCR4_MOUSE     301 HCCLNPILYAFLGAKFKSSAQHALNSMSRGSSLKILSKGKRGGHSSVSTE    350

CXCR4_HUMAN     344 SESSSFHSS    352
                    |||||||||
CXCR4_MOUSE     351 SESSSFHSS    359
```

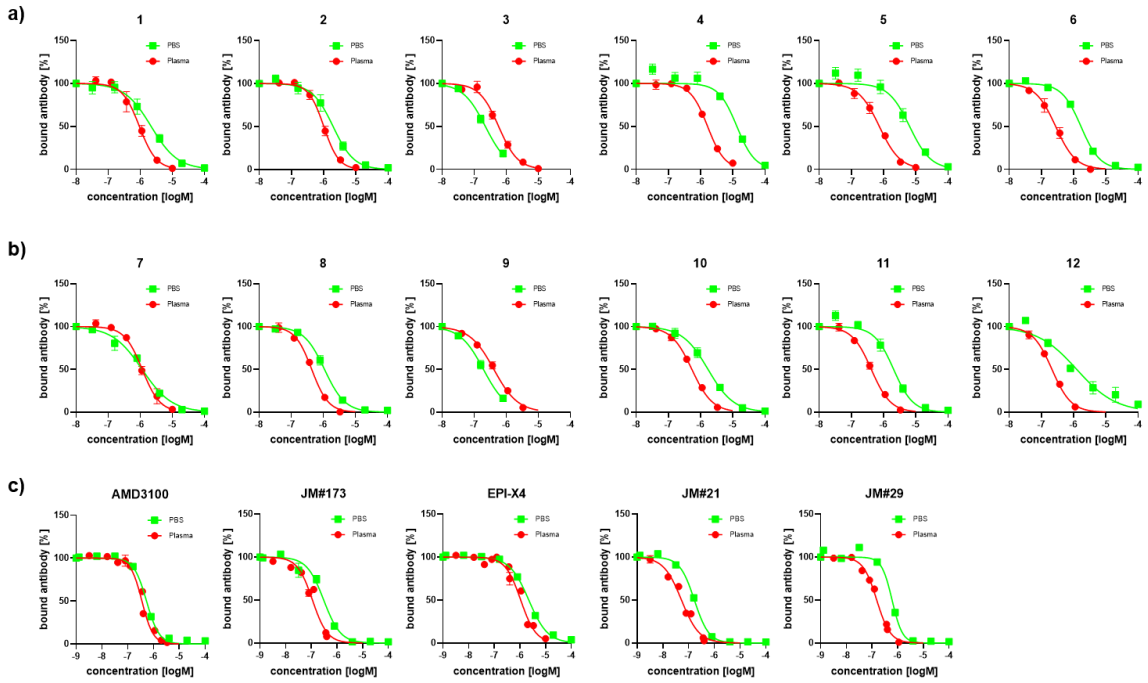
Supplement Figure 1. Human anti-CXCR4 antibody clone 12G5 does not bind to murine CXCR4. (a) Gating strategy using SSC-A, FSC-A and FSC-H to determine living single cells of murine T cell line BW5147 and human T cell line SupT1 whereof fluorescence intensity of anti-CXCR4 antibody clone 12G5 coupled to APC was detected. (b) Pairwise sequence alignment of human and murine CXCR4 was performed using EMBOSS needle. Highlighted in red is the sequence of the second extracellular loop (ECL2) and marked in yellow the amino acids shown before to be crucial for binding of the human anti-CXCR4 antibody clone 12G5[235].



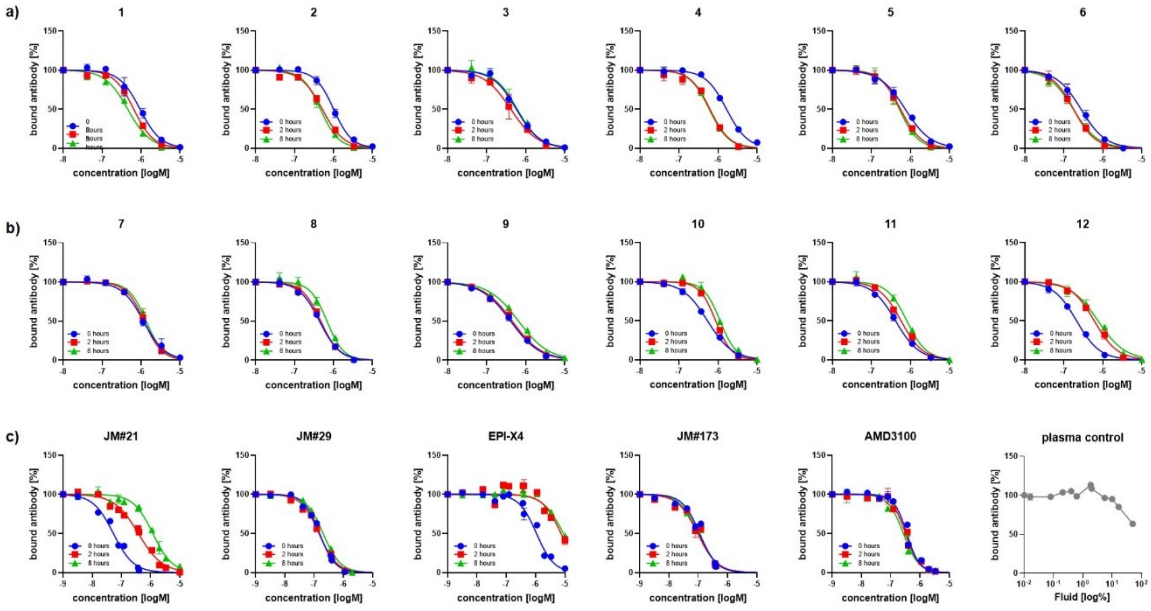
Supplement Figure 2. Comparison of IC_{50} values for the inhibition of CXCL12 induced Erk phosphorylation between murine cell lines Ba/F3, A20, BW5147 and human primary CD4+ T cells. IC_{50} values determined for inhibition of CXCL12 induced Erk phosphorylation were plotted for (a) Ba/F3 cells vs. A20 cells, (b) Ba/F3 cells vs BW5147 cells, (c) A20 cells vs BW5147 cells and A20 cells, Ba/F3 cells and BW5147 cells vs human primary CD4+ T cells (d-f). Dotted lines indicate a perfect correlation with a Pearson correlation coefficient of r=1.0.



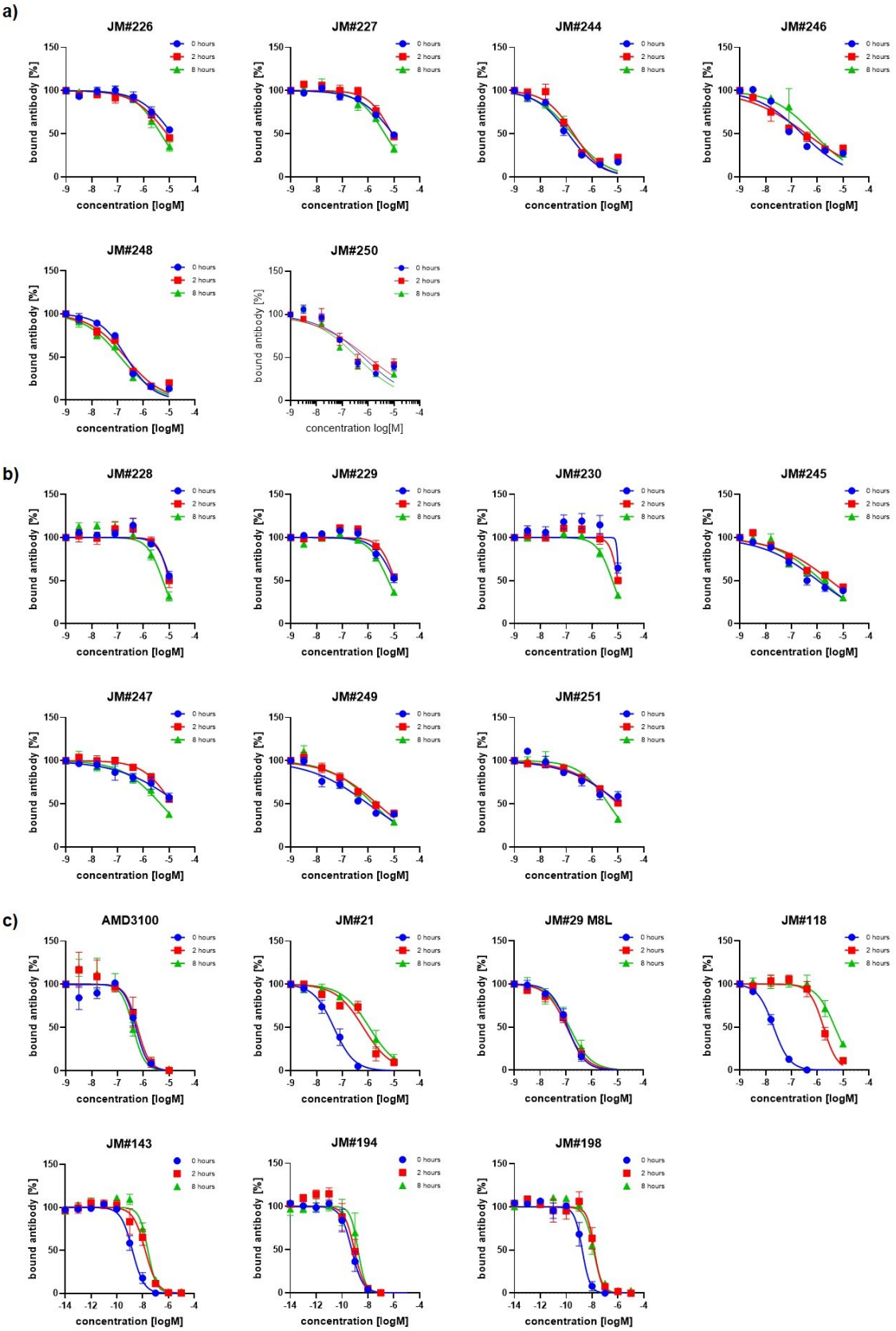
Supplement Figure 3. Antibody competition assay is not meaningful on CLL cell lines. Antibody competition assay was performed for MCL cell lines Jeko-1 and Maver-1 as well as for CLL cell lines HG-3 and Mec-2. Shown are representative overlay histograms for each cell lines in the presence of different concentrations of JM#21 (100 µM=red, 1 µM=blue, 0.01 µM=green and 0 µM=black).



Supplement Figure 4. Plasma increases binding affinity of JM#29 and JM#173 variants coupled to PEG and albumin binders. Variants of JM#29 (a) and JM#173 (b) coupled to PEG and albumin binders, respectively, and controls (c) were spiked into PBS (green) or human plasma (red) reaching a final concentration of 20 µM before antibody competition assay was performed. For this, spiked PBS or plasma was serially diluted in precooled PBS and applied to the SupT1 cells together with a constant concentration of anti-CXCR4 antibody clone 12G5 coupled to APC. After 2 hours at 4°C, unbound antibody was removed cells resuspended in 2% PFA before bound antibody were analyzed using flow cytometry. Shown data are derived from n=3 individual rounds of spiking ± SEM.



Supplement Figure 5. Dose-response curves to determine peptide stability in human plasma. Peptide conjugates of JM#29 (a), JM#173 (b) and respective controls (c) were spiked into human plasma reaching a final concentration of 20 µM. First aliquots, corresponding to t=0, were taken immediately after spiking and stored at -80°C. Remaining mixtures were incubated at 37°C until other aliquots were taken after 2 hours and 8 hours, respectively, which were stored at -80°C as well. Remaining activity was determined by an antibody competition assay. For this, stored aliquots were thaw in parallel and serially diluted in precooled PBS before applied to SupT1 cells together with a constant concentration of anti-CXCR4 antibody clone 12G5 coupled to the fluorophore APC. After 2 hours at 4°C unbound antibodies were removed, and cells fixed with 2% PFA. Bound antibodies were analyzed using flow cytometry. Shown data are derived from n=3 individual experiments ±SEM.



Supplement Figure 6. Dose-response curves to determine plasma stability of diacid variants. C16 diacid variants (a), C18 diacid variants (b) and respective controls (c) were spiked into human plasma reaching a final concentration of 20 µM. Out of each mixture, aliquots were taken immediately (t=0) or after incubation at 37°C for 2 h and 8 h, respectively, and stored at -80°C. Samples were thaw in parallel and serially diluted in precooled PBS before applied to SupT1 cells together with a constant concentration of anti-CXCR4 antibody clone 12G5. After 2 h at 4°C, unbound antibodies were removed, and bound antibody analyzed by flow cytometry. Shown are data derived from n=3 individual experiments ±SEM.

8 Acknowledgements

The acknowledgments have been removed for data protection reasons.

9 Curriculum Vitae

The curriculum vitae has been removed for data protection reasons.

The curriculum vitae has been removed for data protection reasons.

The curriculum vitae has been removed for data protection reasons.

The curriculum vitae has been removed for data protection reasons.